

CELL SIGNALING REGULATORY MECHANISMS CONTROLLING EPITHELIAL-  
MESENCHYMAL TRANSITION IN CARCINOMA

Janine Marie Buonato

A DISSERTATION

in

Chemical and Biomolecular Engineering

Presented to the Faculties of the University of Pennsylvania

in

Partial Fulfillment of the Requirements for the

Degree of Doctor of Philosophy

2015

---

Matthew Lazzara  
Assistant Professor, Chemical and Biomolecular Engineering  
Supervisor of Dissertation

---

Raymond Gorte  
Professor, Chemical and Biomolecular Engineering  
Graduate Group Chairperson

Dissertation Committee:  
Dr. Steven Albelda, Professor, Medicine  
Dr. Scott Diamond, Professor, Chemical and Biomolecular Engineering  
Dr. Dennis Discher, Professor, Chemical and Biomolecular Engineering

CELL SIGNALING REGULATORY MECHANISMS CONTROLLING EPITHELIAL-  
MESENCHYMAL TRANSITION IN CARCINOMA

COPYRIGHT

2015

Janine Marie Buonato

## ACKNOWLEDGMENT

This thesis has been greatly influenced by the guidance and support of a number of people. None of this work would have been possible without Matt, who provided unyielding scientific and professional support and mentorship over the last six years. Looking back I am amazed at all I have learned and the scientist I have become through his advising. The process of becoming a scientist involved a great deal of time spent in lab with some wonderful colleagues on the same journey. I am very appreciative of the friendship and scientific guidance that were always there from Alice, Chris, and Cal in the 'early' years and from Amar, Vaidehi, Evan, and Sarah more recently. My parents, siblings, and extended family have always provided a grounded base for me, and I am forever grateful for their love, support, encouragement, and hesitancy to ask when I was graduating (it's finally here!) over the last six years. Finally, and most importantly, I thank Jamie. It would be impossible to state my gratitude and amazement at his support, but his love has been a truly invaluable component to this work.

# ABSTRACT

## CELL SIGNALING REGULATORY MECHANISMS CONTROLLING EPITHELIAL- MESENCHYMAL TRANSITION IN CARCINOMA

Janine M. Buonato

Matthew J. Lazzara

Epithelial-mesenchymal transition (EMT) is a cellular program normally engaged during development and wound healing that is hijacked in many cancers to drive metastasis and resistance to therapy. The clinical implications of EMT in cancer progression have driven efforts to understand the cellular processes controlling EMT induction. Transforming growth factor-beta (TGF $\beta$ ) and expression of related transcription factors potentiate EMT induction through complex and incompletely understood mechanisms. In this thesis, we investigated specific intracellular signaling pathways controlling maintenance of mesenchymal characteristics and EMT induction in response to growth factors in lung and pancreatic carcinoma cells. In lung carcinoma cells, extracellular signal-regulated kinase-1/2 (ERK1/2) pathway activation, which promotes cell survival and proliferation, was required for complete EMT induction. Furthermore, chronic ERK1/2 inhibition reversed baseline mesenchymal traits while simultaneously augmenting cellular sensitivity to a clinically approved small molecule EGFR inhibitor in cell lines with multiple clinically relevant modes of therapy resistance. In both lung and pancreatic carcinoma cell lines, TGF $\beta$ -mediated EMT was enhanced by co-treatment with epidermal growth factor (EGF), as had been noted in other contexts. We demonstrated that the ability of EGF to enhance TGF $\beta$ -mediated EMT depended on SH2 domain-containing phosphatase-2 (SHP2) activation through tyrosine phosphorylated adapter binding, which is required for complete ERK1/2 activation. Though SHP2 was not directly engaged and activated by TGF $\beta$ , SHP2 was required for TGF $\beta$ -mediated effects. Incomplete or transient effects of ERK inhibition and SHP2 depletion motivated

subsequent systematic evaluation of cell signaling processes engaged during EMT induction to identify other pathways that control mesenchymal dedifferentiation in pancreatic carcinoma cells. We thus developed a data-driven computational model to predict the relationships between multivariate signaling events and EMT-associated phenotypes in response to combinations of TGF $\beta$ , EGF, and hepatocyte growth factor (HGF). Signaling intermediates that co-varied most with mesenchymal traits provided novel potential targets to inhibit EMT phenotype acquisition or restore epithelial traits in carcinoma. Together, this thesis enhanced mechanistic understanding of EMT regulation by SHP2, identified novel strategies to reverse EMT phenotypes in carcinoma cells, and generated a quantitative model to understand mesenchymal dedifferentiation, which can be leveraged in the future to improve clinical outcomes for cancer patients.

# TABLE OF CONTENTS

ACKNOWLEDGMENT .....	III
ABSTRACT .....	IV
TABLE OF CONTENTS .....	VI
LIST OF TABLES .....	IX
LIST OF FIGURES .....	X
CHAPTER 1: INTRODUCTION .....	1
1-1 THE EPITHELIAL-MESENCHYMAL TRANSITION.....	1
1-2 EMT IN CANCER.....	3
1-3 CELL SIGNALING AND EMT .....	5
1-4 EPIDERMAL GROWTH FACTOR RECEPTOR IN CANCER.....	7
1-5 ERK PATHWAY PERTURBATIONS IN CANCER AND EMT .....	10
1-6 THESIS SUMMARY.....	11
CHAPTER 2: ERK1/2 INHIBITION PREVENTS EPITHELIAL-MESENCHYMAL TRANSITION AND PROMOTES SENSITIVITY TO EGFR INHIBITION IN LUNG CANCER CELLS .....	14
2-1 ABSTRACT .....	14
2-2 INTRODUCTION.....	15
2-3 MATERIALS AND METHODS .....	17
Cell culture .....	17
Chronic MEK inhibition in H1666, PC9GR, and PC9 WZR .....	17
Chronic MEK inhibition in H322, H358, and SKBR3.....	18
Transwell migration assay .....	18
Flow cytometry .....	19
Western blotting .....	19
Antibodies and other reagents .....	20
Immunofluorescence.....	20
KRAS <sup>12V</sup> expression.....	20
EGF-mediated EGFR internalization assay.....	20
2-4 RESULTS.....	21
NSCLC cell lines undergo MEK-dependent TGF $\beta$ -induced EMT .....	21
MEK inhibition promotes epithelial phenotypes in NSCLC cells.....	23
Chronic MEK inhibition sensitizes NSCLC cells to EGFR inhibition on a time scale consistent with changes in epithelial and mesenchymal markers .....	23
KRAS <sup>12V</sup> -mediated ERK activation promotes EMT.....	26

MEK inhibition antagonizes mesenchymal phenotypes and acquired resistance to EGFR inhibition in an EGFR mutant-expressing cell line .....	27
2-5 DISCUSSION .....	32
2-6 ACKNOWLEDGEMENTS .....	35
2-7 SUPPLEMENTAL MATERIAL .....	36
<b>CHAPTER 3: EGF AUGMENTS TGF<math>\beta</math>-INDUCED EPITHELIAL-MESENCHYMAL TRANSITION BY PROMOTING SHP2 BINDING TO GAB1..</b>	<b>44</b>
3-1 ABSTRACT .....	44
3-2 INTRODUCTION .....	45
3-3 MATERIALS AND METHODS .....	47
Cell culture and reagents .....	47
Antibodies .....	47
Western blotting .....	47
Immunoprecipitation .....	48
Immunofluorescence staining and image analysis .....	48
Cell scatter experiments and quantification .....	49
Plasmids and viral infections .....	49
Wound closure assay .....	50
Statistical analysis .....	50
3-4 RESULTS .....	52
EGF augments TGF $\beta$ -induced EMT .....	52
EMT-associated changes in migration require TGF $\beta$ and EGF co-treatment .....	54
SHP2 knockdown enhances baseline epithelial characteristics .....	58
EMT induced by TGF $\beta$ with or without EGF is impaired by SHP2 knockdown .....	58
EGF and TGF $\beta$ differentially drive SHP2 association with phosphotyrosine-containing proteins .....	60
SHP2 SH2-domain engagement by phosphotyrosines is essential for EGF-mediated augmentation of EMT .....	61
3-5 DISCUSSION .....	65
3-6 ACKNOWLEDGEMENTS .....	69
3-7 SUPPLEMENTAL MATERIAL .....	70
<b>CHAPTER 4: A PARTIAL LEAST SQUARES REGRESSION ANALYSIS IDENTIFIES CELL SIGNALING EVENTS REGULATING EPITHELIAL-MESENCHYMAL TRANSITION .....</b>	<b>74</b>
4-1 ABSTRACT .....	74
4-2 INTRODUCTION .....	75
4-3 MATERIALS AND METHODS .....	78

Cell culture and reagents .....	78
Antibodies .....	78
Western blotting .....	78
Antibody microarray experiments .....	79
Multiplexed Luminex assay measurements .....	79
Immunofluorescence staining and image analysis .....	80
Cell scatter experiments and quantification .....	81
Partial least squares regression model development .....	81
Statistical analysis .....	83
<b>4-4 RESULTS .....</b>	<b>86</b>
Characterization of EMT-associated shifts in protein expression in response to EGF, HGF, and TGF $\beta$ .....	86
Measuring cell scatter in response to EMT-inducing growth factors .....	88
Antibody microarray reveals EMT-relevant phosphorylated protein targets for further investigation .....	90
Partial least squares regression model predicts signaling events most relevant for EMT phenotype acquisition .....	92
Reducing the X dataset improves PLSR model prediction and reveals key EMT signaling nodes .....	95
A minimal PLSR model identifies key EMT signaling nodes for further validation .....	98
<b>4-5 DISCUSSION .....</b>	<b>100</b>
<b>4-6 ACKNOWLEDGEMENTS .....</b>	<b>103</b>
<b>4-7 SUPPLEMENTAL MATERIAL .....</b>	<b>104</b>
<b>CHAPTER 5: CONCLUSIONS AND FUTURE WORK .....</b>	<b>106</b>
<b>5-1 SUMMARY .....</b>	<b>106</b>
<b>5-2 EFFECTS OF CHRONIC MEK INHIBITION AND FURTHER INVESTIGATION .....</b>	<b>107</b>
<b>5-3 SIGNALING TARGETS FOR EMT REVERSAL AND COMBINATION THERAPIES .....</b>	<b>109</b>
<b>5-4 SHP2 AS A THERAPEUTIC TARGET .....</b>	<b>110</b>
<b>5-5 MEASURING SHP2 ASSOCIATIONS WITH HIGHER SENSITIVITY AND SPATIAL RESOLUTION .....</b>	<b>111</b>
<b>5-6 TGF<math>\beta</math> SIGNALING .....</b>	<b>113</b>
<b>5-7 USING PLSR TO PREDICT CLINICALLY RELEVANT PHENOTYPES .....</b>	<b>115</b>
<b>BIBLIOGRAPHY .....</b>	<b>117</b>

## LIST OF TABLES

Table 4-1 Panel of proteins measured by Luminex. ....	84
Table 4-2 Panel of proteins measured by western blot. ....	85
Table 4-3 Proteins with greatest induction of phosphorylation from microarray.....	91
Table 4-4 Proteins with greatest decrease in phosphorylation from microarray.....	91
Table 4-S1 Protein measurements with VIP > 1.0 from 74-variable PLSR model. ....	105

# LIST OF FIGURES

Figure 1-1: Epithelial-mesenchymal transition.....	2
Figure 1-2: Cancer initiation and progression in epithelial tissues. ....	3
Figure 1-3: Epidermal growth factor receptor activation.....	8
Figure 1-4: ERK pathway signaling downstream of EGFR activation. ....	10
Figure 2-1: MEK inhibition prevents TGF $\beta$ -induced EMT in NSCLC cell lines.....	21
Figure 2-2: MEK inhibition promotes epithelial characteristics in H1666 cells. ....	22
Figure 2-3: Chronic MEK inhibition sensitizes NSCLC cells to EGFR inhibition. ....	25
Figure 2-4: KRAS <sup>12V</sup> expression promotes mesenchymal characteristics in H1666 cells.....	26
Figure 2-5: ERK activity determines epithelial/mesenchymal characteristics in an NSCLC cell line with an EGFR-activating mutation. ....	28
Figure 2-6: ERK2 amplification promotes mesenchymal characteristics in PC9 cells with acquired resistance to an irreversible EGFR inhibitor. ....	30
Figure 2-7: MEK inhibition sensitizes cells with acquired resistance to EGFR inhibitors. ....	31
Figure 2-S1. ....	36
Figure 2-S2. ....	37
Figure 2-S3. ....	37
Figure 2-S4. ....	38
Figure 2-S5. ....	39
Figure 2-S6. ....	40
Figure 2-S7. ....	41
Figure 2-S8. ....	42
Figure 2-S9. ....	43
Figure 3-1: EGF enhances TGF $\beta$ -mediated shifts in epithelial and mesenchymal marker expression.....	53
Figure 3-2: EGF enhances cellular migration in response to TGF $\beta$ . ....	56
Figure 3-3: SHP2 depletion promotes epithelial characteristics. ....	57
Figure 3-4: SHP2 is required for TGF $\beta$ -mediated EMT effects and EGF-mediated EMT augmentation. ....	59
Figure 3-5: EGF, but not TGF $\beta$ , promotes SHP2 association with phosphotyrosine-containing proteins. ....	61
Figure 3-6: SHP2 SH2 domain binding to phosphotyrosines is required for SHP2-mediated EMT effects.....	63
Figure 3-7: Schematic summary of the role of SHP2 in promoting EMT.....	65
Figure 3-S1. ....	70
Figure 3-S2. ....	71
Figure 3-S3. ....	72
Figure 3-S4. ....	73
Figure 4-1: EGF, HGF, and TGF $\beta$ induce differential changes in epithelial and mesenchymal marker expression and localization.....	87
Figure 4-2: EMT inducing growth factors promote cell scatter. ....	89
Figure 4-3: Evaluating total phosphotyrosine content from TGF $\beta$ +EGF time course.....	90
Figure 4-4: Individual protein phosphorylation profiles reveal differences in growth factor-mediated signaling. ....	93
Figure 4-5: A PLSR model reveals an EMT signaling axis.....	95
Figure 4-6: Systematic reduction of X variables improves model quality. ....	97
Figure 4-7: VIP score analysis confirms multivariate EMT regulation. ....	98
Figure 4-8: A minimal PLSR model captures important EMT signaling.....	99
Figure 4-S1: PCA analysis enables systematic exclusion of redundant X-variables. ....	104

# CHAPTER 1: Introduction

## 1-1 THE EPITHELIAL-MESENCHYMAL TRANSITION

Epithelial-mesenchymal transition (EMT) is a cellular program that allows fully differentiated epithelial cells to undergo a series of modifications ultimately leading to acquisition of a less differentiated mesenchymal phenotype. During this process, epithelial cells lose their distinctive morphology with strong cell-cell adhesions, patterned organization, and apical-basal polarity to acquire a more invasive and migratory phenotype with front-back polarity [1]. EMT is engaged during specific stages of normal development including embryonic implantation, gastrulation, and migration from the neural crest as well as in wound healing in mature organisms [2, 3]. In these contexts, EMT induction is necessary for proper development and homeostasis. However, EMT can also produce unfavorable outcomes in disease including fibrosis at sites of inflammation and cancer metastasis [3, 4]. These central roles for EMT in both development and disease have motivated extensive research to characterize and understand the details of this series of coordinated complex alterations within and among cells.

As illustrated in Figure 1-1, EMT induction causes shifts in cellular morphology, dissolution of cell-cell adhesions, and invasion into the basement membrane. These phenotypic outcomes are accompanied by corresponding shifts in expression of proteins that make up the cytoskeleton, compose junctional complexes, and allow degradation of and invasion into the surrounding stroma [5]. Epithelial cells are characterized by expression of junctional proteins E-cadherin and zona occludens-1 (ZO-1) as well as cytokeratin. As cell-cell adhesions dissolve during EMT, expression of these epithelial markers decreases in favor of mesenchymal cell markers, which include vimentin, fibronectin, and N-cadherin [2]. Expression of the zinc-finger binding transcription factors Snail1 or Snail2 (also known as Slug) or one of the basic helix-loop-helix factors Twist1 or ZEB-1 can induce EMT by repressing transcription of genes involved in cell-cell adhesion or promoting transcription of mesenchymal-associated genes [2]. These

transcription factors are upregulated during EMT and are often considered master-regulators of EMT because overexpression of Twist1 [6, 7] or Snail [7] alone, for example, can induce the complex array of EMT processes. In addition to shifts in protein and transcription factor expression, cells undergoing EMT display changes in extracellular matrix (ECM) protein deposition and interaction [5], alternative splicing of mRNA [8], and microRNA expression [9], further highlighting the complexity of EMT.

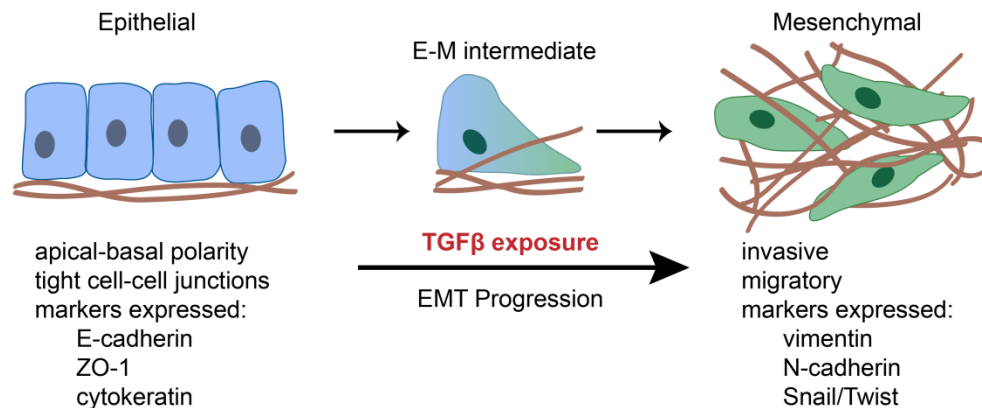


**Figure 1-1: Epithelial-mesenchymal transition.**

Fully differentiated epithelial cells have strong cell-cell contacts, apical-basal polarity, and express the proteins E-cadherin, ZO-1, and cytokeratin. In response to certain cues (e.g., TGFβ), cells lose these traits, undergoing an epithelial-mesenchymal transition (EMT). EMT promotes invasion into the surrounding stroma and expression of vimentin, N-cadherin, and transcription factors including Snail and Twist. Full EMT induction results in complete loss of E-cadherin expression and eliminates all cell-cell contacts. Partial EMT states are observed where cells express both epithelial and mesenchymal proteins.

EMT is initiated by exposure to growth factors of the transforming growth factor-beta (TGFβ) super family. Within this family Nodal, Vg1/GDF-1, and bone morphogenic proteins drive EMT during different stages of embryogenesis [2]. The title family member, TGFβ-1, is more commonly the driver of EMT in inflammation, fibrosis, and wound healing [2, 4]. TGFβ1 itself (hereafter referred to as TGFβ), however, has complex biological roles, producing outcomes of both EMT and apoptosis depending on the cell context [4, 10]. For *in vitro* cell culture models, recombinant TGFβ can be used to induce EMT in immortalized epithelial cell lines. Because of its

pro-apoptotic effects, TGF $\beta$  is often combined with other stimulatory growth factors in these culture models to enhance EMT induction [11]. For example, addition of epidermal growth factor (EGF) with TGF $\beta$  in cell culture has been shown to favor EMT induction over apoptotic outcomes [12, 13] and enhance EMT phenotype acquisition compared to TGF $\beta$  alone [12-14]. This thesis is focused specifically on identifying and quantitatively describing the molecular mechanisms controlling EMT in cancer cells in response to different growth factor treatments or at baseline. Translation of these advances into therapeutic strategies could contribute to improved patient outcomes for multiple reasons, but first a more detailed description of the existing knowledge surrounding EMT must be established to reveal gaps in our understanding.

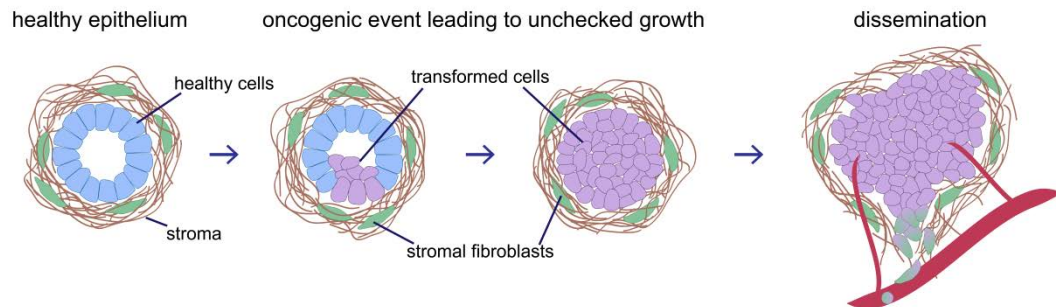


**Figure 1-2: Cancer initiation and progression in epithelial tissues.**

Healthy epithelial cells form acinar structures with a hollow lumen and are surrounded by stroma which contains other cell types including fibroblasts. A tumorigenic event (e.g., oncogenic mutation) causes cell transformation and unchecked proliferation which results in occlusion of the lumen. Further growth and progression leads to rupture of the epithelial structure and dissemination of cells into the stroma and bloodstream.

## 1-2 EMT IN CANCER

In addition to its established roles in development, EMT has been implicated in cancer progression, particularly for solid tumors originating from epithelial tissues. In healthy tissues, epithelial cells exist in highly ordered configurations, often surrounding ducts where they form acinar structures with a hollow lumen surrounded by ECM [15, 16]. As shown in Figure 1-2, unchecked cellular proliferation during cancerous progression leads to occlusion of the lumen [15, 17]. The ability of cells to disseminate from the primary tumor site into the bloodstream requires

cells to invade the surrounding ECM and has therefore been hypothesized to depend upon EMT. This dissemination is required for metastasis, which causes an estimated 90% of cancer-related deaths [18, 19], making deciphering this process of prime importance.

The overlap between traits required for metastatic dissemination and traits conferred to epithelial cells during EMT led investigators over the last 15 years to draw a causal link between these processes with support of *in vitro* and *in vivo* models [3]. There have been detractors of this model, however, due to the lack of direct evidence of cancer cells ‘in the act’ of undergoing EMT to invade the surrounding matrix in histological tumor analysis [20]. Additionally, tumor metastases often display epithelial characteristics similar to the primary tumor cells rather than a mesenchymal phenotype, which further complicated the EMT model [2]. However, in 2012 a mouse model of pancreatic ductal adenocarcinoma provided direct evidence of EMT leading to metastasis, where epithelial-derived cells genetically labeled with a fluorescent protein were seen in the stroma surrounding pancreatic ducts, though apart from their fluorescence they were indistinguishable from stromal fibroblasts [21]. Somewhat surprisingly, EMT induction, invasion, and detection of pancreatic-derived cells in the liver were seen at very early stages of progression from premalignant lesions. Disseminated cells also displayed EMT plasticity consistent with the histological similarity between primary and metastatic tumors as well as observations from previous studies that metastatic colonization requires a mesenchymal-epithelial transition (MET) [22, 23]. Although this establishes concrete evidence for EMT during cancer progression, many questions remain regarding precise cues controlling initial EMT induction and MET reversion.

Further incentive to investigate EMT in the context of carcinoma progression has emerged over the last ten years as accumulating evidence has linked mesenchymal traits to therapeutic resistance across cancer types [24]. Mesenchymal dedifferentiation has been associated with resistance to chemotherapy and targeted therapeutics in cancers including those of the lung [25-28], bladder [29], head and neck [30, 31], pancreas [32], and breast [28, 33]. EMT or EMT-like phenotype switching has also been linked to the ability of initially therapy-sensitive cells to become resistant in lung cancer [28, 34, 35] and melanoma [36]. A more detailed

mechanistic understanding of the processes controlling EMT determination in cancer could thus be leveraged to improve patient response and increase efficacy of targeted drugs and chemotherapeutics.

Another framework for understanding certain features of tumor initiation and progression that has emerged in parallel with EMT investigations is the observation of cancer stem cells (CSCs). CSCs can be defined functionally by proliferative and self-renewal capabilities and the ability of a single cell to seed new tumors that recapitulate the cellular heterogeneity of the original tumor. CSCs have been characterized in acute myeloid leukemia [37] as well as in solid tumors including breast and colon carcinomas [38, 39]. The undifferentiated nature of stem cells and the requirement that disseminated cancer cells (the product of EMT) must be able to form metastatic lesions from a single cell, have linked the concepts of CSCs to EMT [24]. Indeed there has been evidence that after undergoing EMT, cells display certain properties of CSCs, such as tumor-initiating capacity and surface expression of stem cell markers [40]. However, as the CSC concept has matured in the literature, additional properties have been attributed to CSCs that are sometimes in opposition to each other, for example both dormancy and proliferation [41, 42]. Additionally, the inability to purify a stem cell population displaying all attributed CSC surface markers and phenotypic traits has motivated a shift toward characterizing stemness as a property of certain cancer cells rather than focusing on the absolute definition of a CSC population [41]. Thus, rather than defining CSC populations, examining certain stem cell characteristics and attributes will prove useful references to characterize EMT-associated transformations in this work and elsewhere.

### **1-3 CELL SIGNALING AND EMT**

Cellular decision making and acquisition of phenotypes in response to extracellular stimuli, such as EMT in response to TGF $\beta$  or death in response to therapy, is controlled by networks of intracellular signaling pathways. Transmission of information through such signaling networks often originates from transmembrane receptor proteins including receptor tyrosine

kinases (RTKs) and receptor serine/threonine kinases. Receptor extracellular domain binding to soluble or immobilized ligand can lead to receptor dimerization and activation of the intracellular kinase domain [43]. In the case of RTKs, the induced catalytic activity of the kinase domain leads to covalent attachment of phosphates onto tyrosine residues on the receptor itself and/or downstream substrates. Phosphorylated tyrosine residues serve as binding sites for downstream adapters containing SRC-homology-2 (SH2) or phosphotyrosine binding (PTB) domains [44]. Recruitment of such adapter proteins leads to further protein modifications and protein interactions resulting in the activation of downstream signaling pathways such as the mitogen activated protein kinase (MAPK), signal transducer and activator of transcription (STAT), and phosphoinositide 3-kinase (PI3K)/AKT pathways. Signals originating at the plasma membrane ultimately impact cell behavior through transcriptional effects mediated in the cell nucleus. Systematic evaluation of the precise signaling pathways activated in response to cellular stimuli and resulting phenotypic effects can thus reveal mechanisms that predict or control cellular outcomes.

As implied by the complex nature of the EMT program, the signaling networks engaged during EMT downstream of TGF $\beta$ , for example, are extensive and complex [45, 46]. Dimers of TGF $\beta$  bind, and thus bring together, two pairs of receptor serine/threonine kinases [10]. Each pair contains one type I and one type II receptor, and upon binding to TGF $\beta$ , the type II receptor phosphorylates the type I receptor leading to recruitment and phosphorylation of SMAD transcription factors [4]. Due to this direct activation by TGF $\beta$  receptors, the SMAD signaling pathways are often considered 'canonical' TGF $\beta$  signaling pathways. There are, however, many other pathways activated downstream of TGF $\beta$  including the extracellular signal-regulated kinase (ERK), c-Jun N-terminal kinase (JNK), and p38 MAPK pathways [47]. Though the type I and II TGF $\beta$  receptors are well-characterized serine/threonine kinases, the type II receptor displays a low level of autophosphorylation on tyrosine residues [48] and can be tyrosine phosphorylated by the cytosolic kinase SRC [49]. This tyrosine phosphorylation can lead to recruitment of adapter proteins in the MAPK cascades, specifically SHC, GRB2, and SOS [50, 51]. The JNK and p38

pathways are also activated downstream of TRAF6 recruitment to TGF $\beta$  receptor complexes [47]. Additionally, PI3K/AKT pathway activation has been reported downstream of TGF $\beta$  in multiple cell types through less fully described mechanisms [46]. Of these non-SMAD pathways downstream of TGF $\beta$ , there is evidence that ERK activation in particular is necessary for EMT induction [14, 45, 52]. In certain cell types, other growth factors including EGF [53], fibroblast growth factor (FGF) [54], and hepatocyte growth factor (HGF) [54] can induce EMT. The EGF receptor (EGFR) can also be activated in a SRC-dependent manner by TGF $\beta$  receptors, promoting ERK activation [55, 56]. EGFR activation through this intracellular mechanism or by EGF treatment often enhances EMT outcomes *in vitro* compared to TGF $\beta$  treatment alone [12-14, 57].

In addition to displaying differential activation of signaling pathways during EMT induction, cells that have undergone EMT through transcription factor expression, growth factor treatment, or other mechanisms display altered signaling networks. For example, inducible expression of Twist or Snail in the non-small cell lung cancer (NSCLC) cell line H358 reduced basal AKT phosphorylation through downregulation of the EGFR-family member ERBB3 [58]. Similarly, EMT driven by expression of Twist, Snail, or Slug in mammary epithelial cells was accompanied by decreased EGFR and increased platelet-derived growth factor receptor (PDGFR) expression [7]. Additional models of mesenchymal dedifferentiation have also found upregulation of PDGFR [26, 59] as well as other receptors including c-MET (the receptor for HGF) [59], lysophosphatic acid receptor [59], FGF receptor (FGFR) [26], and AXL [28].

#### **1-4 EPIDERMAL GROWTH FACTOR RECEPTOR IN CANCER**

Epidermal growth factor receptor (EGFR) kinases are activated upon ligand binding to the EGFR extracellular domain, which promotes receptor dimerization and trans-autophosphorylation on multiple tyrosine residues in the receptor C-terminal tail (Figure 1-3, reviewed in [43, 60, 61]). Phosphorylated EGFR dimers then recruit downstream signaling adapters through phosphotyrosine-SH2 and -PTB domain interactions. These interactions

ultimately lead to activation of pathways that promote cell survival, proliferation, and growth including AKT, ERK, and STAT3.

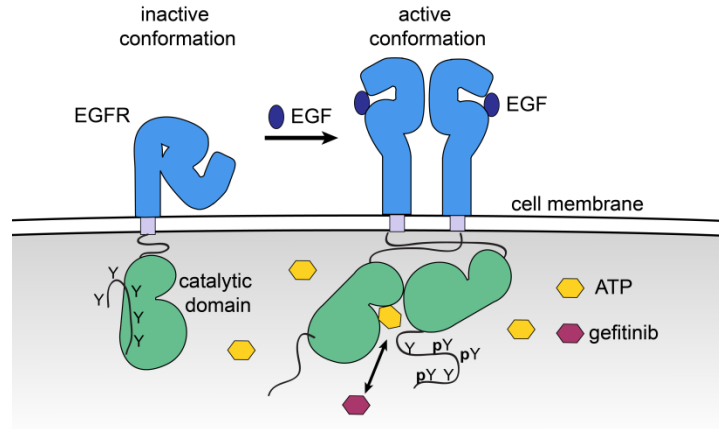


**Figure 1-3: Epidermal growth factor receptor activation.**

Epidermal growth factor receptor (EGFR) activation is initiated by binding of EGF to the extracellular domain of the receptor, inducing receptor dimerization. Asymmetrical interaction of intracellular kinase domains activates their catalytic activity, leading to ATP-dependent phosphorylation (p) of tyrosine residues (Y) on the C-terminal tail in trans. The small molecule gefitinib is an ATP analog, which inhibits this receptor autophosphorylation mechanism.

EGFR overexpression occurs with high frequency in many cancer types including 70-80% of NSCLC [62] and ~50% of glioblastoma multiforme (GBM) [63, 64] tumors. Additionally, EGFR-activating mutations are detected at 10-20% and 25-30% overall in NSCLC and GBM, respectively. Due to these high rates of overexpression and mutation, a number of small molecule inhibitors (e.g., gefitinib) and monoclonal antibodies (e.g., cetuximab) targeting EGFR have been developed and approved for various cancers [65]. Despite their ability to specifically inhibit EGFR signaling these drugs generally confer little clinical advantage, with rare notable exceptions. For example, in NSCLC the subset of tumors expressing kinase-activated mutants of EGFR display significant initial response to small molecule EGFR inhibitors [66-68]. However, though initial response is often dramatic, these patients almost invariably develop resistance to EGFR inhibition, often through acquisition of the EGFR 'gatekeeper' mutation (T790M) [69, 70]. Up-regulation of c-MET [71] and *ERK2* amplification [72] are other mechanisms leading to adaptive

resistance to EGFR inhibition. Interestingly, in addition to EGFR inhibitor response, expression of kinase activated EGFR mutants is correlated with enhanced epithelial characteristics compared to wild type expressing cells [73], and EMT phenotype acquisition is a mechanism of acquired resistance in these cells [35].

The NSCLC-associated EGFR mutants that confer inhibitor sensitivity display elevated kinase activity and impaired endocytosis compared to wild type EGFR, indicating constitutive receptor-mediated signaling from the plasma membrane. Corresponding phosphorylation of downstream signaling components such as AKT and STAT3/5 is elevated in cells harboring these *EGFR* mutations [67]. Interestingly however, the same EGFR mutants also lead to suppressed ERK phosphorylation relative to wild type EGFR, which is linked to the enhanced cellular response to EGFR inhibition [74]. Recent work identified a mechanism for this ERK suppression through functional impairment of the proto-oncogene SH2-domain containing phosphatase-2 (SHP2) [75], a cytosolic protein tyrosine phosphatase (PTP), which is recruited to receptor-bound signaling complexes to promote full ERK activation (Figure 1-4). In the context of wild type receptor activation, ligand-bound EGFR dimers trans-autophosphorylate, leading to recruitment of downstream signaling intermediates growth factor receptor-bound protein 2 (GRB2) and GRB2-associated binding protein 1 (GAB1) [76]. GAB1 is then phosphorylated on multiple tyrosine residues which are recognized by SH2 domains on SHP2, leading to relief of intramolecular SHP2 inhibition and access of the phosphatase domain to substrates (Figure 1-4, refs [77-79]). In the context of kinase-activated EGFR mutants, SHP2 is constitutively associated with GAB1 and endocytosis-impaired EGFR in a way that suppresses its ability to promote ERK activation [75]. As implied by its designation as a proto-oncogene, SHP2-activating mutations have been causally linked to multiple cancers including juvenile myelomonocytic leukemia and acute myelogenous leukemia [80, 81], and SHP2 activity through regulating the ERK pathway has been shown to promote tumorigenesis in models of breast cancer and GBM [82, 83].

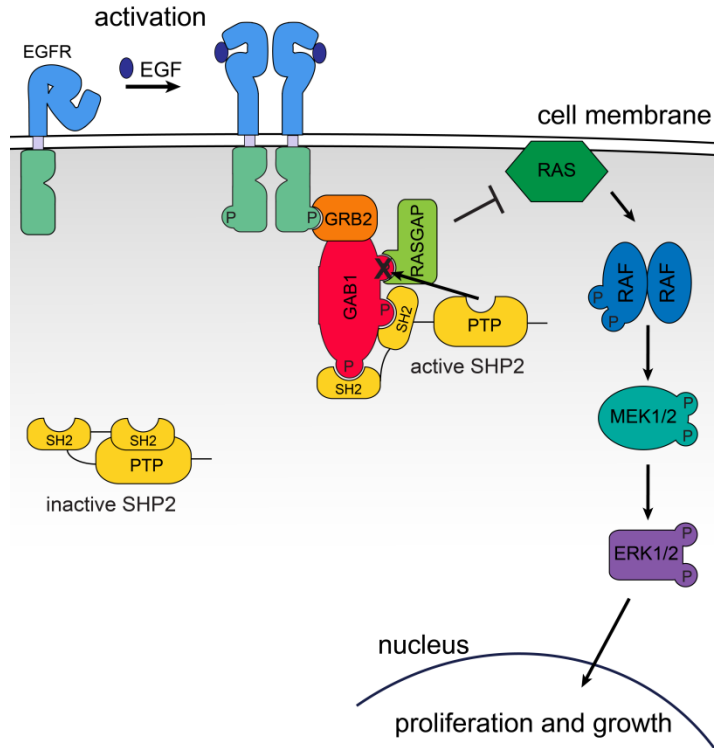


**Figure 1-4: ERK pathway signaling downstream of EGFR activation.**

In cells at rest, EGFR and SHP2 exist in inactive conformations stabilized through intramolecular interactions. EGF-induced EGFR kinase activation and phosphorylation (P) leads to recruitment of the signaling adapters GRB2 and GAB1. Phosphorylation of GAB1 on multiple tyrosine residues recruits binding of SHP2's SH2 domains, which activates SHP2 by relieving an inhibitory interaction of the N-terminal SH2 and PTP domains. SHP2 phosphatase activity promotes ERK pathway activation through multiple routes including dephosphorylation of a binding site on GAB1 for the RAS-inhibitory molecule RASGAP.

### 1-5 ERK PATHWAY PERTURBATIONS IN CANCER AND EMT

ERK1 and ERK2 are the terminal MAPK proteins in a cascade that originates at the plasma membrane with the small GTPase RAS. RAS is activated downstream of many RTKs, as shown for EGFR in Figure 1-4. RAS promotes dimerization and activation of the RAF MAPK-kinase-kinases, which in turn phosphorylate the MAPK-kinases MEK1/2, which phosphorylate ERK1/2. The ERK pathway is well established as promoting cellular survival and proliferation, and mutations within the RAS-RAF-MEK-ERK signaling cascade occur with high frequency in many cancers [84, 85]. The most common mutations in this cascade (and of all oncogenes) are found in the *RAS* family genes – *KRAS* (which represents a large majority of *RAS* mutations),

*NRAS*, and *HRAS* – with high overall *RAS* mutation incidence in pancreatic (~95%), colorectal (~50%), and lung (~30%) adenocarcinomas and notable mutational populations in many other malignancies, including uterine, thyroid, gastric, and cervical carcinomas [86]. *BRAF* mutations also occur with high frequency in certain malignancies including melanoma (~70%), papillary thyroid cancer (~50%), and colon cancer (~10%) [86]. Since the discovery of *RAS* mutations in human cancer in 1982 [87, 88], ongoing research efforts have been devoted to characterizing and targeting *RAS* and *RAF* proteins, but few advances have been made that confer significant clinical benefit. Particular challenges have arisen due to the complex function and difficult-to-target nature of *RAS* signaling [86], as well as the importance of negative feedback loops within the cascade particularly downstream of mutant *BRAF* [89, 90]. Significant efforts have thus focused on targeting proteins downstream of *RAS* such as *MEK* [84, 85]. Trametinib recently became the first FDA-approved *MEK* inhibitor after improved overall survival was demonstrated in metastatic melanoma patients with *BRAF* mutation [91, 92].

This same signaling cascade has been linked to EMT with several studies demonstrating a requirement for *ERK1/2* pathway activity for *TGFβ*-induced EMT in multiple non-transformed cellular backgrounds [14, 45, 52]. The activity of *ERK2* specifically induces EMT in non-transformed mammary epithelial cells [93] and has been implicated as the mediator of oncogenic *KRAS*-induced invasion in pancreatic cancer cells [94]. Furthermore, phosphatases within the *ERK* cascade including *SHP2*, *PTPN14*, and *MKP3* have been implicated in EMT induction [95-97]. In some cell contexts *TGFβ* alone is able to induce *ERK* activation and subsequent EMT [51, 56, 98], while in others *EGF* addition is needed to activate the *ERK* pathway and promote *TGFβ*-driven EMT [14, 57]. The molecular interactions responsible for these effects have not been described, but would provide important insight into routes for controlling EMT.

## **1-6 THESIS SUMMARY**

Clinical intervention strategies to reduce or eliminate the invasive capacity of tumor cells and enhance therapy response have the potential to substantially impact cancer patient

prognosis. With these aims in mind, this thesis focuses on approaches to understand and control EMT induction in cancer cells. In Chapter 2, we studied how suppressing ERK activation using a MEK inhibitor affected EMT induction and baseline mesenchymal characteristics in NSCLC cells. We found that MEK inhibition impaired EMT in response to the combination of TGF $\beta$  and EGF in lung cancer cells. MEK inhibition in the absence of EMT-inducing growth factors also promoted acquisition of epithelial characteristics in cells with either wild type or mutant EGFR expression on a timescale (multiple days) which was much longer than that for ERK pathway suppression (several minutes). Further investigation revealed that prolonged MEK inhibition continued to promote epithelial marker expression while significantly enhancing cell death in response to the EGFR inhibitor gefitinib. This strategy of staggered exposure to MEK- and EGFR-targeted inhibitors led to enhanced cell death response in multiple cell lines with *de novo* or acquired gefitinib resistance, suggesting potential efficacy in different clinical populations of lung carcinoma. The concurrent acquisition of epithelial traits from MEK inhibition and enhanced sensitivity also provided basic validation of the concept that targeting EMT could augment therapeutic response.

The striking effect of MEK inhibition on EMT induction motivated further investigation into upstream components in the ERK pathway. Given previous knowledge about its importance in ERK pathway activation and determining gefitinib response, the role of the cytosolic phosphatase SHP2 in EMT induction was explored in Chapter 3. Specifically, we investigated how the presence and activation of SHP2 contributed to the ability of EGF to enhance EMT induction by TGF $\beta$ . EGF has been shown to augment TGF $\beta$ -mediated EMT in multiple cell settings, which we observed and quantified in lung and pancreatic cancer cell lines. In these cells, EGF significantly enhanced TGF $\beta$ -mediated downregulation of E-cadherin, upregulation of vimentin, and increased migration. We found that basal SHP2 activity is required for EMT in response to TGF $\beta$  alone and that the augmented EMT from EGF addition resulted from induced SHP2 activity through SHP2 SH2-domain binding to tyrosine phosphorylated GAB1. These results suggested that SHP2 is a

key effector in EMT induction whose degree of activation is associated with the extent of EMT observed in response to various stimuli.

In Chapter 4, motivated by the ability to reverse EMT with chronic MEK inhibition, we took a broader view of EMT-relevant signaling networks to identify other targets for inhibiting or reversing mesenchymal dedifferentiation in pancreatic cancer cells. We combined high-throughput temporal protein phosphorylation measurements and quantitative EMT phenotype measurements in response to EMT-inducing growth factor treatments in a partial least squares regression (PLSR) computational model to identify the protein phosphorylation events that are most predictive of EMT induction. We found that different combinations of EGF, HGF, and TGF $\beta$  produced quantitatively different EMT states, which was captured in the reduced dimension principal component space from the PLSR model. Additionally, we specifically identified early and late phosphorylation events that are most predictive of EMT induction. This model will motivate further investigation into additional targets for reversing mesenchymal phenotypes to produce clinically impactful outcomes similar to those observed in Chapters 2 and 3 for ERK pathway inhibition.

In Chapter 5 we discussed the implications of our findings, which have enhanced our understanding of EMT regulation and offered several approaches to improve clinical outcomes through impairing mesenchymal phenotypes. Implementing alternative scheduling of MEK and EGFR inhibitors was proposed as a potential route for improving patient responses, though *in vivo* models will be important tools to evaluate the potential of this approach moving forward. Our findings have also provided further motivation to develop strategies and therapeutic compounds to specifically target SHP2 activity in carcinoma. Finally, we have identified several additional potential targets for inhibiting EMT that should be evaluated for their quantitative impact on the dynamics and strength of EMT induction.

# CHAPTER 2: ERK1/2 Inhibition Prevents Epithelial-Mesenchymal Transition and Promotes Sensitivity to EGFR Inhibition in Lung Cancer Cells<sup>1</sup>

## 2-1 ABSTRACT

Understanding and overcoming the cellular mechanisms underlying *de novo* and acquired resistance to chemotherapy and targeted inhibitors remain challenges in treating many cancers, including non-small cell lung cancer (NSCLC). A number of studies have linked the mesenchymal cellular phenotype and epithelial-mesenchymal transition (EMT) with resistance to multiple classes of cancer therapeutics, which begs the question of whether inhibiting or reversing EMT could be an attractive therapeutic goal. Here, we demonstrate that ERK signaling plays a key role in determining mesenchymal cellular characteristics in NSCLC cells and that this connection can be leveraged to augment cellular response to inhibition of the epidermal growth factor receptor (EGFR). In NSCLC cell lines, MEK inhibition pushed cells toward a more epithelial phenotype and prevented EMT induction by exogenous transforming growth factor beta. Moreover, in cell lines with *de novo* or acquired resistance to the EGFR inhibitor gefitinib, chronic MEK inhibition synergistically enhanced cellular sensitivity to gefitinib and slowed cell migration. These effects only occurred, however, when MEK was inhibited for enough time to observe changes in epithelial and mesenchymal marker expression. Changes in these same phenotypes and associated changes in epithelial/mesenchymal markers also occurred as a result of KRAS mutant expression in a MEK-dependent manner. These results suggest a potential clinical strategy for scheduling targeted inhibitors of MEK or ERK and EGFR in order to induce mesenchymal-epithelial transition as a way overcome naïve or acquired resistance to EGFR-targeted therapy.

---

<sup>1</sup> A version of Chapter 2 was previously published as: Buonato JM and Lazzara MJ, ERK1/2 blockade prevents epithelial-mesenchymal transition in lung cancer cells and promotes their sensitivity to EGFR inhibition, *Cancer Research* 74: 309-319, 2014.

## 2-2 INTRODUCTION

Epidermal growth factor receptor (EGFR) over-expression and -activation are hallmarks of many cancers, including non-small cell lung cancer (NSCLC). Consequently, a number of inhibitors and monoclonal antibodies targeting EGFR have been developed and approved for various cancers. Unfortunately, these drugs are generally ineffective. In NSCLC, response to EGFR inhibitors is limited mainly to the rare patients (~10%) whose tumors harbor somatic, kinase-activated mutants of EGFR [66, 67]. Even these patients almost invariably develop resistance to EGFR inhibitors, often through the EGFR “gatekeeper” mutation (T790M) [69, 70] or through up-regulation of c-MET or other receptors [71]. Combination therapies present a possible strategy to overcome resistance. In NSCLC, recent investigations suggest promise for combining EGFR inhibitors with chemoradiation [99], the multi-kinase inhibitor sorafenib [100], or a c-MET inhibitor [101]. Scheduling multiple drugs such that initial therapy reprograms cells to respond to another drug is another possible strategy. In one recent example, triple-negative breast cancer cells and NSCLC cells were dramatically sensitized to doxorubicin by pre-treatment with the EGFR inhibitor erlotinib [102].

Epithelial-mesenchymal transition (EMT) is another pathway through which cancers of epithelial origin become chemoresistant. EMT is a developmental process whereby epithelial cells lose cell-cell adhesions to become more motile and invasive. Cells undergoing EMT lose expression of epithelial markers (e.g., E-cadherin) and gain expression of mesenchymal markers (e.g., vimentin and fibronectin) through differential expression and activation of transcription factors including Twist, ZEB1, and Snail [2, 103]. EMT is frequently hijacked in metastatic progression, and mesenchymal dedifferentiation has been associated with resistance to EGFR inhibitors, chemotherapy, and other targeted drugs in cancers of the lung [25-27], bladder [29], head and neck [30, 31], pancreas [32], and breast [33]. In NSCLC, *in vitro* acquired resistance to the EGFR inhibitor erlotinib can result from selection of a mesenchymal sub-population [35], and restoring E-cadherin expression in mesenchymal-like NSCLC cells potentiates sensitivity to EGFR inhibitors [104]. Additionally, growing evidence for AXL-mediated EGFR inhibitor

resistance has been tied to EMT [105]. Thus, developing treatments that elicit a mesenchymal-epithelial transition (MET) could be a useful approach for expanding the efficacy of EGFR inhibitors.

Several studies have demonstrated a requirement for extracellular signal-regulated kinase-1/2 (ERK1/2) pathway activity in EMT induced by transforming growth factor beta (TGF $\beta$ ) in non-transformed cells [14, 45, 52]. ERK2, but not ERK1, activity also induces EMT in non-transformed mammary epithelial cells [93] and has been implicated as mediating oncogenic KRAS-induced invasion in pancreatic cancer cells [94]. Interestingly, *ERK2* amplification was recently identified as a mechanism leading to acquired resistance to EGFR inhibitors in NSCLC [72].

Here, we sought to determine ERK's role in governing EMT in NSCLC. In a panel of NSCLC cell lines, MEK inhibitors prevented TGF $\beta$ -induced EMT and promoted epithelial cellular characteristics when administered alone. Conversely, augmented ERK activation, through KRAS<sup>12V</sup> expression or *ERK2* amplification, promoted mesenchymal characteristics. Furthermore, chronic MEK inhibition for times long enough to observe changes in epithelial and mesenchymal marker expression augmented cellular sensitivity to the EGFR inhibitor gefitinib in cell lines with *de novo* or acquired resistance to EGFR inhibitors. These changes were reversible and accompanied by shifts in expression of stem cell-like markers CD24 and CD44. These results suggest the potential utility of drug scheduling strategies first targeting ERK to promote epithelial characteristics prior to targeting EGFR or other oncogenic signaling nodes.

## 2-3 MATERIALS AND METHODS

### *Cell culture*

H1666 cells were obtained from the American Type Culture Collection. H322, gefitinib-resistant PC9 (clone GR4, referred to as GR henceforth), and WZ4002-resistant PC9 cells (clone WZR12, referred to as WZR henceforth) were provided by Dr. Pasi Jänne (Dana-Farber Cancer Institute). Parental PC9 cells were provided by Dr. Douglas Lauffenburger (MIT). Since PC9 cells came from different labs, we confirmed similar expression of important proteins and response to gefitinib for parental stocks from both labs. H358 cells were provided by Dr. Russ Carstens (University of Pennsylvania). PC9 (all variants), H322, and H358 cells were maintained in RPMI 1640 supplemented with 10% FBS, 100 units/mL penicillin, 100 µg/mL streptomycin, and 1 mM L-glutamine. H1666 cells were maintained in ACL4 [74]. Cell culture reagents were from Life Technologies. Cell lines were validated for anticipated responsiveness to gefitinib and were cultured for less than two months from low-passage frozen stocks.

### *Chronic MEK inhibition in H1666, PC9GR, and PC9 WZR*

H1666, PC9 GR, and PC9 WZR cells were maintained in 10 µM, 5 µM, and 20 µM U0126, respectively, with controls maintained in DMSO. Responses to 1 hr or 2 day treatments with a range of U0126 concentrations were evaluated for each cell line to identify U0126 concentrations yielding significantly inhibited ERK phosphorylation (Fig. 2-S1) but minimal background cell death. For culture experiments, media was changed every two days or cells were passed as necessary. When passing, cells were sub-cultured into inhibitor-free media to promote adhesion. U0126 or DMSO was replaced the following day. When appropriate, cells were lysed or gefitinib was added 24 hrs later. Time points in figures with chronic MEK inhibition reflect the total time of U0126 exposure before lysing or gefitinib addition. To probe the reversibility of U0126 effects, cells were split from U0126 cultures after 7 days and maintained in DMSO thereafter. All time courses were performed from freshly thawed cells multiple times to demonstrate reproducibility. Naïve cell death response to U0126 and gefitinib was quantified at

multiple points during time courses, including the beginning and end, to verify that baseline response was not changing.

The MEK inhibitor CI-1040 (LC Labs) stock was prepared in DMSO. All applicable experiments used 3  $\mu$ M CI-1040. Lysate preparation, wound healing measurements, and experiments testing gefitinib sensitivity from chronic MEK inhibition with CI-1040 were performed analogously to experiments described using U0126.

#### *Chronic MEK inhibition in H322, H358, and SKBR3*

H322 cells were cultured in 40  $\mu$ M U0126 and H358 and SKBR3 cells were cultured in 10  $\mu$ M U0126 or DMSO control, analogously to above. After 5 days of U0126 culture, cells were lysed or treated with 5  $\mu$ M gefitinib. Cells treated for 48 hrs were collected and co-stained with TO-PRO3 and Annexin-V FITC conjugate (Southern Biotech) according to manufacturer instructions. Cells were analyzed within 1 hr on a BD Biosciences FACSCalibur flow cytometer. Data for percent apoptotic cells reflects the sum of all cells staining positively for Annexin-V or TO-PRO3.

#### *Wound healing assay.*

Confluent cell monolayers in 6-well plates were scratched with a pipet tip, and media was immediately changed. Phase contrast images were taken with a Zeiss Axiovert 40 CFL microscope (10X objective) every 1-3 hrs for  $\leq$ 11 hrs. Scratch areas were quantified using ImageJ, and closure rates were calculated from linear fits of areas versus time and reported as percent of total image area closed per hr normalized to the conditions indicated in figures. Where inhibitors were used, cells were plated at sub-confluence and treated at appropriate times with media containing inhibitor. Media and inhibitor were changed every two days until wells reached confluence.

#### *Transwell migration assay*

Untreated PC9 GR and WZR cells or H1666 cells treated with U0126 or DMSO for 4 days were trypsinized and resuspended in media containing 0.1% FBS and U0126 or DMSO for

H1666. 20,000 untreated or DMSO-treated cells or 50,000 U0126-treated cells (adjusted for U0126-mediated changes in adhesion) were added to 8  $\mu$ m Transwell membranes (Corning), which were placed in 24-well plates well containing complete media with DMSO or U0126. After 20 hrs, cells on the upper surfaces were removed with a cotton swab. Cells on the lower surfaces were fixed in 4% paraformaldehyde for 30 min and washed with PBS, and nuclei were stained with Hoescht-33342. Membranes were mounted and imaged (10X objective), and nuclei were counted using ImageJ. Counts were normalized to the number of adhered cells from parallel wells for each condition.

#### *Flow cytometry*

For cell death assays, cells were plated in 6-well dishes from their various culture conditions and treated with inhibitors. Floating and adherent cells were collected 48 hrs later, resuspended in PBS containing TO-PRO3 (Life Technologies), and analyzed within 1 hr. For CD24 and CD44 measurements, cells were collected as above, washed with 0.1% BSA in PBS (PBSA), blocked for 10 min in PBSA, and incubated for 1 hr with 3  $\mu$ L each of FITC-conjugated anti-human CD44 antibody (BD Pharmingen, #555478) and Alexa-647 conjugated anti-human CD24 antibody (BioLegend, #311109) in 200  $\mu$ L. Labeled cells were washed again and resuspended in PBS. Cytometry was performed on a BD Biosciences FACSCalibur cytometer, and data were analyzed using FlowJo.

#### *Western blotting*

Cell lysates were prepared using a standard cell extraction buffer (Invitrogen) supplemented with 1 mM PMSF, additional protease inhibitors (Sigma), and phosphatase inhibitors (Sigma). Proteins were resolved by SDS-PAGE and transferred to nitrocellulose membranes, which were blocked in Odyssey Blocking Buffer (LI-COR) and stripped with 0.2 M NaOH as needed. Blots were scanned using a LI-COR Odyssey Infrared Imaging System.

### *Antibodies and other reagents*

pERK T202/Y204 (#4377) and ERK (#4695) antibodies were from Cell Signaling Technology. E-cadherin (sc-8426), vimentin (sc-373717), fibronectin (sc-8422), and GAPDH (sc-32233) antibodies were from Santa Cruz Biotechnology. Stocks of U0126 and gefitinib (LC Labs) were prepared in DMSO. Recombinant human epidermal growth factor (EGF) and TGF $\beta$  were from Peprotech. Infrared dye- and Alexa Fluor®-conjugated secondary antibodies were from Rockland Immunochemicals and Invitrogen, respectively.

### *Immunofluorescence*

Cells were plated on glass coverslips and maintained in 6-well dishes during ligand and/or inhibitor treatments. Cells were then fixed in 4% paraformaldehyde in PBS for 20 min, blocked, stained, and imaged as described previously [106]. E-cadherin was stained using 2  $\mu$ g/mL antibody. Alexa Fluor® 488-conjugated phalloidin at 6.6 nM (Invitrogen; provided by Dr. Deepak Nihilani, University of Pennsylvania) was added to the secondary antibody staining solution. All samples within an experiment used identical image acquisition settings.

### *KRAS<sup>12V</sup> expression*

The pBabe-puro-KRAS-12V expression construct was acquired from Addgene (Dr. Channing Der, University of North Carolina). Retrovirus was produced by calcium phosphate-mediated transfection of amphotropic Phoenix cells (Dr. Gary Nolan, Stanford University). Virus was harvested 24, 30, and 48 hrs post-transfection and used to infect target cells, which were selected in puromycin.

### *EGF-mediated EGFR internalization assay*

PC9 GR and WZR cells were treated for 24 hrs with 80  $\mu$ M Dynasore (Calbiochem), a dynamin inhibitor, or DMSO (control). EGF-mediated EGFR endocytosis rate constants ( $k_e$ ) were then measured using 10 ng/mL <sup>125</sup>I-EGF with corrections for non-specific binding and spill over, as previously described [107, 108].

## 2-4 RESULTS

### *NSCLC cell lines undergo MEK-dependent TGF $\beta$ -induced EMT*

H1666, H322, and H358 cells were cultured in complete media with TGF $\beta$  and EGF with or without U0126 for four days, with a media change after two days (Fig. 2-1). In response to TGF $\beta$  and EGF, E-cadherin expression decreased and vimentin expression increased in all three cell lines, and fibronectin expression increased in H1666 and H358 cells (Fig. 2-1A). U0126 co-treatment inhibited changes in E-cadherin and vimentin, but did not prevent fibronectin induction. The same trends were found in H1666 cells using the alternative MEK inhibitor CI-1040 (Fig. 2-S2). The conditions used in Fig. 2-1A were explored in H1666 cells by immunofluorescence (Fig. 2-1B). Treatment with TGF $\beta$  and EGF promoted an elongated cellular morphology, the appearance of F-actin fibers, and decreased E-cadherin intensity. U0126 addition prevented E-cadherin loss and promoted E-cadherin localization at cell-cell junctions.

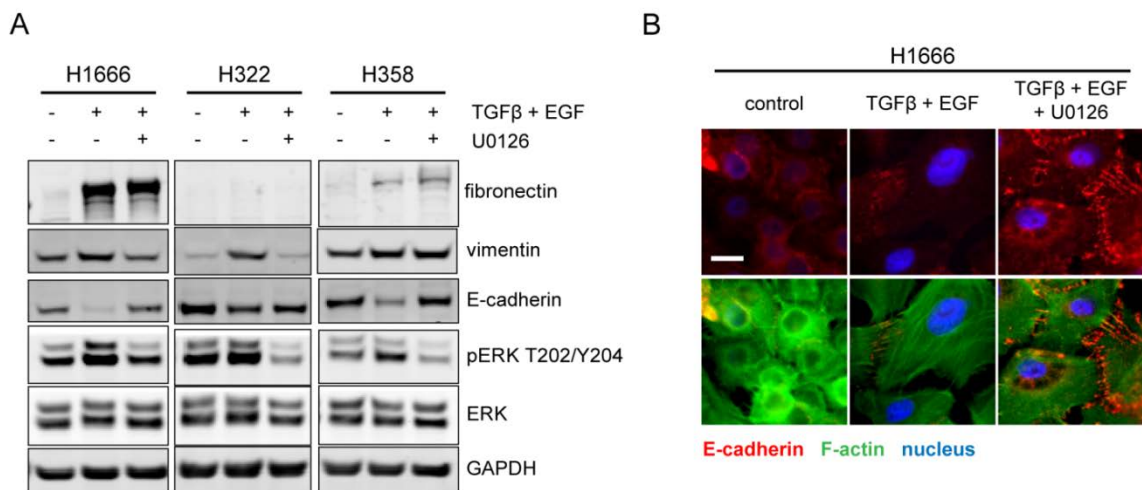


**Figure 2-1: MEK inhibition prevents TGF $\beta$ -induced EMT in NSCLC cell lines.**

(A) H1666, H322, and H358 cells were treated for four days with 10 ng/mL TGF $\beta$  + 50 ng/mL EGF, TGF $\beta$  + EGF and 20  $\mu$ M U0126, or DMSO (control). Whole cell lysates were analyzed by western blot with antibodies against indicated proteins. Images are representative of at least three independent experiments. (B) H1666 cells on glass coverslips were treated as in (A), fixed, and stained for E-cadherin, F-actin, and DNA. Images are representative of three replicates from each of two independent experiments. Scale bar = 20  $\mu$ m.

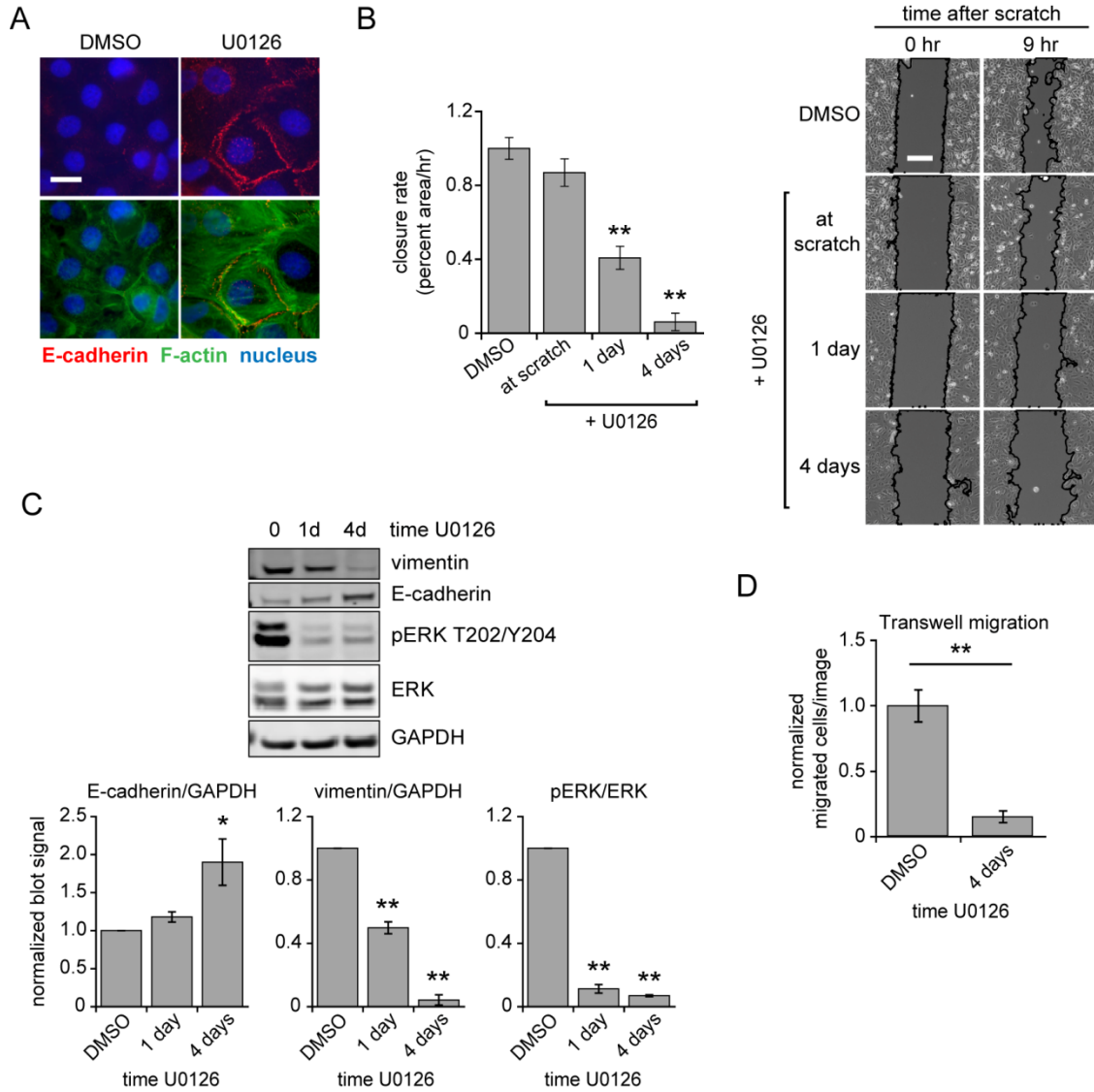


**Figure 2-2: MEK inhibition promotes epithelial characteristics in H1666 cells.**

(A) H1666 cells plated on glass coverslips were treated with 20  $\mu$ M U0126 for 4 days, fixed, and stained for E-cadherin, F-actin, and DNA. Images are representative of three replicates from each of two independent experiments. Scale bar = 20  $\mu$ m. (B) Wound closure rates were measured for H1666 cells treated with DMSO (control) or 20  $\mu$ M U0126 at the time of scratch or for 1 or 4 days prior to scratch. Rates normalized to the control condition for triplicate wells from two different platings ( $n = 6$ ) are reported as averages  $\pm$  s.e.m. Representative phase contrast images are shown, with tracings added to identify open scratch areas. Scale bar = 200  $\mu$ m. (C) Lysates prepared in parallel to (B) were analyzed by western blot using antibodies against indicated proteins. Signals normalized to respective DMSO controls are reported as averages  $\pm$  s.e.m. ( $n = 3$ ). (D) Transwell migration experiments were performed for H1666 cells pre-treated with DMSO or 20  $\mu$ M U0126 for 4 days. Counts normalized to DMSO control for duplicate wells from three separate experiments ( $n = 6$ ) are reported as averages  $\pm$  s.e.m. \* and \*\* indicate  $p < 0.05$  and  $0.005$ , respectively.

### *MEK inhibition promotes epithelial phenotypes in NSCLC cells*

We next explored the ability of MEK inhibition alone to promote epithelial characteristics in H1666 cells. As seen when combined with TGF $\beta$  and EGF, U0126 promoted E-cadherin localization at cell-cell junctions (Fig. 2-2A). MEK inhibition also antagonized H1666 wound healing in a treatment time-dependent manner (Fig. 2-2B, 2-S3). While U0126 inhibited ERK phosphorylation within 1 hr of addition (Fig. 2-S1), U0126 treatment for the duration of the scratch assay (10 hrs) did not significantly affect wound closure rate (“at scratch” condition versus DMSO in Fig. 2-2B). Wound closure rate decreased significantly with 1 day of U0126 pre-treatment and was nearly zero with four days of pre-treatment. Western blots of lysates created in parallel revealed that E-cadherin expression increased and vimentin expression decreased with increasing U0126 exposure time, consistent with the time-dependent changes in wound closure rate (Fig. 2-2C, Fig. 2-S3). U0126-mediated changes in wound healing migration were further confirmed by assessing migration across Transwell inserts (Fig. 2-2D).

### *Chronic MEK inhibition sensitizes NSCLC cells to EGFR inhibition on a time scale consistent with changes in epithelial and mesenchymal markers*

Since epithelial characteristics have been connected to EGFR dependence in NSCLC [27, 104], we explored the ability of MEK inhibition to increase sensitivity to gefitinib (Fig. 2-3). As described in *Materials and Methods Section 2-3*, H1666 cells were maintained in 10  $\mu$ M U0126 or DMSO (control) for up to 3 weeks. Throughout the 3-week period, cells were evaluated for death response to gefitinib. Without U0126 pre-treatment, 2 days of EGFR and MEK co-inhibition led to only 7% cell death in H1666, but this more than doubled with 3 days of U0126 pre-treatment (Fig. 2-3A, 2-S4A). This enhancement further increased with additional U0126 pre-treatment time, reaching a maximum at 11 days. Increased cellular sensitivity to gefitinib was accompanied by increased E-cadherin expression (Fig. 2-3B, 2-S4B). Beyond 11 days, the synergistic effect began to decrease, which was accompanied by increased fibronectin expression and decreased E-cadherin expression. Similar effects were observed in H1666 cells using CI-1040 (Fig. 2-S4C).

H358 and H322 cells and the breast cancer cell line SKBR3 were also evaluated for response to gefitinib following chronic MEK inhibition (Fig. 2-S5). H358 cells harbor a *KRAS* mutation and are ERK-addicted [109]. Not surprisingly therefore, H358 response to gefitinib was not augmented by U0126 pre-treatment. However, H322 and SKBR3 cells were sensitized to EGFR inhibition with 5 days of U0126 exposure, suggesting fairly broad applicability of this strategy.

We also probed the reversibility of the effects of chronic MEK inhibition in H1666 cells (Fig. 2-3C-E, 2-S6). After 7 days, a fraction of cells was split from the U0126 culture and maintained in media containing DMSO (control). This “U0126 removal” culture was subsequently plated in parallel with the cells maintained in U0126. After 7 days of U0126 exposure, removal from U0126 for 4 days completely reversed changes in cellular sensitivity to gefitinib and epithelial and mesenchymal marker expression (Fig. 2-3C-D, 2-S6A).

Stem cell-like sub-populations with intrinsic therapeutic resistance are found within tumors [35, 110] and are typically identified as CD44<sup>high</sup>/CD24<sup>low</sup> [35] or E-cadherin<sup>low</sup> [111]. CD44<sup>high</sup>/CD24<sup>low</sup> enrichment from heterogeneous cultures promotes mesenchymal behaviors including resistance to EGFR inhibitors [35]. Using flow cytometry, we measured the shift in the CD44<sup>high</sup>/CD24<sup>low</sup> sub-population with U0126 addition and subsequent removal (Fig. 2-3E, 2-S6B). U0126-treated cells had fewer CD44<sup>high</sup>/CD24<sup>low</sup> cells and more CD44<sup>low</sup>/CD24<sup>high</sup> cells than controls. As with epithelial/mesenchymal marker expression, U0126 removal for four days reversed the effect on the CD44<sup>low</sup>/CD24<sup>high</sup> population.

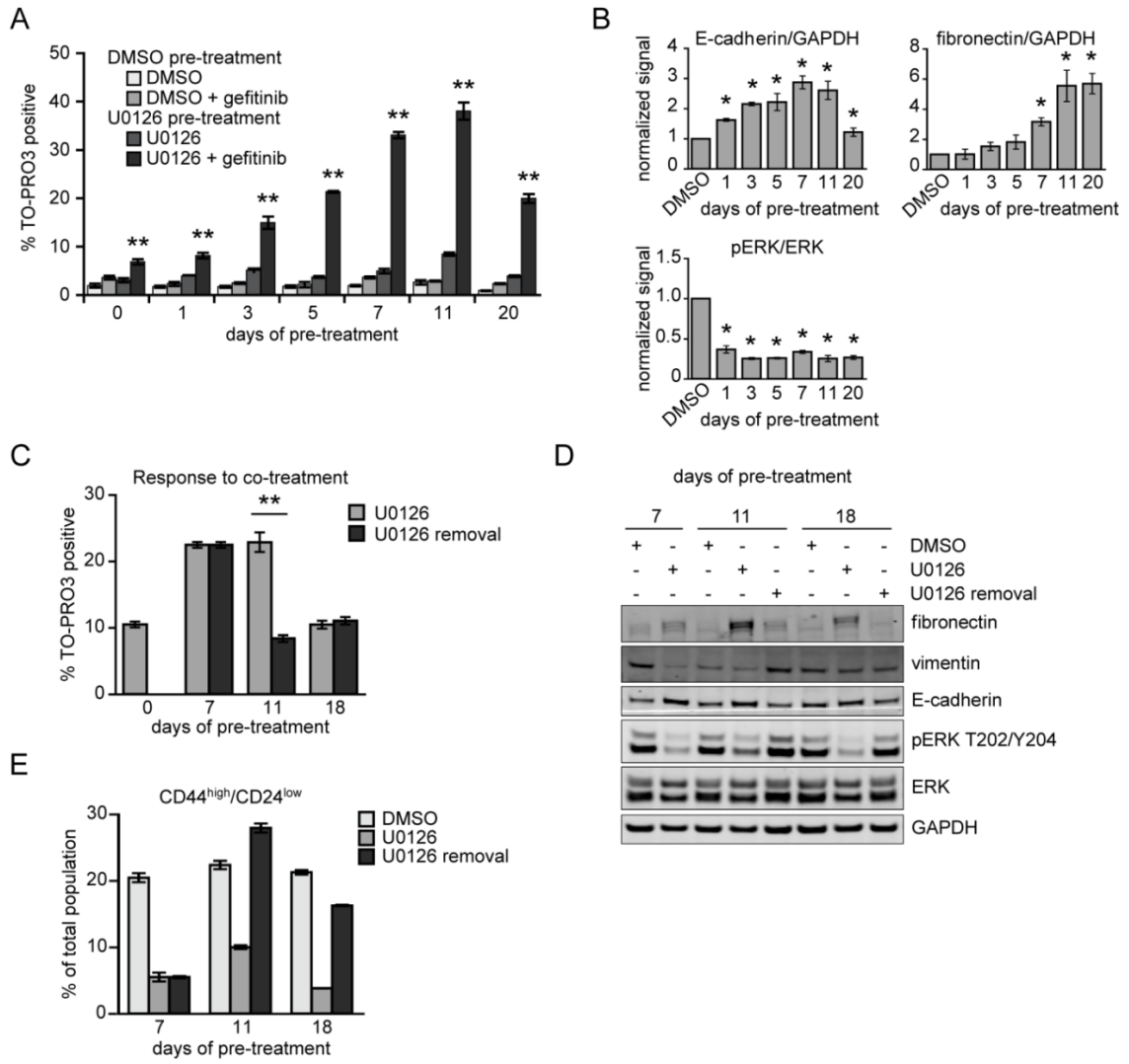


**Figure 2-3: Chronic MEK inhibition sensitizes NSCLC cells to EGFR inhibition.**

(A) H1666 cells were cultured in 10  $\mu$ M U0126 or DMSO (control) for up to 3 weeks and were evaluated for cell death response to 10  $\mu$ M gefitinib for various U0126 exposure times. Cell death was measured by flow cytometry for TO-PRO3 permeability 48 hrs after gefitinib addition. Averaged data are shown  $\pm$  s.e.m. ( $n = 3$ ); significance is relative to any other condition from the same day. (B) Lysates prepared in parallel to (A), before gefitinib addition, were analyzed by western blot with antibodies against the indicated proteins. Signals normalized to respective DMSO controls are reported as averages  $\pm$  s.e.m. ( $n = 3$ ). (C) The reversibility of U0126-mediated effects was assessed as described in *Materials and Methods Section 2-3*. For cells removed from (U0126 removal) or maintained in U0126, response to the same drug co-treatment was assessed by TO-PRO3 permeability at the indicated times. Data are represented as averages  $\pm$  s.e.m ( $n = 3$ ). (D and E) Reversibility of U0126 effects was assessed by western blot (D), using antibodies against indicated proteins, and by flow cytometry for CD44 and CD24 staining (E). Blot images are representative of three replicates. Flow cytometry data are represented as averages  $\pm$  s.e.m. ( $n = 3$ ). Times indicated reflect the total time of U0126 exposure prior to lysis, gefitinib addition, or staining; \* and \*\*  $p < 0.05$  and  $0.005$ , respectively.

*KRAS<sup>12V</sup>-mediated ERK activation promotes EMT*

To further probe the connection between ERK activity and EMT, we expressed KRAS<sup>12V</sup> in H1666 cells. This produced an anticipated increase in ERK phosphorylation and increased vimentin expression (Fig. 2-4A). Gefitinib and U0126 promoted an epithelial shift in control cells, as determined by western blot and wound closure measurements (Fig. 2-4A, B). KRAS<sup>12V</sup> promoted maintenance of ERK phosphorylation in response to gefitinib and largely prevented gefitinib-mediated changes in marker expression and wound closure (Fig. 2-4A, B). Importantly, the effects of KRAS<sup>12V</sup> were MEK-dependent, as demonstrated by the effects of U0126 (Fig. 2-4).

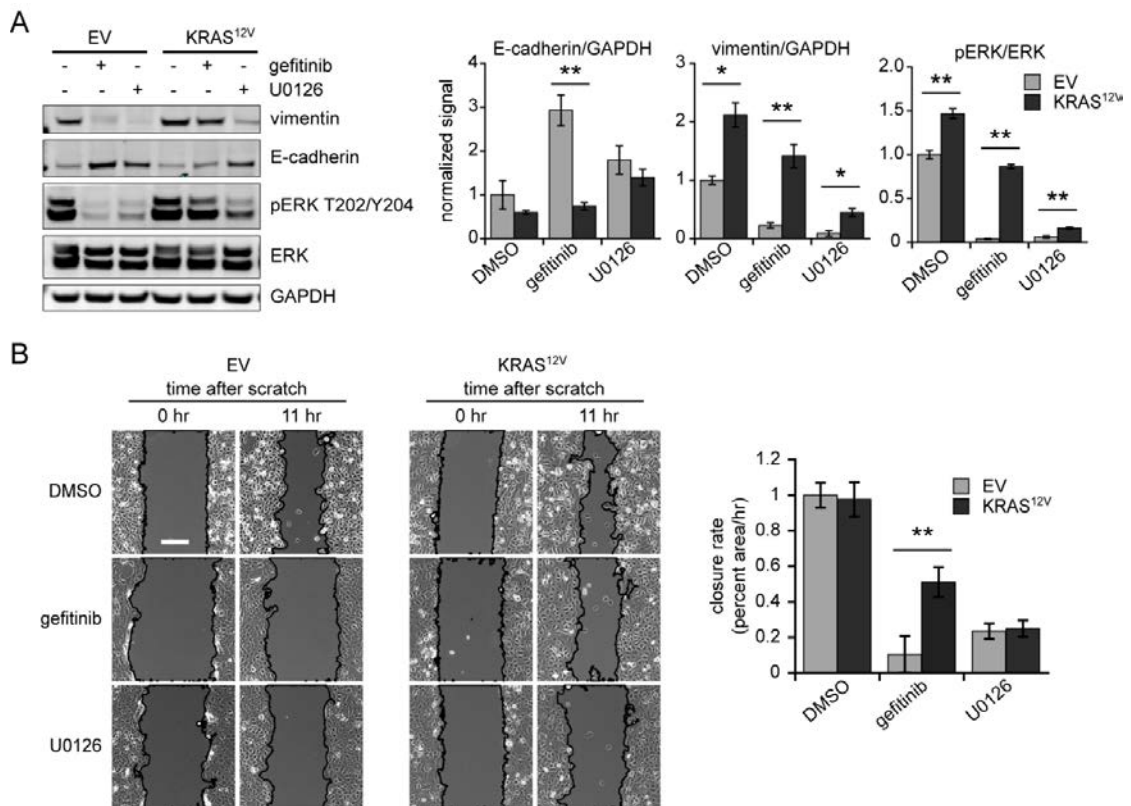


**Figure 2-4: KRAS<sup>12V</sup> expression promotes mesenchymal characteristics in H1666 cells.**

(A) H1666 cells transduced with KRAS<sup>12V</sup> or an empty vector control (EV) treated for three days with DMSO, 2 μM gefitinib, or 20 μM U0126 were lysed and analyzed by western blot with antibodies against indicated proteins. Signals normalized to DMSO-treated EV lysates are reported as averages ± s.e.m. (n = 3). (B) Wound closure rates were measured for EV- and KRAS<sup>12V</sup>-transduced cells treated as in panel (A). Rates normalized to the EV DMSO control condition are reported as averages ± s.e.m. for triplicate wells from two different platings (n = 6). Representative phase contrast images are shown, with tracings added to identify open scratch areas. Scale bar = 200 μm. \* and \*\* indicate p < 0.05 and 0.005, respectively

*MEK inhibition antagonizes mesenchymal phenotypes and acquired resistance to EGFR inhibition in an EGFR mutant-expressing cell line*

We tested the effects of chronic MEK inhibition in a panel of cell lines derived from PC9 cells, which express EGFR<sup>delE746\_A750</sup> and are gefitinib sensitive. In parental PC9 cells, MEK inhibition prevented TGFβ-mediated EMT and drove changes in epithelial/mesenchymal marker expression and wound healing consistent with the effects observed in H1666 cells (Fig. 2-5, 2-S7).

A previous study derived PC9 cells that acquired gefitinib resistance through EGFR<sup>T790M</sup> mutation [72]. Another cell line was then derived from these cells with secondary resistance to the irreversible EGFR inhibitor WZ4002, which potently inhibits EGFR<sup>T790M</sup> [72, 112]. WZ4002 resistance arose through *ERK2* amplification. We used these gefitinib-resistant (GR) and WZ4002-resistant (WZR) clones to examine the effects of ERK2 activity, which has been tied to EMT in non-transformed cells [93]. WZR cells displayed a more mesenchymal marker expression pattern than parental or GR cells, with increased fibronectin and vimentin expression and decreased E-cadherin expression (Fig. 2-6A). WZR cells were also more migratory than GR cells as measured by wound closure and Transwell migration (Fig. 2-6B, C).

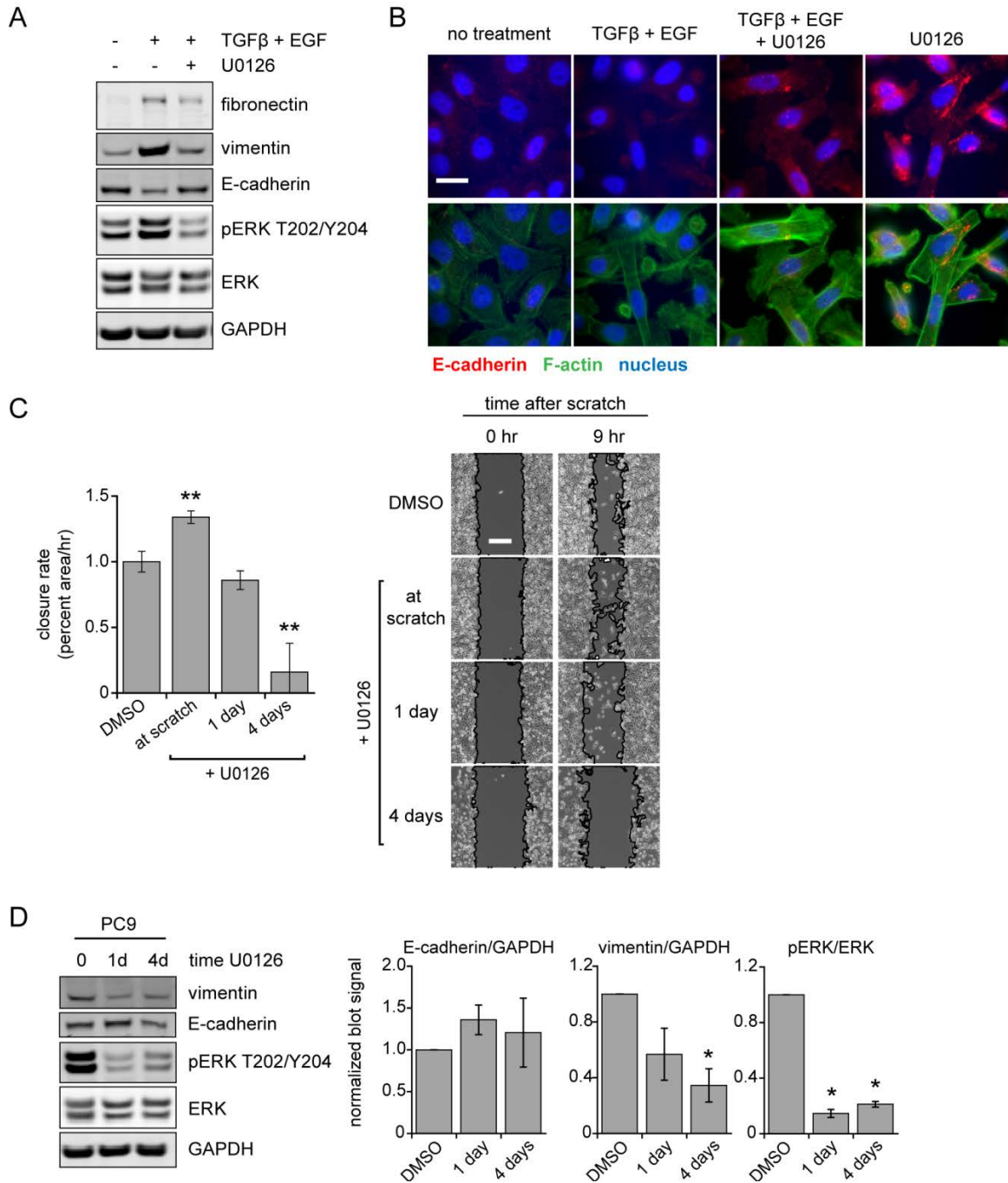


**Figure 2-5: ERK activity determines epithelial/mesenchymal characteristics in an NSCLC cell line with an EGFR-activating mutation.**

(A) Lysates of parental PC9 cells treated for four days with 10 ng/mL TGFβ + 50 ng/mL EGF, TGFβ + EGF and 20 μM U0126, or DMSO (control) were analyzed by western blot with antibodies against indicated proteins. Images are representative of three independent experiments. Scale bar = 20 μm. (B) PC9 cells on glass coverslips were treated as in (A), fixed, and stained for E-cadherin, F-actin, and DNA. Images are representative of three replicates for

each of two independent experiments. **(C)** Wound closure rates were measured for PC9 cells treated with DMSO (control) or 20  $\mu$ M U0126 at the time of scratch or for 1 or 4 days prior to scratch. Rates normalized to the control condition for triplicate wells from two different platings ( $n = 6$ ) are reported as averages  $\pm$  s.e.m. Representative phase contrast images are shown, with tracings added to identify open scratch areas. Scale bar = 200  $\mu$ m. **(D)** Lysates prepared in parallel to **(C)** were analyzed by western blot using antibodies against indicated proteins. Images are representative of three independent experiments. Signals normalized to respective DMSO controls are reported as averages  $\pm$  s.e.m. ( $n = 3$ ); \* and \*\* indicate  $p < 0.05$  and  $0.005$ , respectively, compared to control.

The effects of chronic MEK inhibition were tested in GR and WZR cells, using a higher U0126 concentration for WZR because of the *ERK2* amplification. Death response to co-treatment was enhanced by approximately two-fold with three days of U0126 pre-treatment in both cell lines (Fig. 2-7A, 2-S8A,B). As in H1666 cells, sufficiently long U0126 exposure resulted in an eventual decrease in augmented response to EGFR inhibition. Increased sensitivity to gefitinib correlated with reduced vimentin expression and slight increases in E-cadherin expression, and the eventual decrease in augmentation was accompanied by increased fibronectin expression in WZR cells (fibronectin was not detectable in GR cells) (Fig. 2-7B, 2-S8C).

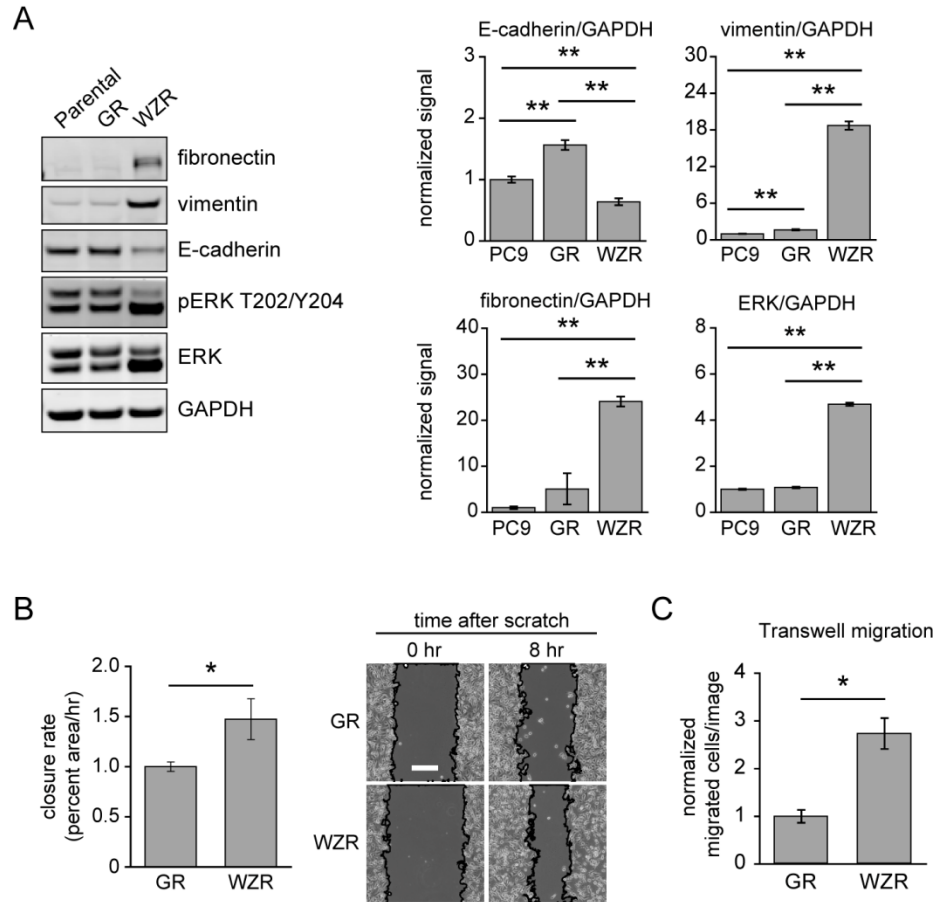


**Figure 2-6: ERK2 amplification promotes mesenchymal characteristics in PC9 cells with acquired resistance to an irreversible EGFR inhibitor.**

(A) Lysates prepared from parental, gefitinib-resistant (GR), and WZ4002-resistant (WZR) PC9 cells grown in complete media were analyzed by western blot using antibodies against indicated proteins. Images are representative of three independent experiments. Densitometry data are shown normalized to PC9 parental signals and are reported as averages  $\pm$  s.e.m. ( $n = 3$ ); \*\* indicates  $p < 0.01$ . (B) Wound closure rates were measured for GR and WZR cells. Rates normalized to GR closure rate are reported as averages  $\pm$  s.e.m. for triplicate wells from each of two different platings ( $n = 6$ ); \* indicates  $p < 0.05$ . Representative phase contrast images are shown, with tracings added to identify open scratch areas. Scale bar = 200  $\mu$ m. (C) Transwell migration measurements were made for GR and WZR cells. Bars represent averages  $\pm$  s.e.m. for duplicate wells from three separate experiments ( $n = 6$ ) normalized to GR cells.

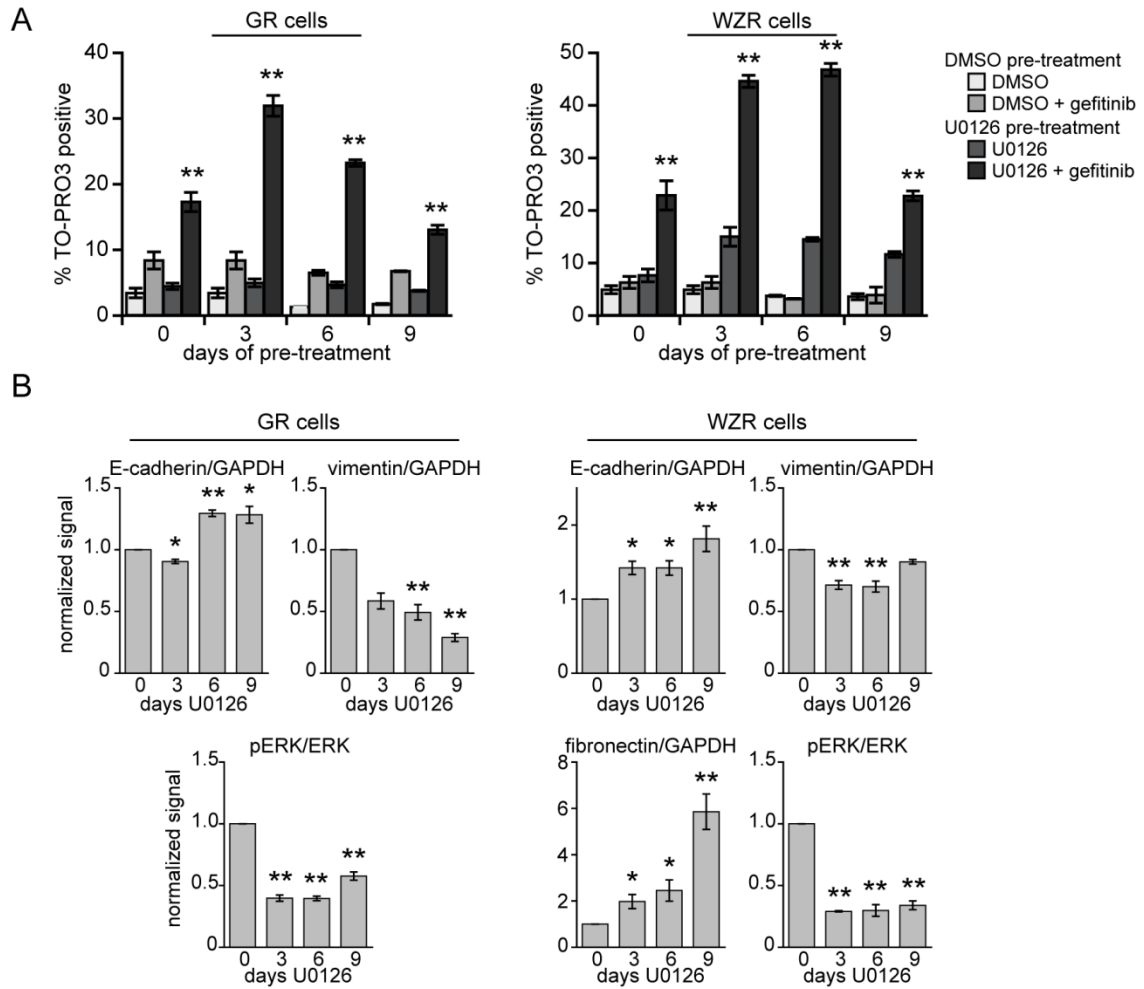


**Figure 2-7: MEK inhibition sensitizes cells with acquired resistance to EGFR inhibitors.**

(A) Gefitinib-resistant (GR) and WZ4002-resistant (WZR) PC9 cells were cultured in 5  $\mu$ M and 20  $\mu$ M U0126, respectively, or DMSO (control) for up to 9 days, as described in *Materials and Methods Section 2-3*, and were evaluated for cell death response to 5  $\mu$ M gefitinib for various U0126 exposure times. Cell death was measured by flow cytometry for TO-PRO3 permeability 48 hrs after gefitinib addition. Time points represent total time exposed to U0126 prior to gefitinib addition or lysis. Data are represented as averages  $\pm$  s.e.m. ( $n = 3$ ); significance is shown relative to any other condition from the same day. (B) GR and WZR cell lysates prepared in parallel to (A) were analyzed by western blot using antibodies against indicated proteins. Average signals normalized to respective DMSO controls are reported  $\pm$  s.e.m ( $n = 3$ ). \* and \*\* indicate  $p < 0.05$  and  $0.005$ , respectively.

## 2-5 DISCUSSION

We characterized the role of ERK in regulating EMT in NSCLC cells. MEK inhibition prevented TGF $\beta$ -induced EMT in NSCLC cell lines expressing wild type EGFR and KRAS (H1666 and H322), wild type EGFR and mutant KRAS (H358), or mutant EGFR (PC9). This suggests a general role for ERK in promoting mesenchymal characteristics across typical NSCLC cell types. MEK inhibition also antagonized mesenchymal-associated characteristics including migration, resistance to EGFR inhibition, and CD44<sup>high</sup>/CD24<sup>low</sup> expression.

The role of ERK in EMT has been explored in other cell types. ERK is an established determinant of EMT in non-transformed cells [14, 113-115], with ERK2 specifically implicated as an EMT driver [93, 94, 116]. This is consistent with findings in breast cancer [117], where MEK inhibition reverses miR-21-mediated EMT, and with studies of phosphatases regulating ERK (i.e., MKP3, PTPN14, and SHP2) [95-97], which also suggest a connection between ERK activity and EMT.

A number of factors regulate ERK activity in NSCLC cells. For example, we previously demonstrated a connection between impaired mutant EGFR endocytosis and impaired ERK activity [74]. More recently, in collaboration with others, we identified a coupling between *ERK2* amplification and increased EGFR endocytosis in the WZ4002-resistant PC9 cells used here [72]. Interestingly, inhibiting EGFR endocytosis in WZ4002-resistant cells reduced ERK phosphorylation and promoted an epithelial marker expression pattern (Fig. 2-S9), drawing a potential connection between EGFR endocytosis and EMT.

In H1666 cells, KRAS<sup>12V</sup>-driven ERK activity promoted mesenchymal marker expression and resistance to gefitinib-mediated MET changes. These findings are generally consistent with studies connecting oncogenic HRAS or KRAS mutants with EMT in mammary epithelia [93], pancreatic cancer [94, 109], and lung cancer [109]. The MEK dependence of our observations with KRAS<sup>12V</sup> may support exploration of MEK and ERK inhibitors in NSCLCs with KRAS mutation.

In addition to promoting epithelial marker expression, MEK inhibition promoted response to EGFR inhibition. Some studies have suggested the efficacy of EGFR and MEK co-inhibition in gastric cancer [118] and pancreatic cancer cells [119], and current clinical trials are testing erlotinib combined with MEK inhibitors in NSCLC. In light of this, it is worth noting that the effects we observed with MEK inhibition occurred on a time scale that was much longer than that for ERK inhibition and more consistent with changes in epithelial and mesenchymal marker expression. This may suggest considering a clinical scheduling approach wherein a MEK inhibitor is initially used alone to promote an epithelial phenotype, followed by addition of an EGFR inhibitor. An analogous staggered drug scheduling approach was effective in triple negative breast cancer cells which were sensitized to doxorubicin by erlotinib pre-treatment *in vitro* and in mouse tumor xenografts [102]. Applying this basic concept to future clinical trial design may allow for lower MEK inhibitor doses to curb toxicities [120] and promote response to EGFR inhibitors. Given that the time windows for augmented response to gefitinib and the useful concentrations of U0126 were variable among cell lines, it will of course be important first to examine this strategy in pre-clinical animal models to assess general efficacy in an *in vivo* setting and optimize timing and dosing.

We note as well that some recent data suggests that MET is required for efficient colonization of distant metastases [22, 23]. Thus, in evaluating different potential strategies for driving MET, the potential to drive proliferation of metastases will have to be weighed against potential ability to kill tumor cells. ERK may be an especially attractive target in this regard. In at least one study, ERK inhibition through microRNA-mediated reduction of SHP2 (a positive regulator of ERK signaling) reduced metastases in an *in vivo* breast cancer model [82], which was due to SHP2's simultaneous regulation of proliferation, invasion, and transcription factor expression. Thus, promoting MET through ERK inhibition, which should additionally inhibit cellular proliferation, may mitigate risks associated with proliferation of micrometastases.

In all three cell lines we tested for effects of chronic MEK inhibition, enhanced gefitinib response eventually decreased. Though initially unresponsive to U0126, U0126-cultured cells

displayed noticeable cell death at mid-range time points (partially reflected by cell death measurements for U0126-only samples in Figs. 2-3 and 2-7). This could result in selection for U0126-resistant cells over time. Since the fraction of CD44<sup>high</sup>/CD24<sup>low</sup> cells in U0126-treated cultures remained low at time points when resistance was observed (Fig. 2-3C,E), the potentially inherently resistant population was apparently not CD44<sup>high</sup>/CD24<sup>low</sup>. Alternatively, resistance could arise from adaptation of the entire cell population, for example through increased fibronectin-mediated signaling, which has been linked to AKT activation and docetaxel resistance in ovarian and breast cancer cells [121]. Indeed, in all cases, the eventual drop in augmented response to gefitinib was accompanied by increased fibronectin expression. Future work should consider effectors of fibronectin-mediated signaling as signaling nodes whose inhibition may augment EGFR inhibitor response.

While our data suggest potential relevance of our findings to *de novo* and acquired EGFR inhibitor resistance, responsiveness to chronic MEK inhibition was not uniform among cell lines, which could result from any of the numerous differences in initial conditions among NSCLC cell lines. For example, while H1666 cells express wild type EGFR and KRAS, they also express the low-activity G446V BRAF mutant [122], which could influence their death response to MEK inhibition. In the future, therefore, investigating the cellular initial conditions that may determine responsiveness to this approach and identifying alternative signaling nodes whose inhibition may result in more stable maintenance of an epithelial cell type will also be important.

## **2-6 ACKNOWLEDGEMENTS**

The authors thank Drs. Pasi Jänne, Douglas Lauffenburger, Deepak Nihilani, and Russ Carstens for generously providing reagents. The authors also thank Calixte Monast, Chris Furcht, and Alice Walsh for technical assistance and guidance.

## 2-7 SUPPLEMENTAL MATERIAL

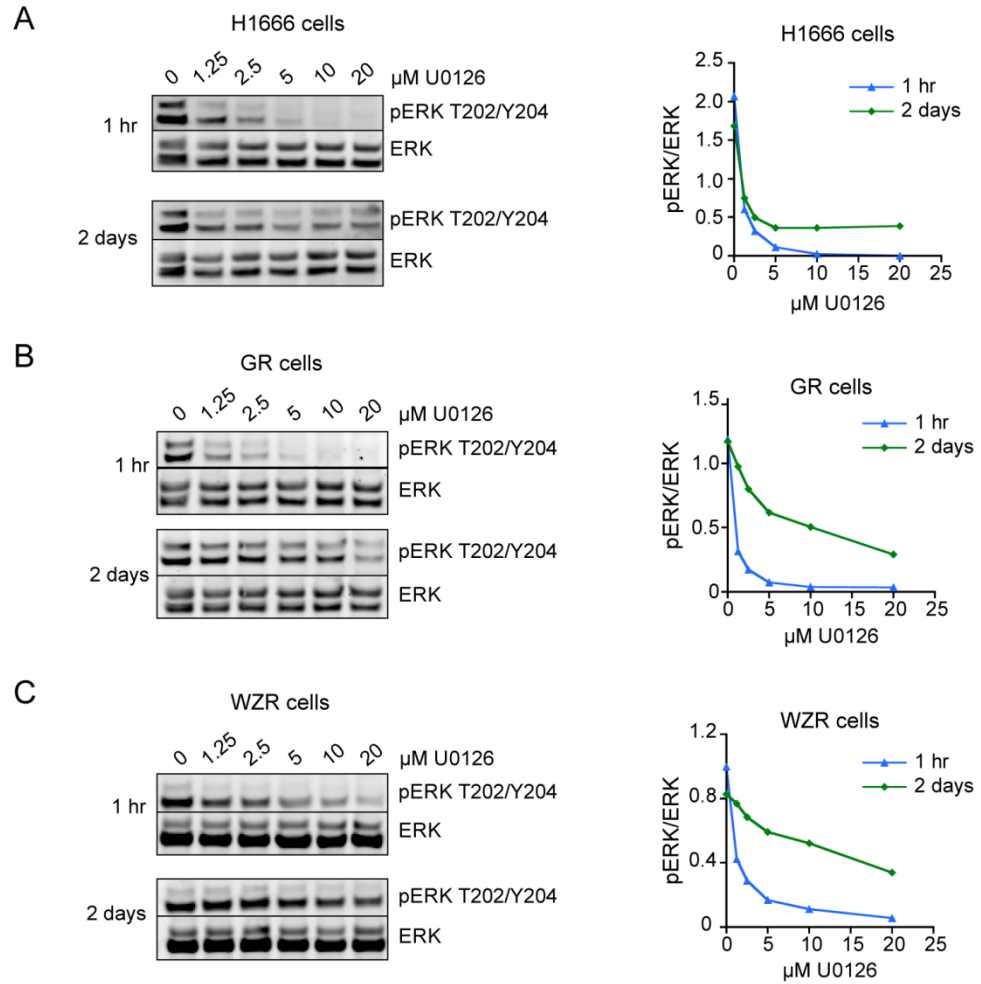


**Figure 2-S1**

Lysates were prepared from (A) H1666, (B) PC9 GR, or (C) PC9 WZR cells treated with a range of U0126 concentrations for 1 hr or 2 days and evaluated by western blot using antibodies against the indicated proteins. Line plots on the right are quantifications of western blot signals.

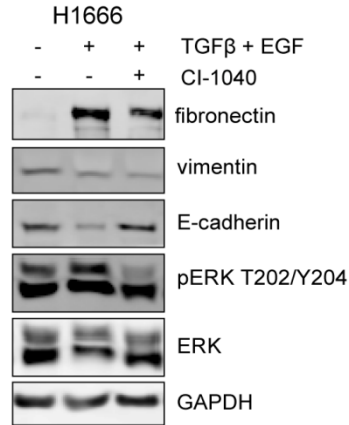


**Figure 2-S2**

H1666 cells were treated for four days with 10 ng/mL TGFβ + 50 ng/mL EGF, a combination of TGFβ + EGF and 3μM CI-1040, or DMSO (control). Whole cell lysates were analyzed by western blot with antibodies against indicated proteins.

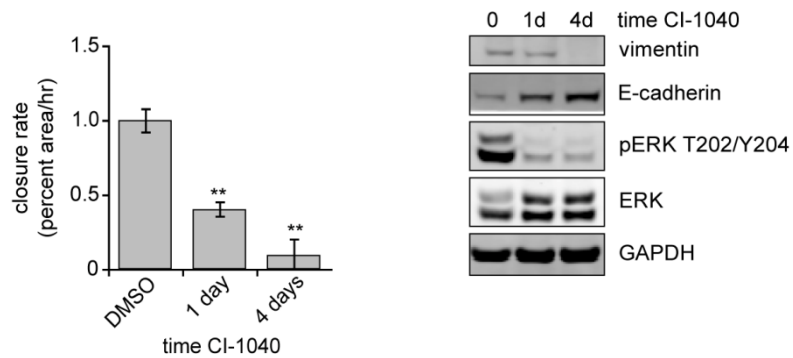


**Figure 2-S3**

Wound closure rates were calculated as described in *Materials and Methods Section 2-3* for H1666 cells treated with DMSO (control) or 3 μM CI-1040 for 1 or 4 days prior to scratch. Rates are reported as averages ± s.e.m. normalized to the control condition for triplicate wells from two independent platings ( $n = 6$ ). Lysates prepared in parallel with wound closure experiments were analyzed by western blot using antibodies against indicated proteins.

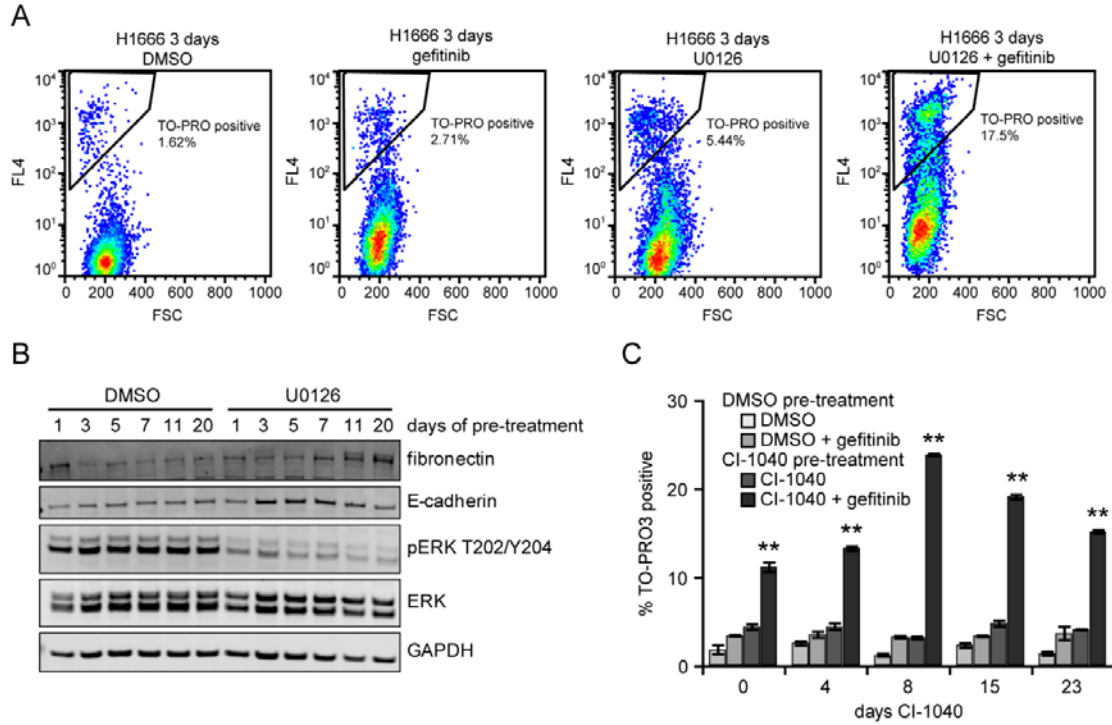


**Figure 2-S4**

(A) H1666 cells were cultured in 10  $\mu$ M U0126 or DMSO (control) for up to 3 weeks, as described in *Materials and Methods Section 2-3*, and were evaluated for cell death response to gefitinib for various U0126 treatment times. At each time point, U0126 pre-treated cells were treated with or without 10  $\mu$ M gefitinib, and cell death was measured by flow cytometry for TO-PRO3 permeability 48 hrs later. Representative flow cytometry dot plots for average data presented in Fig. 2-3A are shown for each condition from the 3 day time point with gating for TO-PRO3 positive cells. (B) Cell lysates prepared in parallel to flow experiments, prior to gefitinib addition, were analyzed by western blot with antibodies against indicated proteins. Image is representative of three replicates, and densitometry analysis is shown in Fig. 2-3B. (C) H1666 cells were cultured in 3  $\mu$ M CI-1040 or DMSO (control) for up to 23 days, as described in *Materials and Methods Section 2-3*, and were evaluated for cell death response to gefitinib for various CI-1040 exposure times. Pre-treated cells were then treated with or without 2  $\mu$ M gefitinib, and cell death was measured by flow cytometry for TO-PRO3 permeability 48 hrs later. Data are represented as averages  $\pm$  s.e.m ( $n = 3$ ); \*\* indicates  $p < 0.005$ , with significance relative to any other condition from the same day.

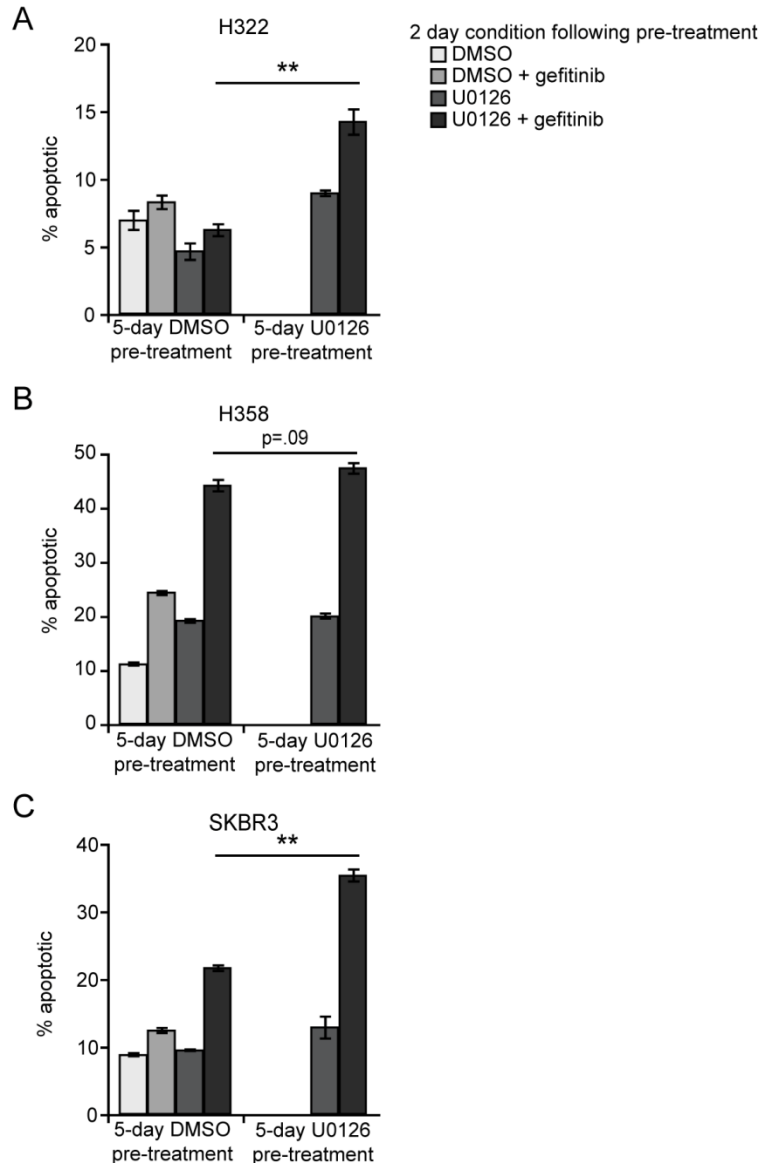


**Figure 2-S5**

(A) H322 cells were cultured in 40  $\mu$ M U0126 and (B) H358 and (C) SKBR3 cells were cultured in 10  $\mu$ M U0126 for a total of 5 days before addition of 5  $\mu$ M gefitinib. Cell death was measured by flow cytometry 48 hrs later using Annexin-V and TO-PRO3 co-staining, described in *Materials and Methods Section 2-3*. Data are represented as averages  $\pm$  s.e.m ( $n = 3$ ); \*\* indicates  $p < 0.005$ .

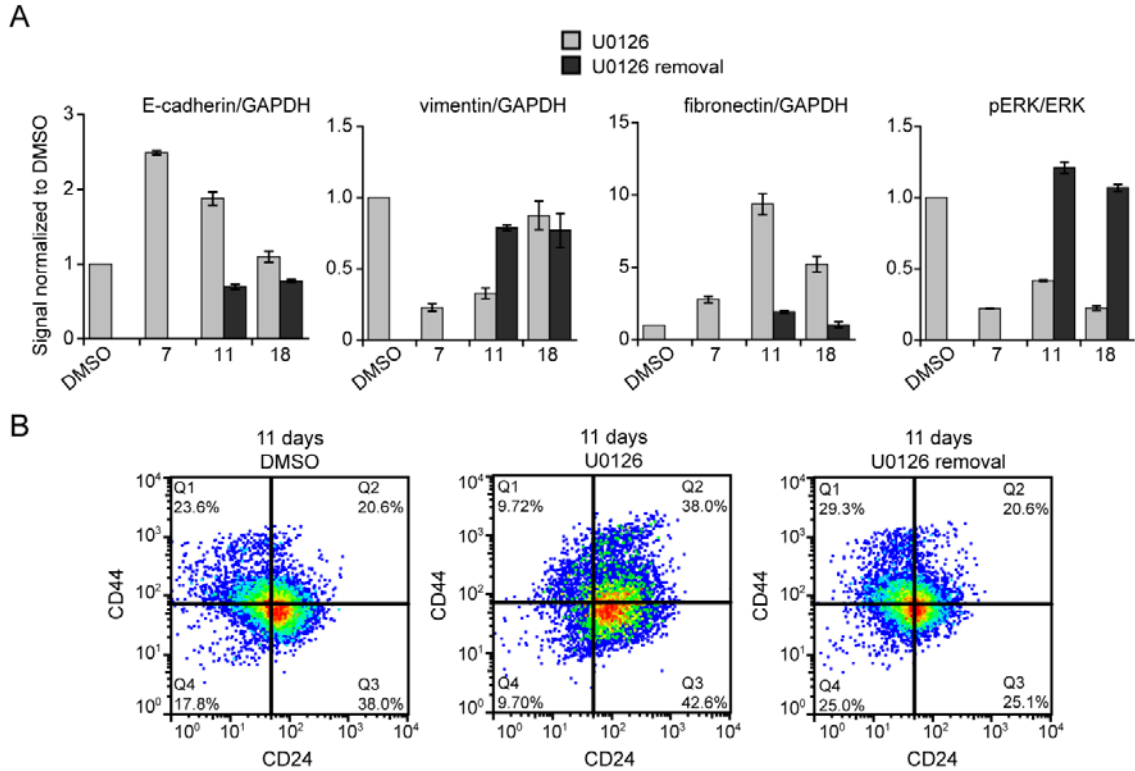


**Figure 2-S6**

Experiments probing the reversibility of U0126-mediated effects were performed by splitting a fraction of cells from U0126 culture after 7 days and maintaining in DMSO (control) thereafter, as described in *Materials and Methods Section 2-3*. **(A)** For the times and treatment conditions indicated, cell lysates were analyzed by western blot using antibodies against indicated proteins. Data are represented as signals normalized to those from DMSO controls (i.e., cells maintained in DMSO throughout the experiment) and are reported as averages  $\pm$  s.e.m. ( $n = 3$ ). A representative blot image is shown in Fig. 2-3D. **(B)** Reversibility was also evaluated by flow cytometry analysis for CD44 and CD24. Representative flow cytometry dot plots for data in Fig. 2-3E are shown for all three conditions of the 11 day time point.

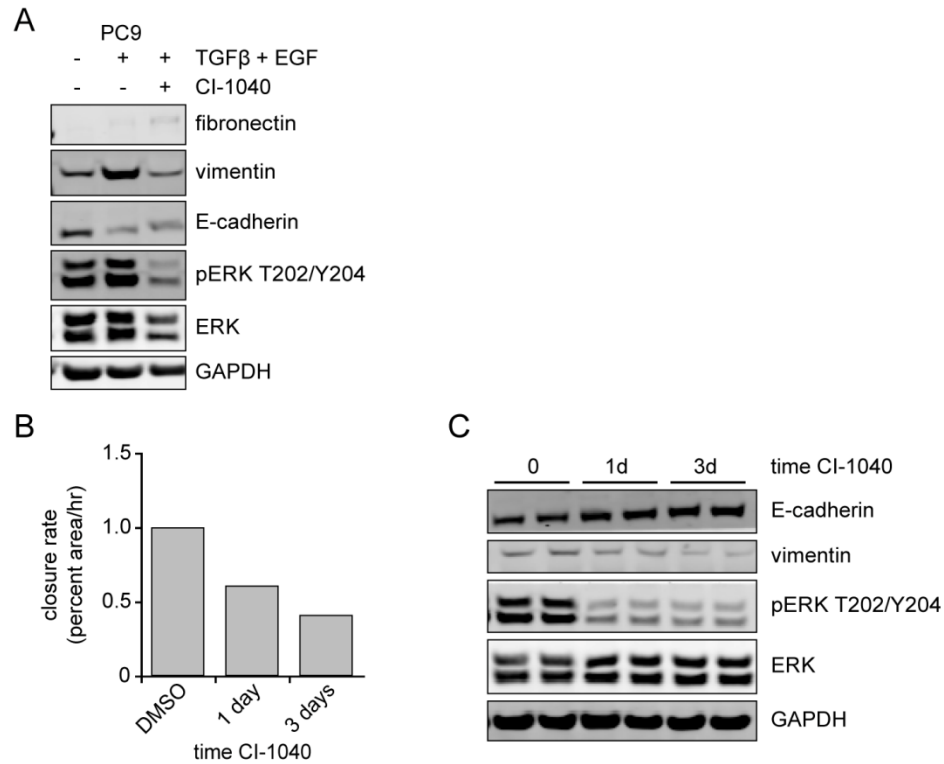


**Figure 2-S7**

(A) PC9 cells were treated for four days with 10 ng/mL TGFβ + 50 ng/mL EGF, a combination of TGFβ + EGF and 3 μM CI-1040, or DMSO (control). Whole cell lysates were analyzed by western blot with antibodies against indicated proteins. (B) Wound closure rates were calculated as described in *Materials and Methods Section 2-3* for PC9 cells treated with DMSO (control) or with 3 μM CI-1040 for 1 or 3 days prior to scratch. Rates are reported as averages normalized to the control condition for duplicate wells. (C) Lysates prepared in parallel with wound closure experiments were analyzed by western blot using antibodies against indicated proteins.

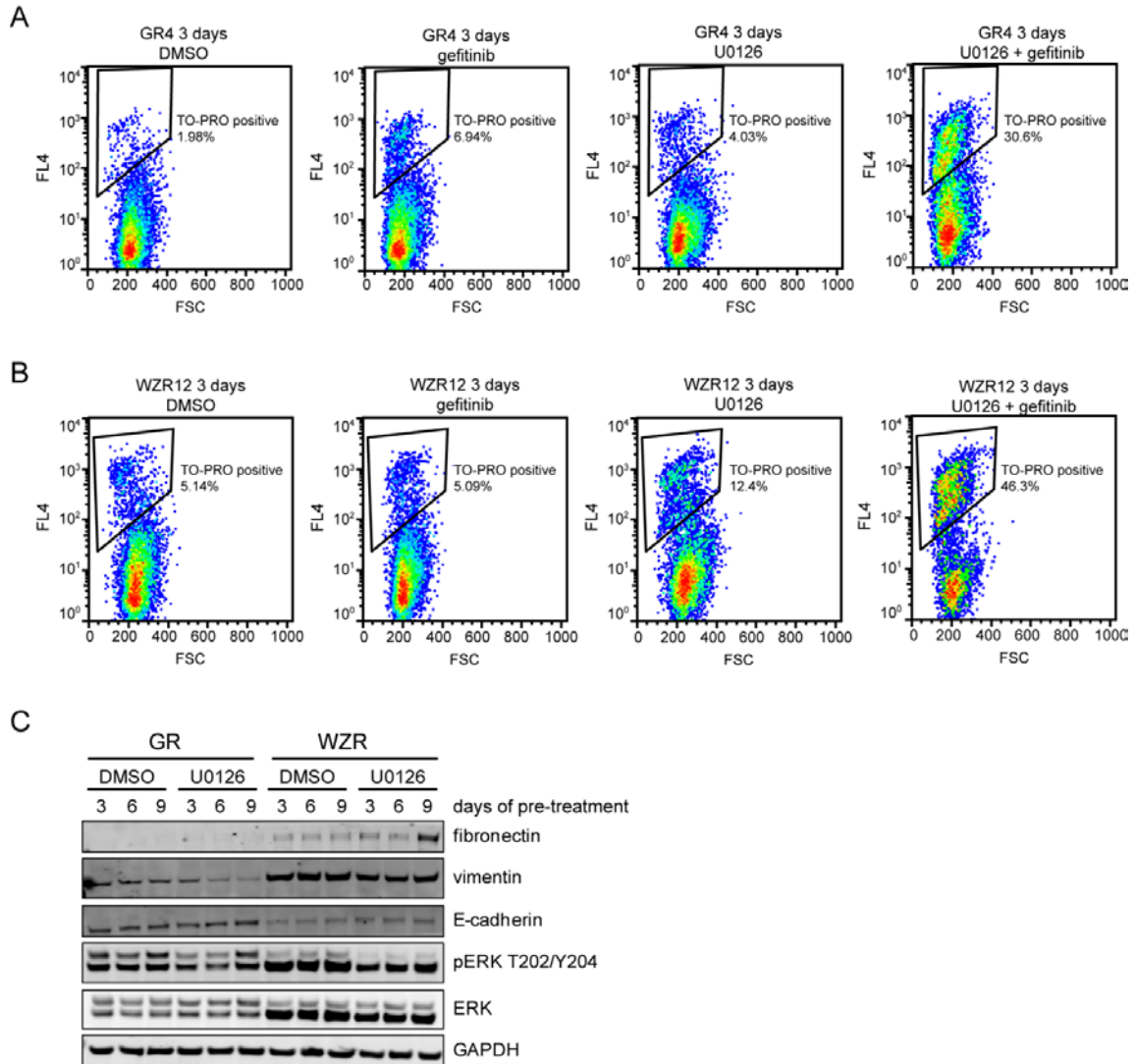


**Figure 2-S8**

(**A** and **B**) PC9 GR and WZR cells were cultured in 5  $\mu$ M and 20  $\mu$ M U0126, respectively, or DMSO (control) for up to 9 days, as described in *Materials and Methods*, and were evaluated for cell death response to gefitinib for various U0126 exposure times. At each time point, U0126 pre-treated cells were treated with or without 5  $\mu$ M gefitinib, and cell death was measured by flow cytometry for TO-PRO3 permeability 48 hrs after gefitinib addition. Representative flow cytometry dot plots for averaged data in Fig. 2-7A are shown for GR cells (**A**) and WZR cells (**B**) from each condition from the 3 day time point with gating for TO-PRO3 positive cells. (**C**) Cell lysates prepared in parallel with flow experiments, prior to gefitinib addition, were analyzed by western blot with antibodies against the indicated proteins. The image is representative of three replicates, and densitometry analysis is shown in Fig. 2-7B.

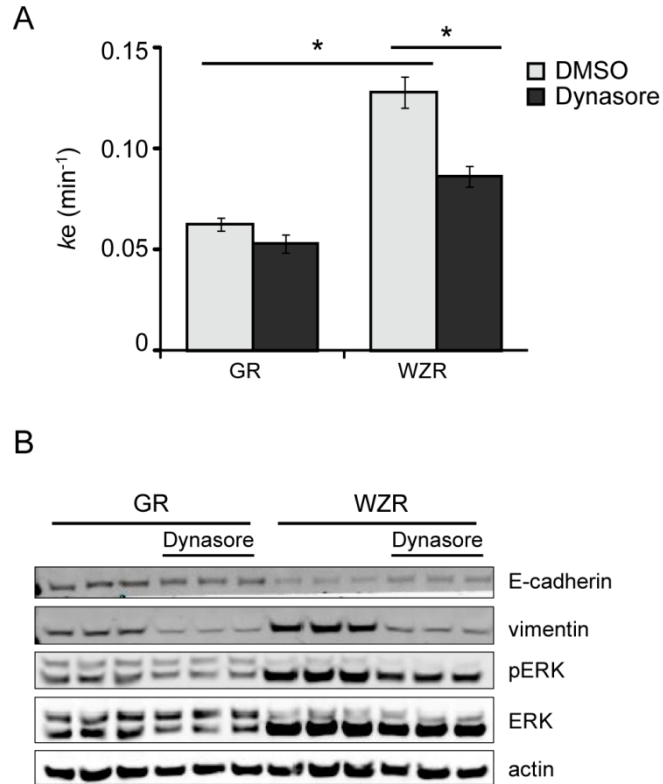


**Figure 2-S9**

(A) EGF-mediated EGFR internalization rate constants ( $k_e$ ) for PC9 GR and WZR cells treated with 80  $\mu\text{M}$  Dynasore or DMSO (control) were measured using 10 ng/mL  $^{125}\text{I}$ -EGF. Data are represented as averages  $\pm$  s.e.m. for two separate experiments performed in triplicate ( $n = 6$ ); \* indicates  $p < 0.05$ . (B) PC9 GR and WZR cells in 6-well plates were treated with 80  $\mu\text{M}$  Dynasore or DMSO (control) for 4 days, and lysates were analyzed by western blot with antibodies against the indicated proteins. Triplicate samples are shown for each condition.

## **CHAPTER 3: EGF Augments TGF $\beta$ -Induced Epithelial-Mesenchymal Transition by Promoting SHP2 Binding to GAB1<sup>2</sup>**

### **3-1 ABSTRACT**

In many epithelial cells, epidermal growth factor (EGF) augments the epithelial-mesenchymal transition (EMT) that occurs when cells are treated with transforming growth factor beta (TGF $\beta$ ). Here, we demonstrate that this augmentation requires activation of SH2 domain-containing phosphatase-2 (SHP2), a proto-oncogene. In lung and pancreatic cancer cell lines, reductions in E-cadherin expression, increases in vimentin expression, and increases in cell scatter rates were larger when cells were treated with TGF $\beta$  and EGF versus TGF $\beta$  or EGF alone. SHP2 knockdown promoted epithelial characteristics basally and antagonized EMT in response to TGF $\beta$  alone or in combination with EGF. While EGF promoted SHP2 binding to tyrosine phosphorylated GAB1, which promotes SHP2 activity, TGF $\beta$  did not induce SHP2 association with phosphotyrosine-containing proteins. Knockdown of endogenous SHP2 and reconstitution with an SHP2 mutant with impaired phosphotyrosine binding ability eliminated the EGF-mediated EMT augmentation that was otherwise restored with wild type SHP2 reconstitution. These results demonstrate roles for basal and ligand-induced SHP2 activity in EMT and further motivate efforts to identify specific ways to inhibit SHP2, given the role of EMT in cancer dissemination and chemoresistance.

---

<sup>2</sup> A version of Chapter 3 is under revision at a peer-reviewed journal and includes co-author Ingrid Lan

### 3-2 INTRODUCTION

Epithelial-mesenchymal transition (EMT) is a cellular program in which epithelial cells lose polarity and strong cell-cell adhesions and partially dedifferentiate to become more motile and invasive [2]. EMT is accompanied by shifts in transcription factor expression, cytoskeletal arrangement, RNA splicing, and cell signaling [2-4]. While EMT is required for normal development and wound healing, aberrant EMT has also been linked to metastasis [21, 123] and tumor resistance to therapy [124]. In lung and pancreatic cancer cells, sensitivity to therapeutic agents can be increased by promoting an epithelial phenotype [104, 125, 126]. These findings have motivated studies to decipher the signaling and regulatory mechanisms underlying EMT [127-129].

EMT is efficiently driven *in vitro* and *in vivo* by transforming growth factor- $\beta$  (TGF $\beta$ ) [4], which initiates a network of cellular signaling pathways including SMADs, extracellular signal-regulated kinase-1/2 (ERK1/2), p38, and c-Jun N-terminal kinase [46, 47]. Activity of ERK1/2 (hereafter referred to as ERK) has been identified as particularly important for TGF $\beta$ -driven EMT [14, 45, 126]. Epidermal growth factor (EGF), which initiates its own signaling network including ERK, is often combined with TGF $\beta$  to enhance EMT outcomes *in vitro* [12-14, 57], and the augmented EMT that results has been attributed to ERK activation [14, 57]. In some cell settings, TGF $\beta$  cross-activates the EGF receptor (EGFR), which augments ERK pathway activation [55, 56, 98].

Downstream of EGFR and other receptor tyrosine kinases (RTKs), complete ERK activation depends upon the activity of SH2 domain-containing phosphatase-2 (SHP2), a cytosolic protein tyrosine phosphatase. In the basal state, an auto-inhibited SHP2 conformation is stabilized wherein the N-terminal SH2 domain binds and occludes the catalytic domain [77, 130]. Binding of SHP2 SH2 domains to phosphotyrosines on various RTKs or on adaptor proteins such as GRB2 associated binding protein-1 (GAB1) [76, 78] relieves this intramolecular inhibitory mechanism and allows SHP2 phosphatase domain access to substrates [79, 131, 132]. Point mutations of the  $\beta$ B5 arginine residues in the FLVRES motifs of either or both of the SH2

domains reduce the ability of phosphotyrosine peptides to induce SHP2 phosphatase activity, with greater effects for the more N-terminal SH2 domain arginine, Arg<sup>32</sup> [79, 133]. Furthermore, SHP2 isoforms with either or both of these SH2 domain point mutants (R32K/R138K) display impaired ability to induce downstream signaling [134, 135] and lead to developmental defects in mice [135, 136], again with greater dependence on Arg<sup>32</sup> functionality. SHP2 is a proto-oncogene, with SHP2 mutations or overexpression linked to a number of malignancies [80]. In breast cancer models, endogenous wild type SHP2 promotes tumor progression and metastasis in mice [82] and promotes mesenchymal marker expression and phenotypes in cultured breast cancer cell lines [97]. SHP2 has also been identified as a promoter of TGF $\beta$ -mediated EMT in A549 lung carcinoma cells [137], but whether differential SHP2 activation and regulation of ERK activity play a role in the ability of EGF to enhance TGF $\beta$ -mediated EMT is unknown.

We used lung and pancreatic cancer cell lines to explore the role of SHP2 in driving EMT in response to TGF $\beta$ . While TGF $\beta$  alone produced EMT effects in both cell lines, combining EGF with TGF $\beta$  enhanced EMT as determined by increased cell scatter and by larger decreases in E-cadherin expression and larger increases in vimentin expression observed by immunoblot and immunofluorescence. In contrast to TGF $\beta$ , EGF (alone or in combination with TGF $\beta$ ) induced SHP2 activity by promoting SHP2 association with phosphorylated GAB1. Knockdown of endogenous SHP2 promoted baseline epithelial cell characteristics and inhibited EMT-associated changes in response to TGF $\beta$  with or without EGF. Reconstitution with SHP2<sup>WT</sup> restored EMT in response to TGF $\beta$  and the ability of EGF to enhance the effects of TGF $\beta$ , but reconstitution with SHP2<sup>R32,138K</sup>, a mutant with impaired ability to bind phosphorylated GAB1, did not improve EMT induction from either growth factor treatment compared to empty vector controls. These results suggest that basal SHP2 activity is needed for the incomplete EMT observed in response to TGF $\beta$ , but that the activation of SHP2 induced by its association with phosphotyrosine-containing proteins such as GAB1 is needed for the more complete EMT observed when ligands such as EGF are combined with TGF $\beta$ .

### **3-3 MATERIALS AND METHODS**

#### *Cell culture and reagents*

H322 cells (Dr. Pasi Jänne, Dana-Farber Cancer Institute), H358 cells (Dr. Russ Carstens, University of Pennsylvania), PC9 cells (Dr. Douglas Lauffenburger, MIT), and AsPC1 and HPAF-II cells (Dr. Carl June, University of Pennsylvania) were maintained in RPMI supplemented with 10% FBS, 1 mM L-glutamine, 100 units/mL penicillin, and 100 µg/mL streptomycin. CAPAN-2 cells (Dr. Carl June) were maintained in DMEM supplemented as RPMI above. Cell culture reagents were from Life Technologies (Carlsbad, CA). Recombinant human EGF and TGFβ were purchased from Peprotech (Rocky Hill, NJ).

#### *Antibodies*

pERK T202/Y204 (4377), ERK (4695), pSMAD2/3 S465/467/S423/425 (8828), and pGAB1 Y627 (3233) antibodies were from Cell Signaling Technology (Danvers, MA). E-cadherin (sc-8426), vimentin (sc-373717), SHP2 (sc-7384), GAB1 (sc-9049) and GAPDH (sc-32233) antibodies were from Santa Cruz Biotechnology (Dallas, TX). Phosphotyrosine antibody (4G10) was from Millipore (Billerica, MA). Infrared dye- and Alexa Fluor®-conjugated secondary antibodies were from Rockland Immunochemicals (Gilbertsville, PA) and Life Technologies, respectively.

#### *Western blotting*

Whole cell lysates were prepared in a standard cell extraction buffer (Life Technologies) supplemented with protease inhibitors and phosphatase inhibitors (Sigma-Aldrich, St. Louis, MO). Lysates were cleared by centrifugation at 16,100 *g* for 10 min, and total protein concentrations were determined by micro-bicinchoninic acid (BCA) assay (Thermo Fisher Scientific, Waltham, MA). Proteins were resolved on 4-12% gradient polyacrylamide gels (Life Technologies) under denaturing and reducing conditions and transferred to 0.2 µm nitrocellulose membranes (Bio-Rad Laboratories, Hercules, CA). Membranes were imaged using a LI-COR Odyssey Imaging System. As needed, membranes were stripped with 0.2 M NaOH.

### *Immunoprecipitation*

Cells were lysed in an immunoprecipitation lysis buffer (Cell Signaling Technologies) supplemented with protease and phosphatase inhibitors. Lysates were prepared and assayed for total protein as described above, and 500 µg of protein was incubated with protein G agarose beads conjugated to SHP2 or normal mouse IgG control antibodies at 4°C overnight. Beads were washed three times with cold lysis buffer, re-suspended in LDS sample buffer (Life Technologies) and boiled before western blotting.

### *Immunofluorescence staining and image analysis*

Cells were plated on glass coverslips and maintained in 6-well plates. Following the indicated time of treatment with growth factors, cells were washed and fixed for 20 min in 4% paraformaldehyde and permeabilized with 0.25% Triton X-100 in PBS for 5 min. Washed coverslips were incubated with an anti-E-cadherin or anti-vimentin antibody in a humidified chamber for 3 hr at 37°C. Washed coverslips were incubated with Alexa Fluor-conjugated anti-mouse secondary antibodies and Hoechst-33342 DNA stain (Sigma-Aldrich) for 1 hr at 37°C. Coverslips were mounted on microscope slides using Prolong Gold Antifade mounting media (Life Technologies) and dried overnight. Fixed slides were imaged on a Zeiss Axiovert 40 CFL microscope using an A-Plan 20X objective (vimentin) or 100X oil objective (E-cadherin) and a SPOT Insight CCD camera. Identical acquisition settings were used across all images from a single experiment.

E-cadherin junctional localization was quantified using ImageJ and a method similar to that described in Loerke et al. 2012 [138]. Each cell-cell junction was traced with a 15-pixel (1.1 µm) wide freehand line (corresponding to the average thickness of E-cadherin stained junctions in the untreated condition), for which the area ( $A_j$ ), integrated density ( $ID_j$ ), and area-averaged mean intensity ( $M_j$ ) were measured.  $M_j$  was taken to be the average junctional signal. The three measurements,  $A_{total}$ ,  $ID_{total}$ ,  $M_{total}$ , were then taken for an increased thickness of 100 pixels (7.5 µm) encompassing junctional and peri-junctional E-cadherin staining. In order to find the mean cytoplasmic density ( $M_c$ ),  $A_j$  and  $ID_j$  were first subtracted from  $A_{total}$  and  $ID_{total}$ , respectively, to obtain

the cytoplasm-only quantities  $A_c$  and  $ID_c$ .  $M_c$  was then calculated by dividing  $ID_c$  by  $A_c$ . In order to quantify the extent of junctional localization of E-cadherin, the ratio  $M/M_c$  was calculated for each junction. All full junctions contained within an image were analyzed.

Quantification of percent of cells positive for vimentin was also performed using ImageJ. Nuclei were counted in each image from Hoechst staining to obtain the total number of cells. In the corresponding vimentin image, cell outlines were drawn using a freehand tool from which mean intensities of vimentin staining were recorded. Cells with mean intensities higher than the intensity of background non-specific staining were considered to be vimentin-positive, and the total number of vimentin-positive cells was divided by the number of nuclei to obtain the percentage of vimentin-positive cells in each image.

#### *Cell scatter experiments and quantification*

Cells were plated in complete medium at low density (500 cells per well in 12-well plates). When individual cells had expanded into well-defined colonies 4-5 days later, the scatter experiment was initiated by the addition of complete medium containing EGF (50 ng/mL), TGF $\beta$  (10 ng/mL), or a combination of the two ligands. Individual cell clusters were monitored and phase contrast images were captured with a Zeiss Axiovert 40 CFL microscope (10X objective) over 24 hr. Image segmentation was performed using the MATLAB image processing toolbox (MathWorks, Natick, MA) to identify all objects (cell clusters) within each image and record their area and perimeter. As described previously [139], a circularity index was calculated as  $4\pi(\text{area}/\text{perimeter}^2)$  (=1 for a circle) for each cluster.

#### *Plasmids and viral infections*

DNA oligonucleotides encoding short hairpins targeting human *SHP2* (Integrated DNA Technologies, San Jose, CA) were cloned into the pSicoR vector (Tyler Jacks, MIT; [140]). The shRNA-1 targeted nucleotides 1780-1798 of *SHP2* mRNA (5'-GGACGTTTCATTGTGATTGA-3'), shRNA-2 targeted nucleotides 5890-5908 (5'-GTATTGTACCAGAGTATTA-3'), and shRNA-3 targeted nucleotides 4931-4949 (5'-GCTGGTGGGTATTAATAT-3'). Control vectors were

created using shRNA sequences that do not target a known human mRNA. For stable shRNA expression, lentivirus was produced by calcium phosphate-mediated transfection of 293FT cells (Life Technologies) with pSicoR plasmids along with the packaging plasmids pCMV-VSV-G, pMDL-gp-RRE, and pRSV-Rev (Dr. Marilyn Farquhar, University of California San Diego). Virus-containing media was collected 48 and 72 hrs post-transfection and filtered using 0.45  $\mu$ m syringe filters prior to infecting target cells, which were subsequently selected and maintained in 2  $\mu$ g/mL puromycin.

SHP2 cDNA encoding SHP2<sup>WT</sup> or SHP2<sup>R32,138K</sup> (Ben Neel, Ontario Cancer Institute) was inserted between the BamHI and EcoRI sites of the pBabe.Hygro vector. Retrovirus was produced by calcium phosphate-mediated transfection of amphotropic Phoenix cells (Dr. Gary Nolan, Stanford University) with vector. Virus-containing media was harvested 24 and 48 hrs post-transfection and used to infect target cells, which were selected and maintained in 200  $\mu$ g/mL hygromycin. All expression and shRNA constructs were validated by sequencing.

#### *Wound closure assay*

A scratch was formed on confluent cell monolayers in 6-well plates using a pipet tip, and media was changed immediately thereafter. Phase contrast images were taken with a Zeiss Axiovert 40 CFL microscope (10X objective) every 1-3 hrs for up to 11 hrs. Open scratch areas were quantified using ImageJ, and closure rates were calculated from linear fits of scratch areas versus time and reported as percent of total image area closed per hr. For experiments with different pre-treatment conditions, cells were plated at appropriately modified densities such that all wells within an experiment reached confluence on the same day.

#### *Statistical analysis*

Statistical significance was determined using one- or two-way ANOVA in Kaleidagraph 4.0 (Synergy Software, Reading, PA). One-way ANOVA *p*-values were determined using Student-Newman-Keuls test for multiple comparisons in Kaleidagraph 4.0. Two-way ANOVA *p*-values were determined using the Bonferroni correction for multiple comparisons using the

GraphPad online QuickCalcs calculator for ANOVA  $p$ -values (GraphPad Software Inc., La Jolla, CA).

### 3-4 RESULTS

#### *EGF augments TGF $\beta$ -induced EMT*

To evaluate the EMT-inducing effects of TGF $\beta$  and EGF, H322 and H358 lung carcinoma cells and HPAF-II and CAPAN-2 pancreatic cancer cells were treated with EGF (50 ng/mL), TGF $\beta$  (10 ng/mL) or both ligands for 5 days (Fig. 3-1, 3-S1A,B). These cell lines were chosen because they display baseline epithelial characteristics [141-143] and represent common genotypes for their respective diseases – wild type *EGFR*, *RAS* and *RAF* for H322 and mutant *KRAS* for H358, HPAF-II, and CAPAN-2 [68, 143]. *SMAD4* participates in signaling directly downstream of the TGF $\beta$  receptors and the *SMAD4* gene is mutated or deleted in approximately 50% of pancreatic cancers. However, there are conflicting reports regarding whether *SMAD4* mutation promotes or antagonizes EMT [25, 26] and thus HPAF-II and CAPAN-2 cell lines were chosen for their wild-type *SMAD4* status to avoid interfering effects. TGF $\beta$  treatment reduced expression of the epithelial marker E-cadherin, increased expression of the mesenchymal marker vimentin, and altered cell morphology from cobblestone to more spindle-like in all cell lines (Fig. 3-1A,B). Although EGF produced a modest reduction in E-cadherin expression by itself, its combination with TGF $\beta$  led to significantly enhanced shifts in E-cadherin and vimentin expression and associated morphological changes compared to EGF or TGF $\beta$  alone in both H322 and HPAF-II.

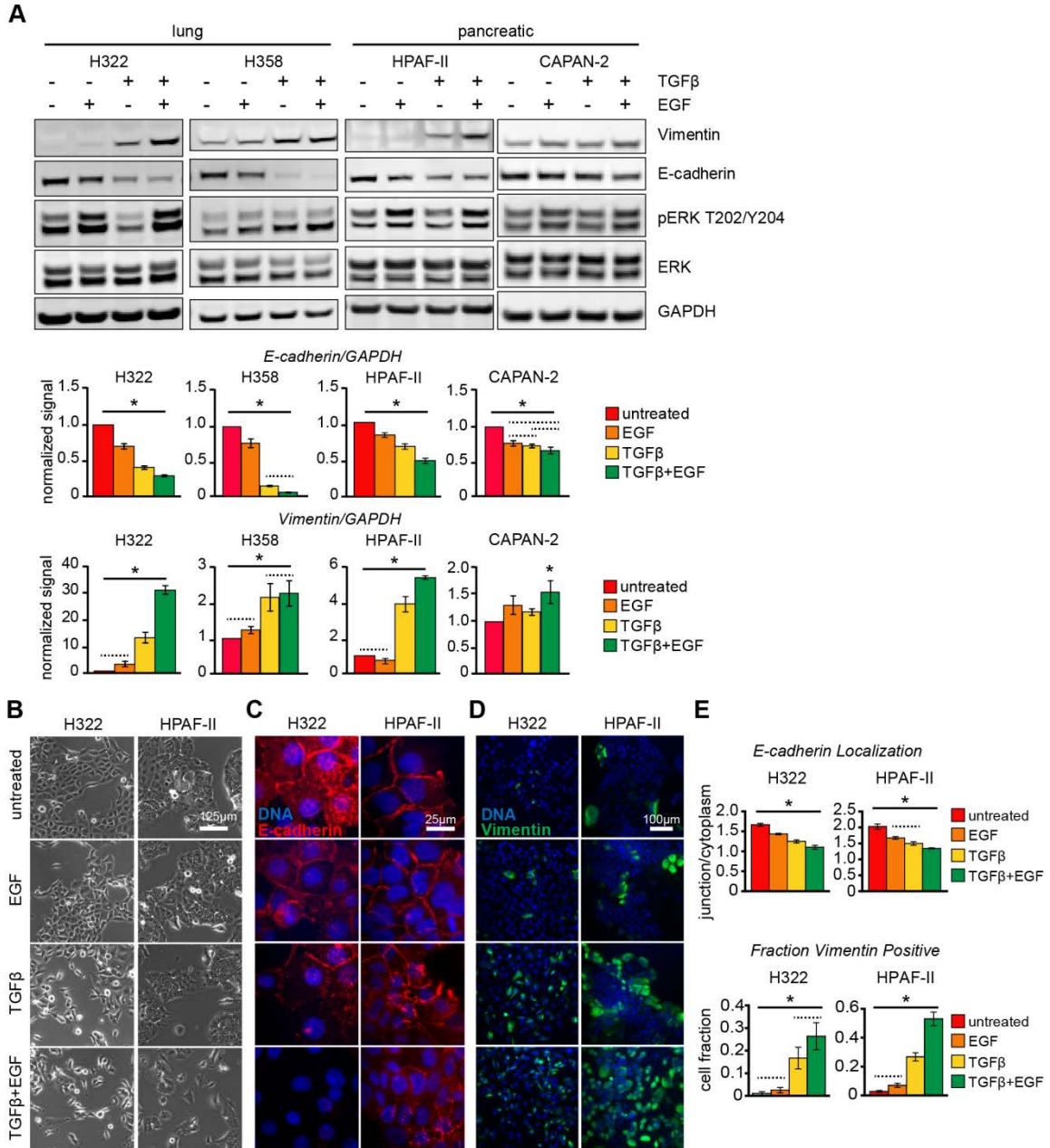


**Figure 3-1: EGF enhances TGF $\beta$ -mediated shifts in epithelial and mesenchymal marker expression.**

(A) H322, H358, HPAF-II, and CAPAN-2 cells were treated for 5 days with EGF (50 ng/mL), TGF $\beta$  (10 ng/mL), or both and lysates were analyzed by western blotting using antibodies against the indicated proteins. Densitometry data normalized to results from untreated samples are represented as mean  $\pm$  s.e.m. ( $n = 3$ ); \*  $p < 0.05$  for all pairwise comparisons unless indicated not significant (dotted line); for vimentin expression in CAPAN-2, only significant comparison is untreated vs. TGF $\beta$ +EGF. (B) H322 and HPAF-II cells were treated as in A and subsequently imaged by phase contrast microscopy. (C and D) H322 and HPAF-II cells were treated as in

panel A and stained for (C) E-cadherin and DNA or (D) vimentin and DNA. (E) Image quantification for replicate images from C and D were performed. E-cadherin localization quantification comparing the relative intensity at cell-cell junctions versus peri-junctional regions was calculated as described in *Materials and Methods Section 3-3* for all junctions within an image. The mean ratio per image was averaged for four images from each of two independent experiments ( $n = 8$ ). The percent of vimentin-positive cells was calculated as described in *Materials and Methods Section 3-3* for four images from each of two independent experiments ( $n = 8$ ). Data are represented as mean  $\pm$  s.e.m; \*  $p < 0.05$  for all pairwise comparisons except where indicated as not significant (dotted line).

Quantitative analysis of immunofluorescence staining for E-cadherin and vimentin in H322 and HPAF-II (Fig. 3-1C-E) confirmed the trends described in Fig. 3-1A and provided additional information at the individual cell level. Quantifying the ratio of E-cadherin staining at individual cell-cell junctions relative to junction-proximal regions demonstrated that the overall decrease in E-cadherin expression observed by western blot was accompanied by a delocalization of E-cadherin from cell-cell junctions in response to TGF $\beta$  with or without EGF. A similar E-cadherin localization analysis was used to support findings related to reduced cell adhesion [138, 139]. Analysis of vimentin staining revealed that the higher total levels of vimentin expression measured by western blot reflected an increased percentage of vimentin-positive cells within the population. These effects were most profound when EGF was combined with TGF $\beta$ . Of note, EGF addition results in robust activation of the ERK pathway, which is required for EMT in H322 and HPAF-II cells (Fig. 3-S1C, and [126]) and which TGF $\beta$  is unable to do on its own in these cells (Fig. 3-1A). Since EGF alone was unable to drive EMT despite high ERK phosphorylation, this ERK activation may be necessary but insufficient for EMT induction.

#### *EMT-associated changes in migration require TGF $\beta$ and EGF co-treatment*

Accompanying the shifts in adhesion and cytoskeletal protein expression, cells undergoing EMT often become more migratory and invasive [2]. We assessed the differential effects of TGF $\beta$  and/or EGF on cell scatter from clusters and on collective migration of cells grown in a monolayer for H322 and HPAF-II cells which displayed the greatest differential growth factor responses (Fig. 3-2). Weakening cell-cell junctions within preformed epithelial cell clusters

can lead to disrupted cluster circularity and scatter of cells away from these clusters [138]. These changes can be monitored by calculating a cluster circularity index (CI), calculated as  $4\pi(\text{area}/\text{perimeter}^2)$ , which has a value of 1 for a circle and a value of 0 for a line [139]. H322 and HPAF-II cell clusters containing ~10-20 cells were grown from individual cells and subsequently monitored for scatter and morphological changes over 24 hr in response to EGF, TGF $\beta$ , or both (Fig. 3-2A,B). Both H322 and HPAF-II cells displayed reduced CI over this time period, with the only statistically significant decreases observed for cells treated with both TGF $\beta$  and EGF.

In wound closure migration assays, H322 cells pre-treated for three days with EGF or TGF $\beta$  alone did not display enhanced migration (Fig. 3-2C). However, combining EGF and TGF $\beta$  for the three day treatment led to a 2.7-fold increase in the migration rate of H322 cells. This was accompanied by the appearance of individual cells migrating away from the cell sheet (arrowheads in the corresponding phase contrast image). In contrast, HPAF-II cells did not display enhanced migration in a monolayer for any of the ligand treatments (Fig. 3-2D). This may have occurred because of the reduced ability to observe EMT induction at the high cell density required for this monolayer assay in HPAF-II but not H322 (Fig. 3-S2). Notably, for changes in cell scatter in both H322 and HPAF-II and wound closure in H322, TGF $\beta$  did not produce a significant effect on its own, and the effect of combining EGF with TGF $\beta$  exceeded an additive effect of the single growth factor treatments. Thus, we observed that the addition of EGF to TGF $\beta$  promoted more complete shifts in marker expression and measurable changes in migration while also enhancing signaling through ERK (Figs. 3-1, 3-2).

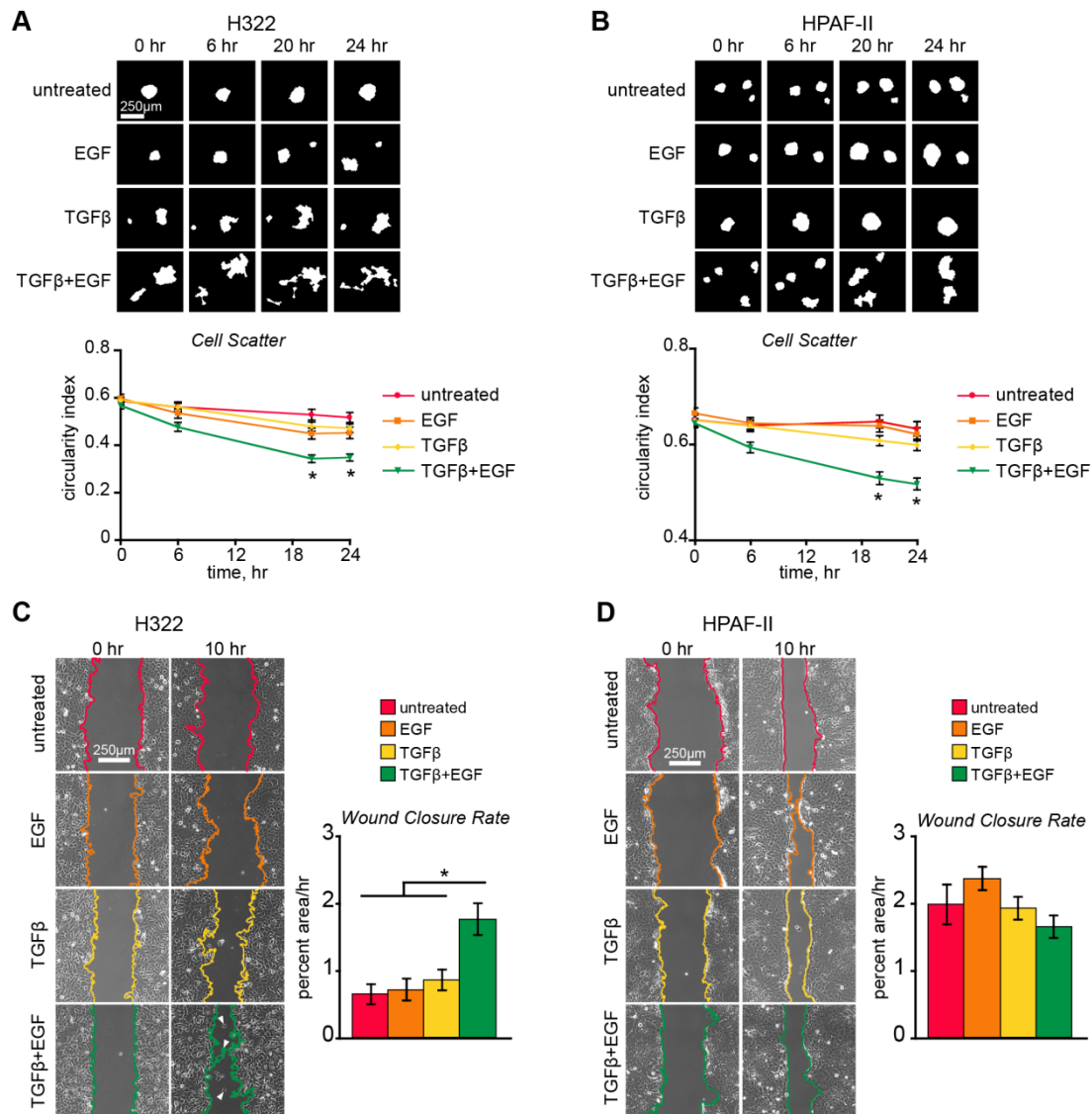


**Figure 3-2: EGF enhances cellular migration in response to TGFβ.**

(A) H322 and (B) HPAF-II cell clusters grown in 12-well plates from single cells were treated with EGF (50 ng/mL), TGFβ (10 ng/mL), or both and monitored for 24 hr for cell scatter. Silhouettes from MATLAB analysis of representative cell cluster images are shown. Circularity indices versus time for clusters from twelve frames per condition in each of three independent experiments were quantified as described in *Materials and Methods Section 3-3* and are reported as averages ± s.e.m. ( $n > 45$ ); \*  $p < 0.05$  for all comparisons with TGFβ + EGF. Wound closure rates were measured for (C) H322 cells treated for 3 days and (D) HPAF-II cells treated for 4 days with EGF (50 ng/mL), TGFβ (10 ng/mL), or both prior to scratch. Rates for triplicate wells from two different platings ( $n = 6$ ) are reported as averages ± s.e.m.; \*  $p < 0.05$  for all comparisons with TGFβ + EGF. Representative phase contrast images are shown, with tracings added to identify open scratch areas. White arrowheads indicate individual cells that migrated away from the cell monolayers into the open wound area.

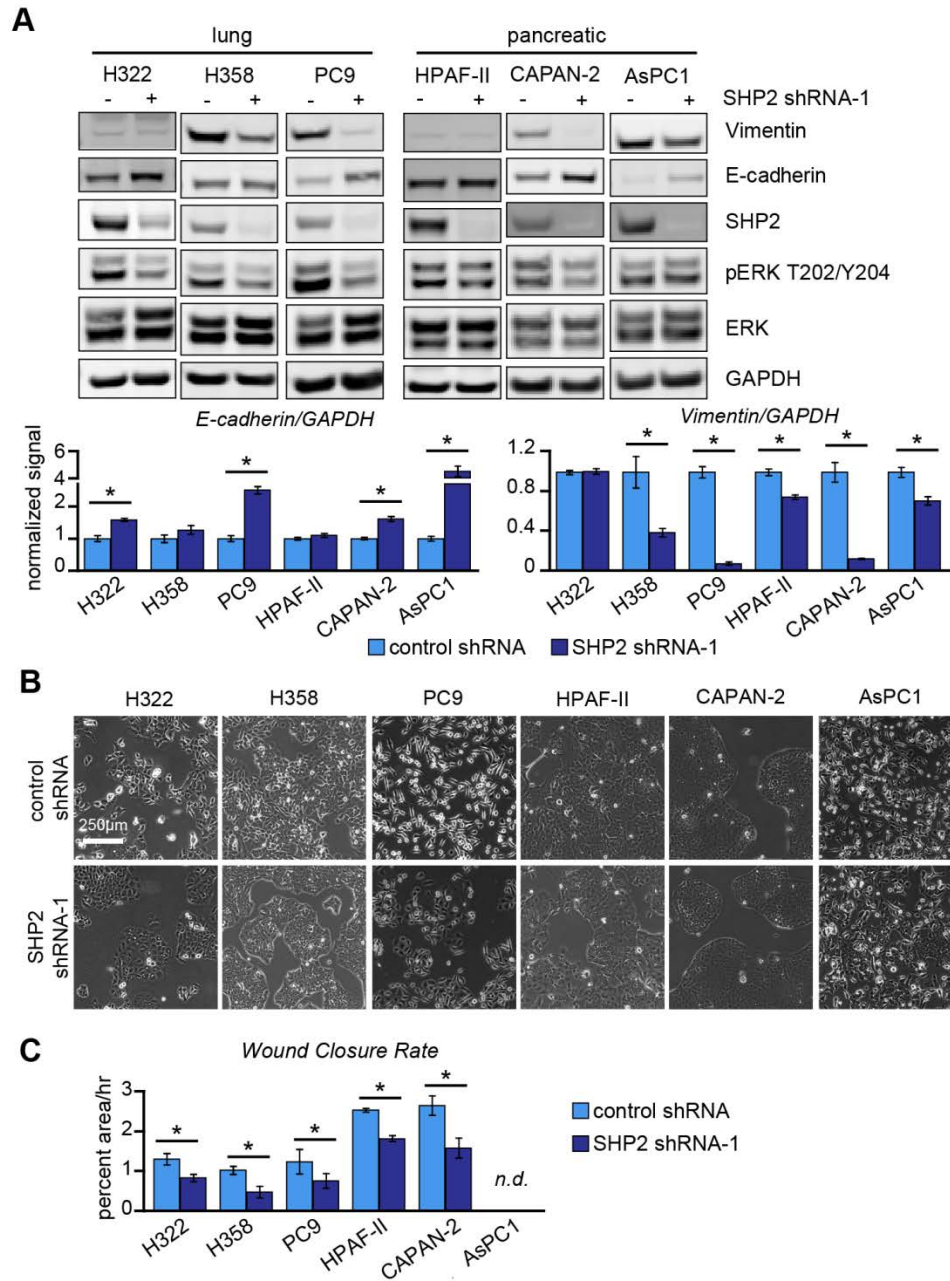


**Figure 3-3: SHP2 depletion promotes epithelial characteristics.**

SHP2-targeting shRNA (SHP2 shRNA-1) or a control shRNA was stably expressed in H322, H358, PC9, HPAF-II, CAPAN-2, and AsPC1 cells. **(A)** Cells expressing control or SHP2 shRNA-1 grown in complete medium were lysed and analyzed by western blotting using antibodies against the indicated proteins. Densitometry data normalized to control shRNA samples are represented as mean  $\pm$  s.e.m. ( $n = 3$ ); \*  $p < 0.05$ . **(B)** Representative phase contrast images of the same cells grown in complete medium are shown. **(C)** Wound closure rates were measured for the indicated cell lines expressing control or SHP2 shRNA-1 grown to confluence in complete medium for triplicate wells from two independent experiments ( $n = 6$ ) and are reported as averages  $\pm$  s.e.m.; \*  $p < 0.05$ ; no data (*n.d.*) for AsPC1 due to inability to form monolayer.

### *SHP2 knockdown enhances baseline epithelial characteristics*

Given the established importance of ERK activation in EMT induction, we assessed how SHP2, a positive regulator of ERK activity, contributes to EMT phenotypes, looking first at baseline cellular characteristics. SHP2 was depleted by stable shRNA expression in H322, H358, HPAF-II, and CAPAN-2 cells as well as one additional lung and pancreatic cancer cell line, PC9 and AsPC1, which display higher mesenchymal character at baseline (Fig. 3-3). Across these six cell lines SHP2 knockdown generally promoted E-cadherin expression and reduced vimentin expression (Fig. 3-3A). Importantly, SHP2 knockdown also reduced baseline ERK phosphorylation. Cells with SHP2 knockdown had increased cobblestone morphology compared to control shRNA cells, an effect that was especially apparent in PC9 and AsPC1, which typically display very spindle-like morphology with very few cell-cell contacts (Fig. 3-3B). These morphological and protein expression shifts toward epithelial characteristics were accompanied by corresponding decreases in migration of SHP2 knockdown cells compared to control (Fig. 3-3C). Thus, SHP2 knockdown promoted a mesenchymal-epithelial transition (MET) of cells grown in unstimulated conditions.

### *EMT induced by TGF $\beta$ with or without EGF is impaired by SHP2 knockdown*

We next evaluated how SHP2 knockdown impacted cellular response to TGF $\beta$  with or without EGF. SHP2 depletion inhibited induction of vimentin expression and reduction of E-cadherin expression in response to growth factor treatment in H322, H358, HPAF-II, and CAPAN-2 cell lines (Fig. 3-4A,B and 3-S3). This corresponded to impaired ERK phosphorylation in cells with SHP2 knockdown, which was most apparent in EGF treatment conditions. These western blot measurements were supported by immunofluorescence staining in H322 and HPAF-II (Fig. 3-4C,D). Cells with SHP2 depletion displayed some loss of total E-cadherin levels in response to TGF $\beta$  with or without EGF, but E-cadherin remained strongly maintained at cell-cell junctions. The appearance of a vimentin-positive cell population was significantly inhibited by SHP2 knockdown in both cell lines. Importantly, SHP2 depletion inhibited EMT induction in response to

TGF $\beta$  with or without EGF addition, indicating that the role of SHP2 in this setting extends beyond regulating only response to EGFR activation.

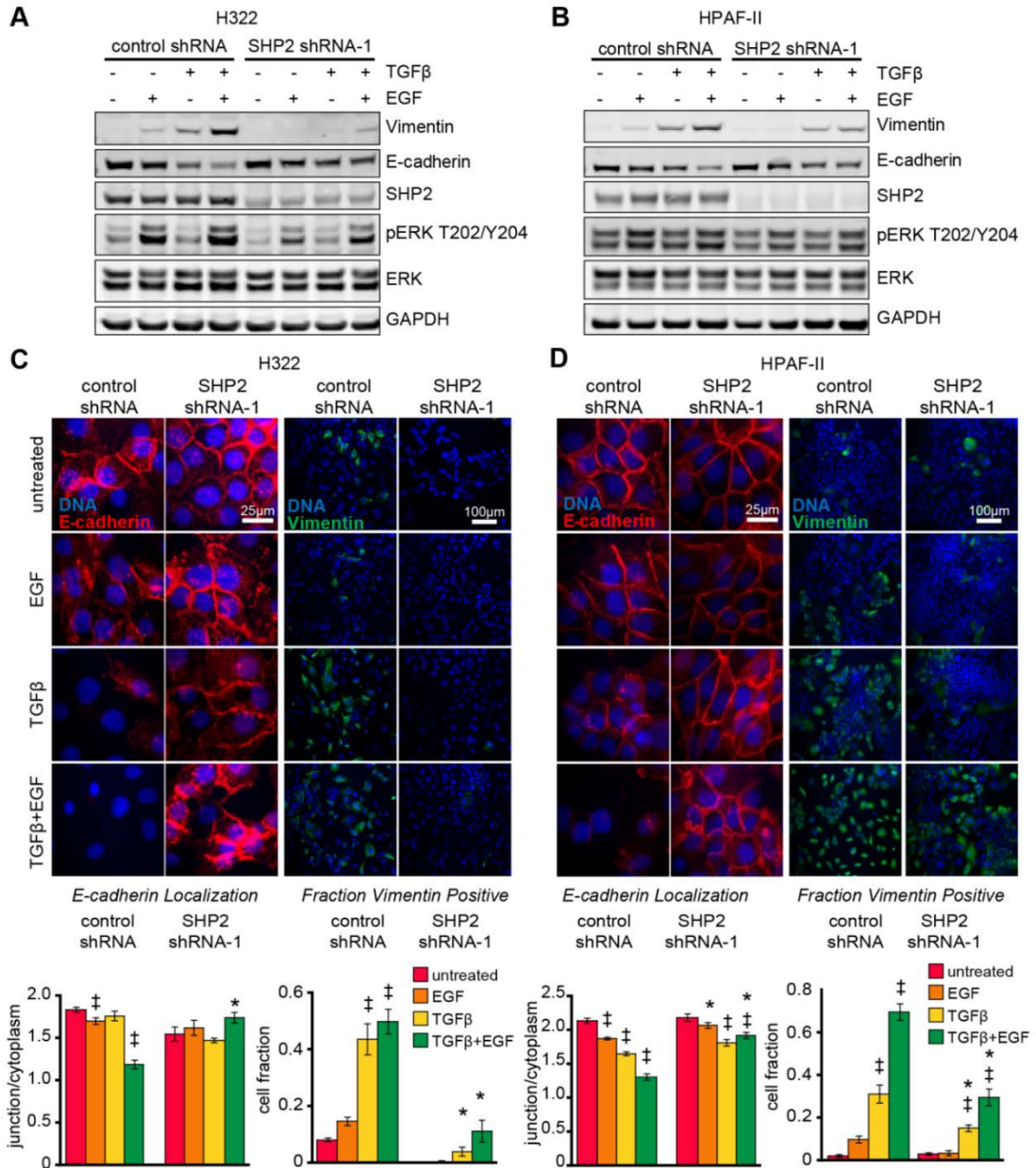


**Figure 3-4: SHP2 is required for TGF $\beta$ -mediated EMT effects and EGF-mediated EMT augmentation.**

(A) H322 and (B) HPAF-II cells expressing a control or SHP2-targeting shRNA (SHP2 shRNA-1) were treated with EGF (50 ng/mL), TGF $\beta$  (10 ng/mL), or both for 5 days and subsequently analyzed by western blotting with antibodies against the indicated proteins. Images are representative of three independent experiments. (C) H322 and (D) HPAF-II cells plated on glass

coverslips were treated as in panels A and B, fixed, and stained for E-cadherin or vimentin and DNA. Quantification of the relative E-cadherin intensity at cell-cell junctions versus peri-junctional regions was calculated as described in *Materials and Methods Section 3-3* for all junctions within an image. The mean ratio per image was averaged for four images from each of two independent experiments ( $n = 8$ ). The percent of vimentin-positive cells was calculated as described in *Materials and Methods Section 3-3* for four images from each of two independent experiments ( $n = 8$ ). Data are represented as mean  $\pm$  s.e.m; \*  $p < 0.05$  compared to control sample with same treatment,  $\neq p < 0.05$  compared to untreated sample from same cells.

#### *EGF and TGF $\beta$ differentially drive SHP2 association with phosphotyrosine-containing proteins*

The results of Figure 3-4 suggested an importance of SHP2 activity for EMT induction in response to TGF $\beta$  alone or the combination of TGF $\beta$  and EGF, which leads to high ERK activation and produces the greatest EMT. To assess the extent of induced SHP2 activity under conditions of varying EMT potential, we probed for SHP2 associations with phosphotyrosine containing proteins in response to EGF, TGF $\beta$ , or a combination of the two through SHP2 immunoprecipitation experiments (Fig. 3-5A). Since SHP2 binds to phosphotyrosine-containing proteins through its SH2 domains, which stabilizes an active SHP2 conformation, increased SHP2 phosphotyrosine binding generally correlates with increased SHP2 activity [133]. In response to EGF, a phosphotyrosine-containing protein of approximately 110 kDa co-immunoprecipitated with SHP2. This protein was confirmed to be GAB1 phosphorylated at Tyr<sup>627</sup>. SHP2 association with GAB1 was detected in samples from both H322 and HPAF-II cells treated with EGF and the strength of this association in response to EGF was insensitive to TGF $\beta$  addition. Interestingly, TGF $\beta$  itself did not drive any SHP2-phosphotyrosine associations. The 30 min treatment time for this experiment corresponded to observed phosphorylation of downstream signaling intermediates in response to EGF or TGF $\beta$  (Fig. 3-5B), suggesting that TGF $\beta$  had initiated signaling that did not involve SHP2 activation. Direct comparison of immunoprecipitates from H322, HPAF-II, and H358 demonstrated that the less significant effect of EGF on enhancing TGF $\beta$ -mediated EMT in H358 was associated with the lowest levels of EGF-induced GAB1-SHP2 association compared to the other cell lines (Fig. 3-S4).

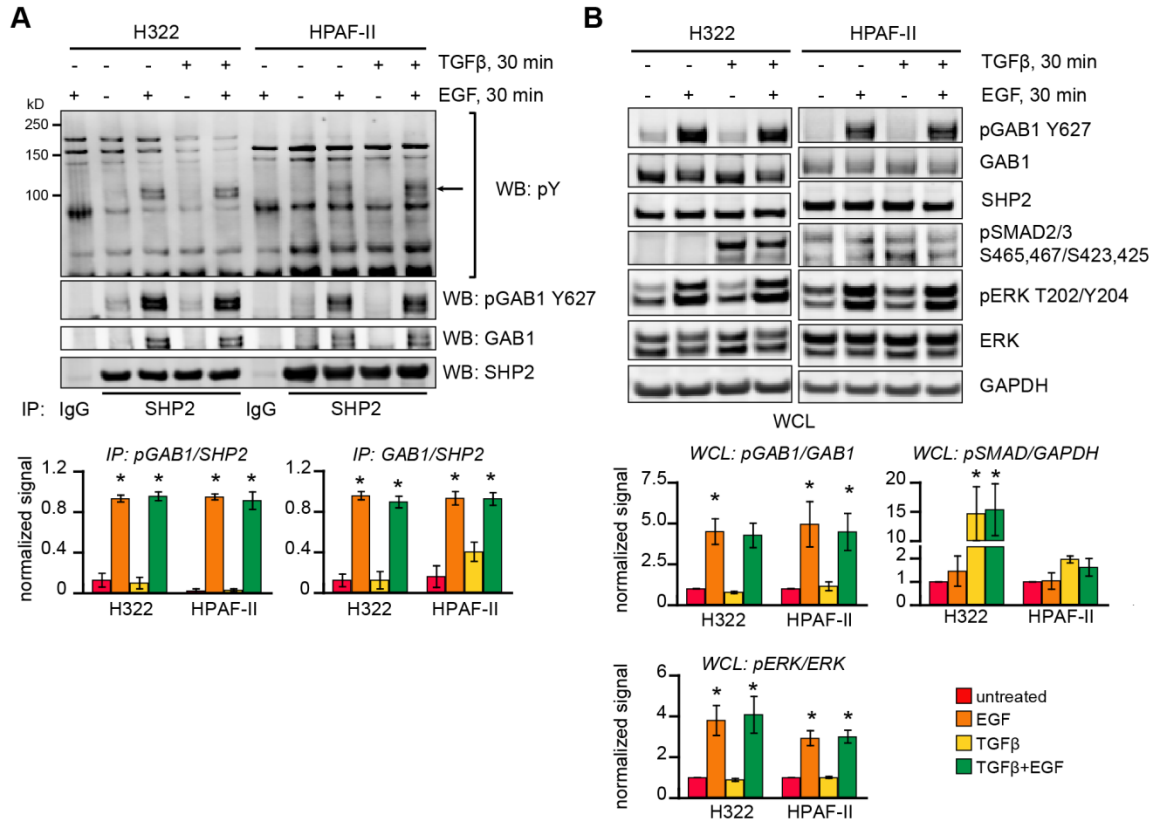


**Figure 3-5: EGF, but not TGFβ, promotes SHP2 association with phosphotyrosine-containing proteins.**

(A) SHP2 or IgG control immunoprecipitates from serum starved H322 and HPAF-II cells treated for 30 min with EGF (50 ng/mL), TGFβ (10 ng/mL), or both were analyzed by western blotting using antibodies against the indicated proteins. Arrow indicates phosphorylated GAB1 detected with total phospho-tyrosine (pY) antibody. Densitometry data normalized to maximum value are represented as mean ± s.e.m. ( $n = 3$ ); \*  $p < 0.05$  compared to untreated sample from same cells. (B) Whole cell lysates (WCL) were analyzed by western blotting using antibodies against the indicated proteins. Images are representative of three independent experiments. Densitometry data normalized to results from untreated samples are represented as mean ± s.e.m. ( $n = 3$ ); \*  $p < 0.05$  compared to untreated sample from same cells.

*SHP2 SH2-domain engagement by phosphotyrosines is essential for EGF-mediated augmentation of EMT*

The observations that EMT depended on SHP2, which was activated by EGF but not TGFβ, and that EGF augmented TGFβ-driven EMT outcomes suggested that EGF-induced SHP2 activation may be responsible for its ability to augment EMT. Since TGFβ alone drove SHP2-dependent EMT without inducing SHP2-phosphotyrosine binding, this also suggested that basal

SHP2 activity was sufficient for some degree of EMT. To test this model for the contribution of SHP2 binding to phosphotyrosine-containing proteins in EMT, we reconstituted cells with knockdown of endogenous SHP2 with either wild type SHP2 or the double SH2-domain mutant SHP2<sup>R32,138K</sup>. For these experiments, knockdown of endogenous SHP2 was accomplished using two shRNA sequences targeting the 3' untranslated region (UTR) of *SHP2* (SHP2 shRNA-2&3) in HPAF-II cells to allow for RNAi-resistant reconstitution using SHP2 constructs not containing the UTRs (Fig. 3-S3, 3-6). The R-K mutations antagonize the ability of SHP2 SH2 domains to bind phosphotyrosines downstream of SHP2-activating stimuli [134, 135]. In HPAF-II cells, SHP2<sup>WT</sup> reconstitution rescued the ability of TGFβ, with or without EGF, to induce E-cadherin loss and vimentin increase (Fig. 3-6A). Cells with SHP2<sup>R32,138K</sup> reconstitution, however, responded more closely to cells with knockdown, displaying E-cadherin maintenance and impaired vimentin induction in response to TGFβ and EGF. Though ERK phosphorylation rebounded in shRNA-2&3 cells with empty-vector control relative to shRNA-2&3 only, cells with SHP2<sup>R32,138K</sup> reconstitution displayed significant impairment of ERK phosphorylation, which was associated with impaired EMT induction (Fig. 3-6A, 3-S3). Immunofluorescence confirmed that SHP2<sup>R32,138K</sup> reconstitution impaired shifts in E-cadherin and vimentin expression in response to TGFβ with and without EGF compared to cells with SHP2<sup>WT</sup> reconstitution (Fig. 3-6B). Immunoprecipitation experiments confirmed that SHP2<sup>R32,138K</sup> did not associate with tyrosine phosphorylated proteins in response to EGF treatment (Fig. 3-6C). Thus, the ability of SHP2 to promote EMT in response to exogenous ligands depends upon SHP2 engagement of phosphotyrosine residues on cognate adaptor proteins such as GAB1, and the complete EMT observed when EGF and TGFβ were combined was due to SHP2 activation driven by EGF specifically.

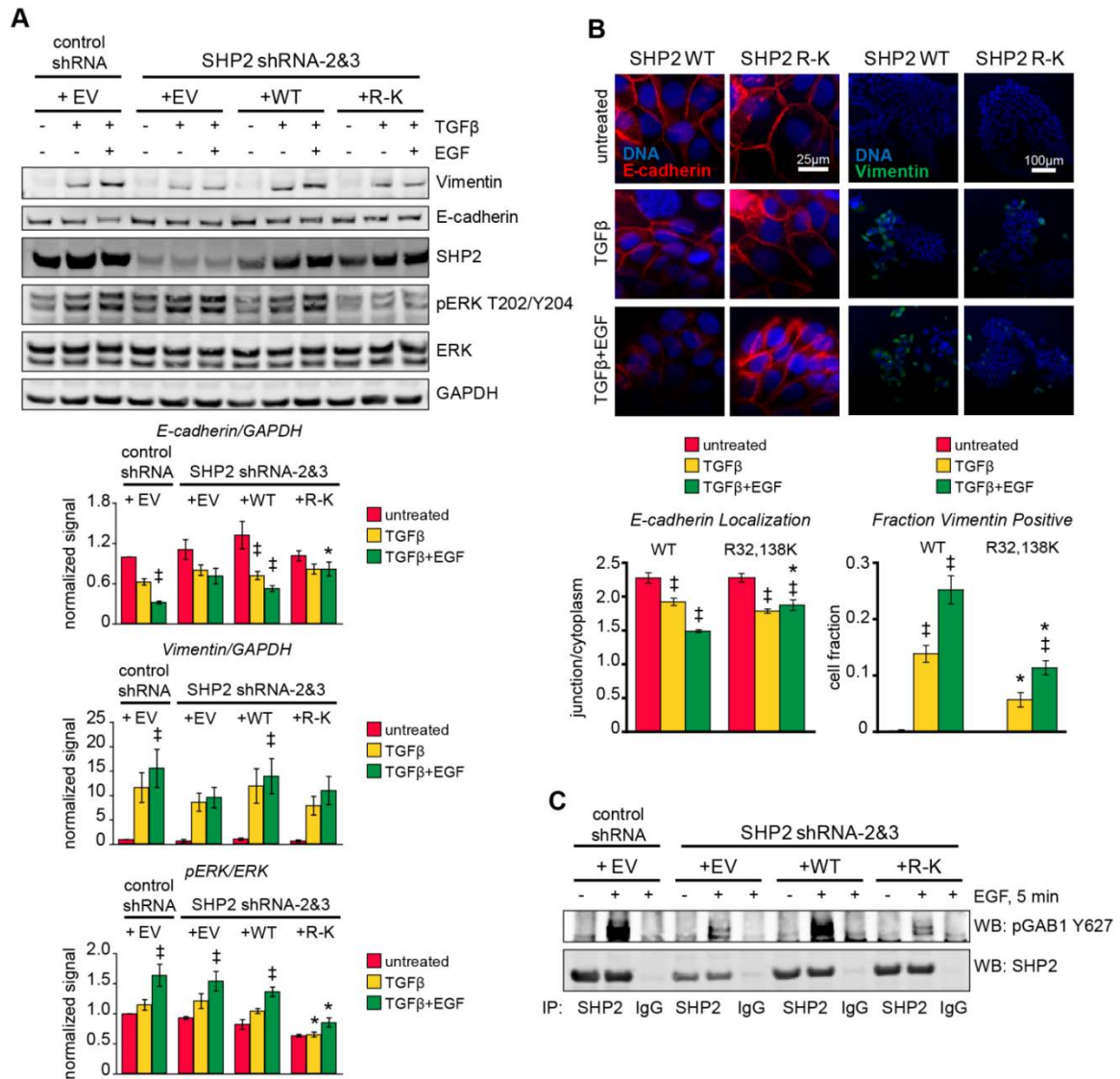


**Figure 3-6: SHP2 SH2 domain binding to phosphotyrosines is required for SHP2-mediated EMT effects.**

HPAF-II cells expressing control shRNA or two shRNAs targeting the 3' untranslated region of the human *SHP2* transcript (SHP2 shRNA-2&3) were transduced with an empty pBabe vector (EV) or pBabe vector encoding *SHP2*<sup>WT</sup> (WT) or *SHP2*<sup>R32,138K</sup> (R-K). (A) Cells treated for 5 days with TGFβ (10 ng/mL) with or without EGF (50 ng/mL) were lysed and analyzed by western blotting using antibodies against the indicated proteins. Western blot images are representative of four independent experiments. Densitometry data are represented as mean ± s.e.m. ( $n = 4$ ); \*  $p < 0.05$  compared to control + EV sample with same treatment, †  $p < 0.05$  compared to untreated sample of same cells. All significant comparisons are shown. (B) The same cells plated on coverslips were treated as in panel A and stained for E-cadherin or vimentin and DNA. E-cadherin staining quantification comparing the relative intensity at cell-cell junctions versus perijunctional regions was calculated as described in *Materials and Methods Section 3-3* for all junctions within an image. The mean ratio per image was averaged for four images from each of two independent experiments ( $n = 8$ ). The percent of vimentin-positive cells was calculated as

described in *Materials and Methods Section 3-3* for four images from each of two independent experiments ( $n = 8$ ). Data are represented as mean  $\pm$  s.e.m; \*  $p < 0.05$  compared to SHP2<sup>WT</sup> sample with same treatment, †  $p < 0.05$  compared to untreated sample of same cells. All significant comparisons are shown. (C) SHP2 or IgG control immunoprecipitates from serum starved cells treated for 5 min with EGF (50 ng/mL) were analyzed by western blotting using antibodies against the indicated proteins. Images are representative of three independent experiments.

### 3-5 DISCUSSION

Our results identify for the first time a mechanism wherein SHP2 SH2 domain engagement of a phosphotyrosine-containing protein contributes to EMT and thus uncovers a new aspect of the well-documented ability of EGF to augment the EMT that occurs in response to TGF $\beta$ , as summarized in Figure 3-7. In our proposed model, TGF $\beta$  binding to its receptors activates some pathways that promote a partial EMT but does not elevate SHP2 activity above its low basal level. The low basal activity of SHP2 nonetheless plays a role in EMT driven by TGF $\beta$  alone. When EGF is combined with TGF $\beta$ , GAB1 becomes tyrosine phosphorylated and SHP2 SH2 domain engagement by phosphorylated GAB1 increases SHP2 activity, promoting stronger EMT induction. EGF-mediated activation of SHP2 is not sufficient for strong EMT induction without the additional signaling processes driven by TGF $\beta$ .

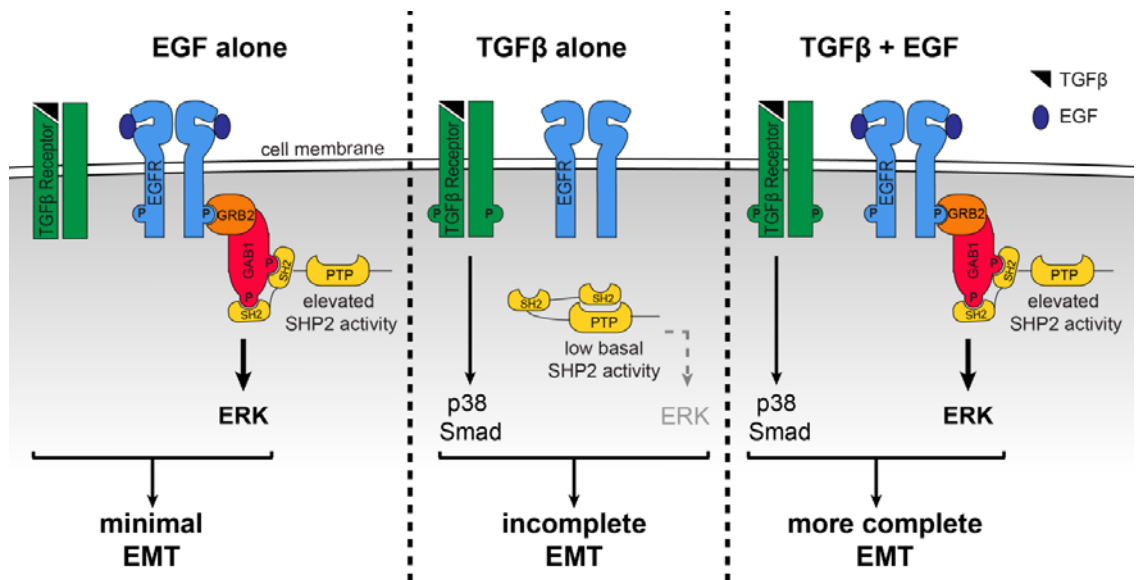


**Figure 3-7: Schematic summary of the role of SHP2 in promoting EMT.**

EGF alone efficiently drives SHP2 and ERK activation, but without concomitant TGF $\beta$ -mediated signaling, minimal EMT is driven. In the presence of TGF $\beta$  alone, cells undergo an incomplete EMT due to activation of pathways including p38 and SMADs, while ERK and SHP2 activities remain at low basal levels. When EGF is combined with TGF $\beta$ , EGFR activation leads to GAB1 phosphorylation and binding to SHP2, which promotes SHP2 activity. SHP2 activation augments ERK activity and drives stronger EMT-related shifts in marker expression, cell morphology, and migratory phenotypes.

Previous work has established that EGFR activation enhances TGF $\beta$ -mediated EMT [55-57]. We analyzed that effect in detail here in terms of expression and localization of the prototypical epithelial and mesenchymal markers E-cadherin and vimentin, respectively, and through cellular migration measurements. In all cases, EGF addition to TGF $\beta$  augmented the EMT-associated effects observed, and in some cases no effect was observed with TGF $\beta$  alone. Other studies have linked the presence of exogenous or autocrine-released growth factors including HGF [11], oncostatin-M [11], PDGF [144], and IL-6 [35] to enhanced TGF $\beta$ -mediated effects. Signaling downstream of many of these ligands involves SHP2, but it is unclear if SHP2 participates in the augmented EMT that accompanies the combination of these ligands with TGF $\beta$ .

Another effect uncovered in this study was the cell line-dependent ability of high cell density to inhibit EMT induction. Specifically, EMT induction in the pancreatic carcinoma cell line HPAF-II was completely inhibited at high plating densities, whereas the lung carcinoma cell line H322 showed no such dependence. Previous work in the human keratinocyte cell line HaCaT showed that high cell density significantly impaired TGF $\beta$ -induced formation of nuclear SMAD3-SMAD4 complexes [145]. Recent investigation by Nallet-Staub and colleagues also captured the density dependence of SMAD nuclear localization in HaCaT cells, but intriguingly not all cell lines displayed this density effect [146]. The effect of cell density on EMT induction may be particularly important *in vivo* where cellular environments correspond to 'high density', though microenvironmental cues not present *in vitro* may enable cells to escape the inhibitory effect of high cell density for EMT induction. Within the SMAD pathway, it will also be informative to evaluate the effect of *SMAD4* deletion and mutation, which is present in approximately 50% of pancreatic carcinomas [147], on the TGF $\beta$  and EGF-mediated effects reported here. HPAF-II and CAPAN-2 are both *SMAD4* wild-type, whereas AsPC1 has a *SMAD4* mutation. Though all three cell lines demonstrated SHP2-dependent mesenchymal traits, concrete determination of the role of *SMAD4* in EMT will require further studies in an isogenic cell background

Based on our previous work and evidence from other studies demonstrating the importance of ERK activation in EMT [93, 126], SHP2-mediated augmentation of ERK activity is likely to be a critical factor in SHP2-mediated effects on EMT. Though ERK pathway regulation by SHP2 is important downstream of EGFR, SHP2 contributes to many other signaling processes, some of which may have relevance to EMT induction. For example, SHP2 has been shown to dephosphorylate focal adhesion kinase (FAK) at the leading edge of a cell to promote focal adhesion turnover [148]. Through regulating FAK and other components of focal adhesions SHP2 promotes cellular migration, polarity, and mechanical sensing [148, 149], phenotypes with clear connections to EMT. Other work demonstrated that inhibiting or stably depleting FAK inhibits TGF $\beta$ -driven signaling, EMT induction, and tumorigenesis in mice [150]. We recently described a mechanism by which EGFR activation leads to formation of SHP2-GAB1 complexes that can remain associated distal from the receptor [151]. In the mechanism we identified, Src family kinases (SFKs) served as effectors activated by EGFR that maintained GAB1 phosphorylation, and therefore GAB1-SHP2 complexes, distal from EGFR through multiple rounds of GAB1-SHP2 dissociation and tyrosine dephosphorylation. Others have identified SFKs as necessary intermediates for EGFR-dependent TGF $\beta$ -mediated transformation [55, 56], a finding which could be related to the ability of SFKs to promote SHP2 activation via GAB1 phosphorylation and GAB1-SHP2 complex formation.

Of course, a role for SHP2 driving EMT is consistent with its identification as a proto-oncogene and the concept of SHP2 as a driver of malignancy and therapeutic resistance. SHP2-activating mutations occur in cancers including juvenile myelomonocytic leukemia, acute myelogenous leukemia, and lung and colon carcinomas, as well as Noonan syndrome, a developmental disorder leading to increased risk of certain malignancies [81, 152]. In mouse tumor xenograft studies of breast and brain cancer cells, SHP2 promotes tumorigenesis [82, 83]. SHP2 activity also contributes to cellular resistance to EGFR inhibition in non-small cell lung carcinoma cells [75]. These and other findings provide continued motivation for the ongoing search for specific inhibitors of SHP2. New strategies developing SHP2 inhibitors that target

allosteric binding sites unique to SHP2 have shown promise toward achieving SHP2 specificity [153, 154]. Therapies developed using such strategies would have promise in many diseases based on the evidence above. In particular, our findings suggest SHP2 may be a potential target for reversing the mesenchymal dedifferentiation process in malignant tumor cells through chronic inhibition prior to administration of another targeted cancer therapeutic, analogous to a strategy we described previously wherein chronic ERK inhibition led to enhanced EGFR inhibitor response in NSCLC cells [126].

### **3-6 ACKNOWLEDGEMENTS**

The authors thank Drs. Carl June, Pasi Jänne, Douglas Lauffenburger, and Russ Carstens for providing cells and thank Dr. Ben Neel for providing SHP2 DNA constructs. JMB was supported by the National Science Foundation (NSF) Graduate Research Fellowship (DGE-08220) and by NSF CBET Award 1450751.

### 3-7 SUPPLEMENTAL MATERIAL

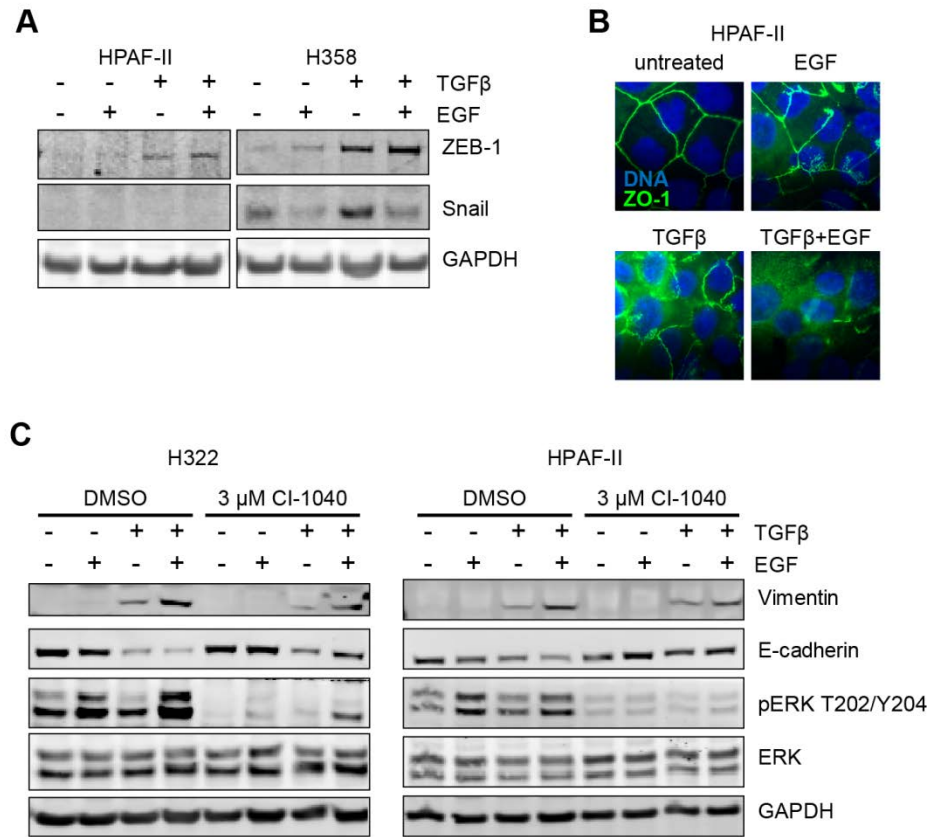


**Figure 3-S1**

(A) HPAF-II and H358 cells were treated for 5 days with EGF (50 ng/mL), TGF $\beta$  (10 ng/mL), or a combination of the two ligands and lysates were analyzed by western blot using antibodies against the indicated proteins. (B) HPAF-II cells were treated as in A and stained for ZO-1 and DNA. (C) H322 and HPAF-II cells were treated for 5 days with EGF (50 ng/mL), TGF $\beta$  (10 ng/mL), or a combination of the two ligands and 3  $\mu$ M CI-1040 (a MEK inhibitor) or DMSO as a control. Lysates were analyzed by western blotting with antibodies against the indicated proteins.

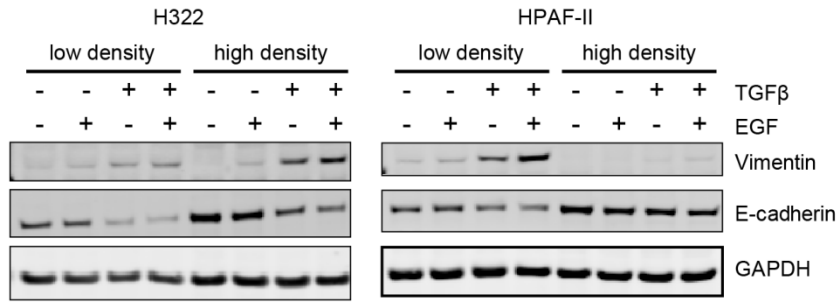


**Figure 3-S2.**

H322 and HPAF-II cells were plated at low (50,000 cells/well) and high ( $\geq 300,000$  cells/well) densities in 6-well plates, and treated 24 hr later with EGF (50 ng/mL), TGFβ (10 ng/mL), or a combination of the two ligands. The low and high densities reflect the plating conditions used for western blotting experiments and wound closure assays, respectively. Cells were lysed after 3 days of treatment with ligands and analyzed by western blotting using antibodies against the indicated proteins.

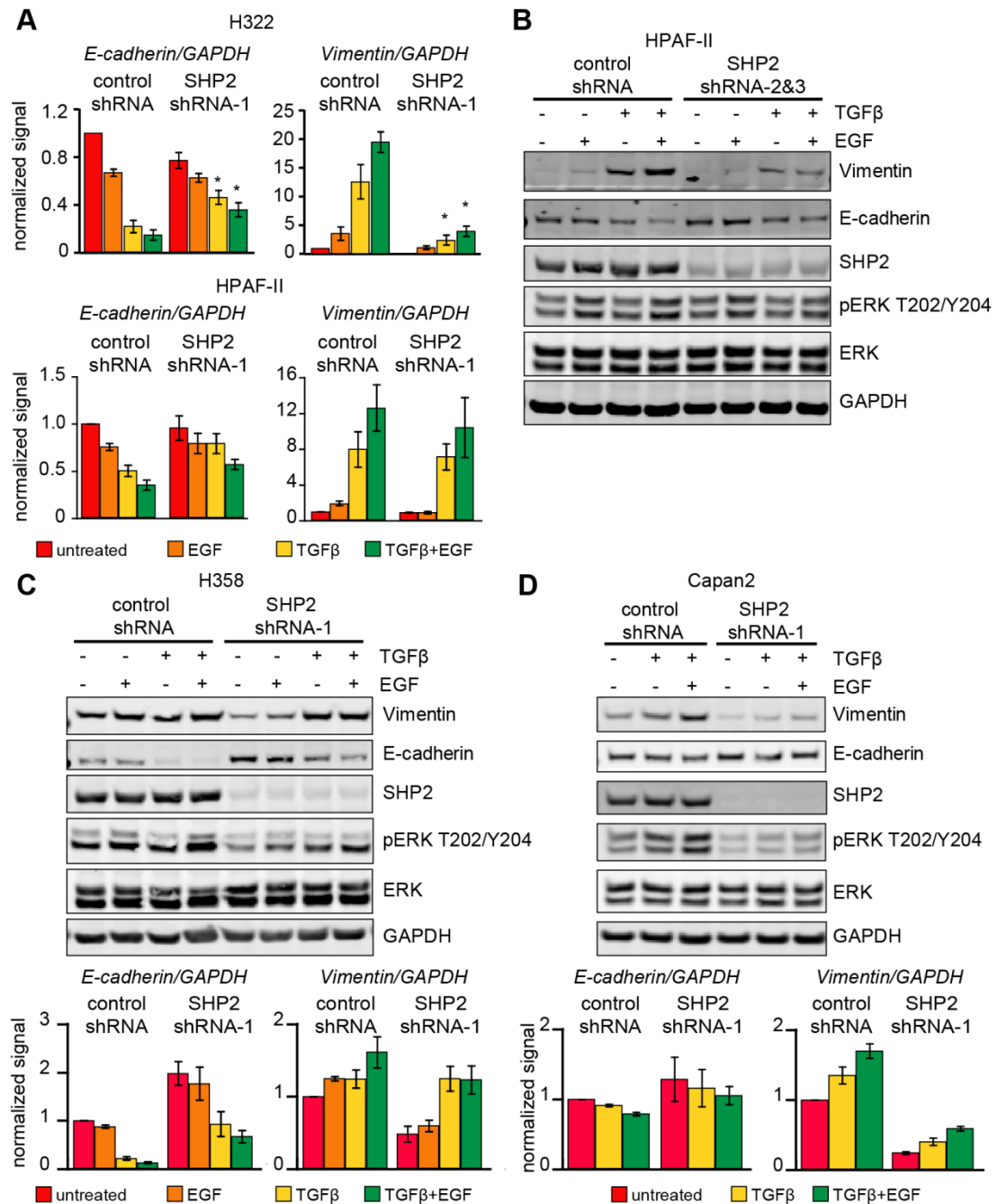


**Figure 3-S3.**

(A) H322 and HPAF-II cells expressing control shRNA or SHP2-targeting shRNA (SHP2 shRNA-1) were treated with EGF (50 ng/mL), TGFβ (10 ng/mL), or both for 5 days and subsequently analyzed by western blotting. Densitometry data normalized to untreated control cells are represented as mean ± s.e.m. ( $n = 3$ ); \*  $p < 0.05$  compared to control sample with same treatment. (B) HPAF-II cells expressing a control shRNA or two independent shRNAs targeting the 3' untranslated region of the human SHP2 transcript (SHP2 shRNA-2&3) were treated as in

panel A. Lysates were analyzed by western blotting with antibodies against the indicated proteins. Images are representative of three independent experiments. (C) H358 (D) and CAPAN-2 cells expressing control shRNA or SHP2-targeting shRNA (SHP2 shRNA-1) were treated with EGF (50 ng/mL), TGF $\beta$  (10 ng/mL), or both for 5 days and subsequently analyzed by western blotting. Densitometry data normalized to untreated control cells are represented as mean  $\pm$  s.e.m. ( $n = 3$ ).

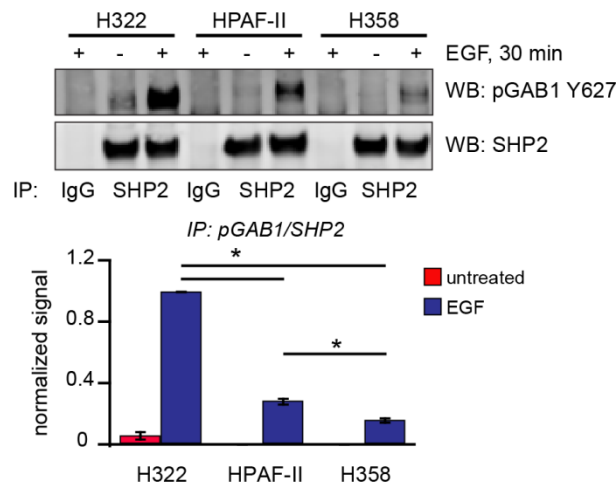


**Figure 3-S4: SHP2 knockdown with UTR-targeting hairpins inhibits EMT induction.**

SHP2 or IgG control immunoprecipitates from serum starved H322, HPAF-II, and H358 cells treated for 30 min with EGF (50 ng/mL) were analyzed by western blotting using antibodies against the indicated proteins. Densitometry data normalized to maximum value are represented as mean  $\pm$  s.e.m. ( $n = 3$ ); \*  $p < 0.05$ .

# CHAPTER 4: A Partial Least Squares Regression Analysis Identifies Cell Signaling Events Regulating Epithelial- Mesenchymal Transition<sup>3</sup>

## 4-1 ABSTRACT

Epithelial-mesenchymal transition (EMT) is a cellular process hijacked in many cancers to drive metastasis and increased resistance to therapy, motivating efforts to understand the cellular processes controlling EMT induction. In particular, the roles of specific signaling pathways controlling EMT induction have been described in some cases, but it is clear that EMT results from integration of multivariate signaling through many pathways. To provide a more complete understanding of EMT induction with an appreciation for this network integration, we performed a systematic analysis of the cell signaling processes that regulate EMT in pancreatic cancer cells. Our approach relies upon the development of a partial least squares regression (PLSR) statistical model to predict the relationships between multivariate signaling events and EMT-associated phenotypes, using a cell culture model of EMT induction in response to transforming growth factor beta, epidermal growth factor, and hepatocyte growth factor alone or in various combinations. In our model, quantitative protein phosphorylation measurements were combined with phenotypic measurements of EMT marker expression and measurements of cell migration. The results of our validated statistical model will be used to rationally identify signaling nodes whose inhibition will antagonize or reverse EMT. Such signaling nodes would be candidate therapeutic targets whose inhibition may slow tumor metastasis or promote tumor cell sensitivity to therapy.

---

<sup>3</sup> Chapter 4 was completed as part of a collaboration with co-authors Erica L. Carpenter and Stephanie S. Yee

## 4-2 INTRODUCTION

Pancreatic cancer is the fourth-leading cause of cancer deaths in the United States, with an estimated 5-year survival rate of only 4% [155]. This poor prognosis is due in part to a combination of low rates of surgically resectable tumors at diagnosis and overall poor response to chemotherapeutic agents [155]. Despite significant advances in molecular and pathological characterization of pancreatic tumors and development of molecularly-targeted therapies, there has been little translation of these advancements to predicting patient outcomes [156]. Identifying strategies to revert tumor malignancy and enhance therapeutic response are needed to improve pancreatic cancer prognosis. Here we describe the generation of a data-driven statistical model to identify key regulators of epithelial-mesenchymal transition (EMT), a cellular process that contributes to malignant progression and therapeutic resistance in many cancers.

EMT is a cellular program engaged during normal development and wound healing in which epithelial cells, such as those lining pancreatic ducts, lose apical-basal polarity and strong cell-cell adhesions to partially dedifferentiate becoming more motile and invasive [1-3]. EMT can be monitored through loss of epithelial markers, such as E-cadherin, and increased expression of mesenchymal markers such as vimentin. While EMT is required for normal development and wound healing [3], aberrant EMT has also been linked to metastasis [123] and has been observed to occur from pre-cancerous pancreatic lesions to promote metastasis during cancerous progression [21], suggesting clinical relevance for EMT at the earliest stages of pancreatic cancer. EMT has emerged as a common predictor of poor prognosis in pancreatic cancer and other carcinomas [24]. Additionally, EMT is associated with therapeutic resistance in pancreatic cancer cells [32, 125], as well as other cancer types [25, 29, 30, 33]. Promoting an epithelial cellular phenotype can confer enhanced therapeutic response [104, 126].

EMT is efficiently driven *in vitro* and *in vivo* by transforming growth factor- $\beta$  (TGF $\beta$ ) [4], a ligand which initiates signaling through a network of pathways including SMADs, extracellular signal-regulated kinase-1/2 (ERK1/2), p38, and c-Jun N-terminal kinase (JNK) [46, 47]. Multiple studies have indicated that activation of ERK1/2 [14, 45, 126], p38 [157], or nuclear factor kappa-

light-chain-enhancer of activated B cells (NF $\kappa$ B) [158] signaling are necessary for EMT induction in different cell types, but little work has assessed the impact of multivariate pathway integration. In addition to TGF $\beta$ , other growth factors such as epidermal growth factor (EGF) [53] and hepatocyte growth factor (HGF, the ligand for c-MET receptor) [11, 159] can induce EMT on their own or be combined with TGF $\beta$  to enhance EMT induction [11-14, 57]. These growth factors are known to promote signaling through their own defined networks that share certain common elements among them (e.g., ERK pathway activation by each EGF [160], HGF [161], and TGF $\beta$  [47]). The dynamics, strength, and balance of signaling events within each network, however, are distinct to each growth factor, and such differences can influence phenotype determination [162].

High throughput analysis of signaling dynamics in response to EGF, HGF, and TGF $\beta$  could reveal unique and overlapping elements to each network, but synthesizing this information to determine the key factors determining cellular outcome cannot be achieved by inspection. Instead, a systematic and unbiased approach is needed to quantitatively evaluate which signaling measurements are most predictive of resulting cellular phenotype. Partial least squares regression (PLSR) is a statistical modeling technique popularized in the field of chemometrics [163, 164] that has been adapted in multiple areas of study to integrate large multivariate data sets to identify key variables determining system outputs. In particular, systems biology approaches to understand how cell signaling impacts phenotype determination have employed PLSR modelling [102, 165, 166]. For example, previous work has identified network 'signatures' predictive of migration and proliferation in response to growth factor treatments [167] or expression of the EGFR-family member HER2 [166]. These approaches, however, have not yet been utilized to relate the extent of EMT induction in response to various stimuli to the activation of key signaling components.

Here we characterize the quantitative changes in EMT-associated phenotypic measures in response to EGF, HGF, TGF $\beta$ , and the combinations TGF $\beta$ +EGF and TGF $\beta$ +HGF in the pancreatic cancer cell line HPAF-II. HGF produced the greatest EMT of any single ligand and its combination with TGF $\beta$  produced the greatest EMT overall. EMT was measured by quantitative

western blotting for E-cadherin and vimentin, image analysis for protein localization, and cellular migration assays. A phosphoprotein antibody microarray was used in a screen to identify proteins involved in EMT response. Hits from this screen were combined with signaling intermediates with known roles in growth factor-dependent EMT to form a panel of 45 proteins for quantitative analysis by Luminex and western blotting. Protein phosphorylation across this panel was measured at five time points in response to the growth factor treatments and a PLSR model was built using these profiles to predict EMT responses. PLSR analysis revealed protein phosphorylation events that are most associated with EMT induction and provided potential targets for inhibiting mesenchymal dedifferentiation.

### **4-3 MATERIALS AND METHODS**

#### *Cell culture and reagents*

HPAF-II cells (Dr. Carl June, University of Pennsylvania) were maintained in RPMI supplemented with 10% FBS, 1 mM L-glutamine, 100 units/mL penicillin, and 100 µg/mL streptomycin. Cell culture reagents were from Life Technologies (Carlsbad, CA). Recombinant human EGF, HGF, and TGFβ were purchased from Peprotech (Rocky Hill, NJ). In all experiments, growth factor concentrations were 50 ng/mL for EGF and HGF and 10 ng/mL for TGFβ. During treatment, media containing growth factors was replenished every 48 hr.

#### *Antibodies*

pERK T202/Y204 (4377), ERK (4695), pSTAT3 Y705 (9145), pALK Y1604 (3341), p-p38 T180/Y182 (4511), and pSMAD2 S465/467/pSMAD3 S423/425 (8828) antibodies were from Cell Signaling Technology (Danvers, MA). E-cadherin (sc-8426), vimentin (sc-373717), and GAPDH (sc-32233) antibodies were from Santa Cruz Biotechnology (Dallas, TX). pSRC Y418 (44660G) was from Life Technologies. p-p27/Kip1 T157 (AF1555) was from R&D Systems (Minneapolis, MN). Phosphotyrosine antibody (4G10) was from Millipore (Billerica, MA). Infrared dye- and Alexa Fluor®-conjugated secondary antibodies were from Rockland Immunochemicals (Gilbertsville, PA) and Life Technologies, respectively.

#### *Western blotting*

Whole cell lysates were prepared in a standard cell extraction buffer (Life Technologies) supplemented with protease inhibitors and phosphatase inhibitors (Sigma-Aldrich, St. Louis, MO). Lysates were cleared by centrifugation at 17,000 g for 10 min, and total protein concentrations were determined by micro-bicinchoninic acid (BCA) assay (Thermo Fisher Scientific, Waltham, MA). Proteins were resolved on 4-12% gradient polyacrylamide gels (Life Technologies) under denaturing and reducing conditions and transferred to 0.2 µm nitrocellulose membranes (Bio-Rad Laboratories, Hercules, CA). Membranes were imaged using a LI-COR Odyssey Imaging System. As needed, membranes were stripped with 0.2 M NaOH.

### *Antibody microarray experiments*

Cell lysates were prepared and cleared as for western blotting from cells treated with or without TGF $\beta$  + EGF for 30 min following overnight serum starvation. Phospho Explorer Antibody Array (Full Moon Biosystems, Sunnyvale, CA) sample processing, array conjugation, and raw data analysis were performed at Full Moon Biosystems. Quantification of duplicate array dots per condition was performed and fold-changes in phosphorylated-to-total peptide signal ratios were calculated as treated/untreated.

### *Multiplexed Luminex assay measurements*

Multiplexed Luminex kits NF- $\kappa$ B Signaling (48-630MAG), Early Apoptosis (48-669MAG), RTK Mitogenesis Phosphoprotein (48-672MAG), Akt/mTOR phosphoprotein (48-611MAG), and MAPK/SAPK Signaling (48-660MAG) were purchased from Millipore to measure a total of 39 phospho proteins, listed in Table 4-1. Whole cell lysates were prepared in kit-supplied lysis buffer supplemented with protease inhibitors from cells treated with indicated growth factor combinations in complete medium. Lysates were first clarified by centrifugation at 21,000 g for 10 min, and further purified by passing through supplied filters from Millipore. Luminex assay was performed at the University of Pennsylvania Human Immunology Core, using standard techniques. Mean fluorescence intensity (MFI) values from the Luminex assay were background corrected by subtracting MFI signal from assay buffer-only samples from all other values. Initial calibration assays were performed for each kit using serial dilution of untreated and TGF $\beta$  + EGF stimulated cell lysates to verify detection of induced signals as well as signal linearity. Protein loading for each kit was chosen based on calibration assay results. For final data collection biological triplicates were analyzed for all treatment conditions. Any analytes with non-linear signals were not included in final data set.

Excess lysate from the Luminex assay preparation was analyzed by western blotting for phosphorylated proteins for which no Luminex bead was available or Luminex signal was not linear, listed in Table 4-2. Since all treatment conditions could not fit on a single western blot, untreated samples were included on each gel for direct comparison.

### *Immunofluorescence staining and image analysis*

Cells were plated on glass coverslips in 6-well plates and maintained in full serum media supplemented with the indicated growth factors 24 hr after plating. Following the indicated time of treatment, cells were washed and fixed for 20 min in 4% paraformaldehyde and permeabilized with 0.25% Triton X-100 in PBS for 5 min. Washed coverslips were incubated with an anti-E-cadherin or anti-vimentin antibody in a humidified chamber for 3 hr at 37°C. Washed coverslips were incubated with Alexa Fluor-conjugated anti-mouse secondary antibodies and Hoechst-33342 DNA stain (Sigma-Aldrich) for 1 hr at 37°C. Coverslips were mounted on microscope slides using Prolong Gold Antifade mounting media (Life Technologies) and dried overnight. Fixed slides were imaged on a Zeiss Axiovert 40 CFL microscope using an A-Plan 20X objective (vimentin) or 100X oil objective (E-cadherin) and a SPOT Insight CCD camera. Identical acquisition settings were used across all images from a single experiment.

E-cadherin junctional localization was quantified using ImageJ and a method similar to that described in Loerke et al. 2012 [138]. Each cell-cell junction was traced with a 15-pixel (1.1  $\mu\text{m}$ ) wide freehand line (corresponding to the average thickness of E-cadherin stained junctions in the untreated condition), for which the area ( $A_j$ ), integrated density ( $ID_j$ ), and area-averaged mean intensity ( $M_j$ ) were measured.  $M_j$  was taken to be the average junctional signal. The three measurements,  $A_{total}$ ,  $ID_{total}$ ,  $M_{total}$ , were then taken for an increased thickness of 100 pixels (7.5  $\mu\text{m}$ ) encompassing junctional and peri-junctional E-cadherin staining. In order to find the mean cytoplasmic density ( $M_c$ ),  $A_j$  and  $ID_j$  were first subtracted from  $A_{total}$  and  $ID_{total}$ , respectively, to obtain the cytoplasm-only quantities  $A_c$  and  $ID_c$ .  $M_c$  was then calculated by dividing  $ID_c$  by  $A_c$ . In order to quantify the extent of junctional localization of E-cadherin, the ratio  $M_j/M_c$  was calculated for each junction. All full junctions contained within an image were analyzed.

Quantification of the percent of cells positive for vimentin was also performed using ImageJ. Nuclei were counted in each image from Hoechst staining to obtain the total number of cells. In the corresponding vimentin image, cell outlines were drawn using a freehand tool from which mean intensities of vimentin staining were recorded. Cells with mean intensities higher than

the intensity of background non-specific staining were considered to be vimentin-positive, and the total number of vimentin-positive cells was divided by the number of nuclei to obtain the percentage of vimentin-positive cells in each image.

#### *Cell scatter experiments and quantification*

Cells were plated in complete medium at low density (500 cells per well in 12-well plates). When individual cells had expanded into well-defined colonies 3-4 days later, the scatter experiment was initiated by the addition of complete medium containing EGF, HGF, TGF $\beta$ , or a combination of the ligands. Individual cell clusters were monitored, and phase contrast images were captured with a Zeiss Axiovert 40 CFL microscope (10X objective) over 3 days. Image segmentation was performed using the MATLAB image processing toolbox (MathWorks, Natick, MA) to identify all objects (cell clusters) within each image and record their area and perimeter. As described previously [139], a circularity index was calculated as  $4\pi(\text{area}/\text{perimeter}^2)$  (=1 for a circle) for each cluster.

#### *Partial least squares regression model development*

PLSR model generation was performed using SIMCA-P software (Umetrics, Umeå, Sweden) as described previously [166], based on mathematical models detailed in Geladi & Kowalski, 1986 and Wold et al., 2001 [163, 164]. For the initial PLSR model, the 6x160 data matrix,  $\mathbf{X}$ , was composed of Luminex and western blot phosphoprotein measurements. The M = 6 rows corresponded to the following cellular conditions: untreated, EGF, HGF, TGF $\beta$ , TGF $\beta$ +EGF, and TGF $\beta$ +HGF. The N = 160 columns corresponded to protein phosphorylation measurements for 32 proteins x 5 time points (15 min, 30 min, 1 hr, 4 hr, and 48 hr) for each condition. The 6x5 output matrix,  $\mathbf{Y}$ , was generated from EMT measurement data for the same conditions, with the K = 5 columns being measurements for total E-cadherin, total vimentin, E-cadherin junctional localization, fraction of vimentin-positive cells, and circularity index after a 3 day treatment. All data columns were mean centered and scaled to unit variance prior to PLSR analysis. Using

SIMCA-P the non-linear iterative partial least squares (NIPALS) algorithm was implemented to solve the linear regression:

$$\mathbf{Y} = \mathbf{XB} + \mathbf{G} \quad (1)$$

Where  $\mathbf{B}$  is a matrix of regression coefficients and  $\mathbf{G}$  represents the residual. To achieve this,  $\mathbf{X}$  is decomposed into scores vectors,  $\mathbf{t}$ , that span sample space and loadings vectors,  $\mathbf{p}$ , that span X-variable space such that the residual  $\mathbf{E}$  is small in the outer product representation:

$$\mathbf{X} = \mathbf{TP}' + \mathbf{E} \quad (2)$$

$\mathbf{Y}$  is equivalently decomposed into Y-scores vectors,  $\mathbf{u}$ , and Y-weights vectors,  $\mathbf{c}$ , that span  $\mathbf{Y}$  with residual  $\mathbf{F}$ :

$$\mathbf{Y} = \mathbf{UC}' + \mathbf{F} \quad (3)$$

In PLSR, the X-scores  $\mathbf{t}$ , which are small in number, represent new latent variables termed principal components (PCs) that maximally capture covariance between the  $\mathbf{X}$  and  $\mathbf{Y}$  data matrices. The  $\mathbf{t}$ 's are linear combinations of the original X-variables with weights  $\mathbf{w}^*$ :

$$\mathbf{T} = \mathbf{XW}^* \quad (4)$$

The X-scores must also be good models of  $\mathbf{Y}$  such that the residual  $\mathbf{G}$  is small:

$$\mathbf{Y} = \mathbf{TC}' + \mathbf{G} \quad (5)$$

Combining equations (4) and (5) and relating back to equation (1) gives:

$$\mathbf{B} = \mathbf{W}^*\mathbf{C}' \quad (6)$$

In the NIPALS algorithm, the  $\mathbf{X}$ -matrix is deflated after each component and the  $a^{\text{th}}$  PC is solved using the  $\mathbf{X}$ - residual from the previous component (note:  $\mathbf{E}_0 = \mathbf{X}$ ):

$$\mathbf{E}_a = \mathbf{E}_{a-1} - \mathbf{t}_a\mathbf{p}_a' \quad (7)$$

$$\mathbf{t}_a = \mathbf{E}_{a-1} \mathbf{w}_a \quad (8)$$

The scores and weights vectors for the  $a^{\text{th}}$  PC,  $\mathbf{t}_a$  and  $\mathbf{w}_a$ , are found such that they maximally capture  $\mathbf{X}$ - $\mathbf{Y}$  covariance remaining after  $a-1$  PCs, and are therefore determined from the residual matrix. Thus the  $\mathbf{w}$ 's correspond to weights for the residual matrices, while  $\mathbf{w}^*$ 's relate to the original  $\mathbf{X}$ -matrix. For relating back to the full model,  $\mathbf{w}^*$ 's are found using the following relation:

$$\mathbf{W}^* = \mathbf{W} (\mathbf{P}'\mathbf{W})^{-1} \quad (9)$$

Each weight vector  $\mathbf{w}_a$  is the normalized eigenvector associated with the greatest eigenvalue of the covariance matrix  $\mathbf{X}_a' \mathbf{Y}_a \mathbf{Y}_a' \mathbf{X}_a$ . Given that each PC is solved after subtracting the contribution from the previous PC, together the  $\mathbf{w}_a$ 's represent an orthonormal set defining directions in the  $\mathbf{X}$  data space to maximally capture  $\mathbf{Y}$ -relevant information.

The PLSR model was tested for goodness of prediction,  $Q^2$ , using a leave-one-out cross-validation approach and information captured,  $R^2Y$  and  $R^2X$ , after each successive component using standard calculations.

#### *Statistical analysis*

Statistical significance was determined using one-way ANOVA and  $p$ -values were determined using Student-Newman-Keuls test for multiple corrections in Kaleidagraph 4.0 (Synergy Software, Reading, PA).

**Table 4-1 Panel of proteins measured by Luminex**

	Protein	Phosphorylation
1	AKT	S473
2	ATF2	T71
3	BAD	S112
4	BCL-2*	S70
5	Caspase 8*	active
6	Caspase 9	active
7	c-Jun	S73
8	c-MET	panY
9	c-MYC	
10	EGFR	panY
11	ERBB3	panY
12	ERBB4*	panY
13	ERK1/2	T185/Y187
14	FADD	S194
15	GSK3 $\alpha$	S21
16	GSK3 $\beta$	S9
17	HER2	panY
18	HSP27*	S78
19	IGF-IR*	Y1135/1136
20	IGF-IR*	panY
21	IKK $\alpha/\beta$ *	S177/181
22	IR*	Y1162/1163
23	IR*	panY
24	IRS1	S363
25	I $\kappa$ B	S32
26	JNK	T183/Y185
27	MEK	S222
28	MSK	S212
29	mTOR	S2448
30	NF $\kappa$ B	S536
31	p38*	T180/Y182
32	p53*	S15
33	p53	S46
34	p70S6K	T412
35	PTEN*	S380
36	RPS6	S235/236
37	STAT1*	Y707
38	TNFR1	
39	TSC2	S939

\* analytes that did not produce linear Luminex signal and were removed from PLSR model construction; text color corresponds to kit: **cell cycle+apoptosis**, **AKT/mTOR**, **MAPK**, **NF $\kappa$ B**, **receptors**

**Table 4-2 Panel of proteins measured by western blot**

	Protein	Phosphorylation
1	<b>ALK</b>	Y1604
2	<b>p27</b>	T157
3	<b>p38</b>	T180/Y182
4	<b>SMAD2/3</b>	S465/467 S423/425
5	<b>SRC</b>	Y418
6	<b>STAT3</b>	Y705

Where appropriate, text color corresponds to Luminex kit functions; proteins with other pathway functionality are colored grey: **cell cycle+apoptosis**, **MAPK**, **receptors**, other

#### 4-4 RESULTS

##### *Characterization of EMT-associated shifts in protein expression in response to EGF, HGF, and TGF $\beta$*

The HPAF-II pancreatic cancer cell line was used to analyze the ability of different culture conditions to induce EMT (Fig. 4-1). This cell line displays differentiated epithelial characteristics, harbors mutations in *KRAS*, *p16*, and *p53*, and is *SMAD4* wild type [143]. We have previously described the ability of different combinations of EGF and TGF $\beta$  to induce varying extents of EMT induction in HPAF-II (Chapter 3). In addition to EGF and TGF $\beta$ , we analyzed cellular response to HGF in this study, which is known to induce mesenchymal cellular characteristics on its own in certain cellular contexts [54]. Cells were monitored for EMT induction when maintained in complete medium supplemented with EGF (50 ng/mL), HGF (50 ng/mL), TGF $\beta$  (10 ng/mL), TGF $\beta$ +EGF, or TGF $\beta$ +HGF. After 5 days of treatment, cells had undergone EMT as indicated by acquisition of spindle-like morphology with fewer cell-cell junctions, decreased E-cadherin expression, and increased vimentin expression, with the degree of these changes dependent on treatment condition (Fig. 4-1A-D). Across conditions, HGF produced the greatest EMT as a single ligand, and the combination of TGF $\beta$ +HGF produced the greatest EMT overall. Western blot quantification for total protein abundance and quantitative immunofluorescence analysis of individual cell expression of E-cadherin and vimentin produced largely similar comparisons between conditions, but the profiles had some distinct differences (Fig. 4-1B-D). For example, western blotting results reflected greater differences in vimentin expression between HGF and TGF $\beta$  treatments as well as greater differences in E-cadherin among HGF, TGF $\beta$ , TGF $\beta$ +EGF, and TGF $\beta$ +HGF. These comparisons demonstrate consistency and complementarity between the two methods for analyzing changes in prototypical epithelial and mesenchymal markers.

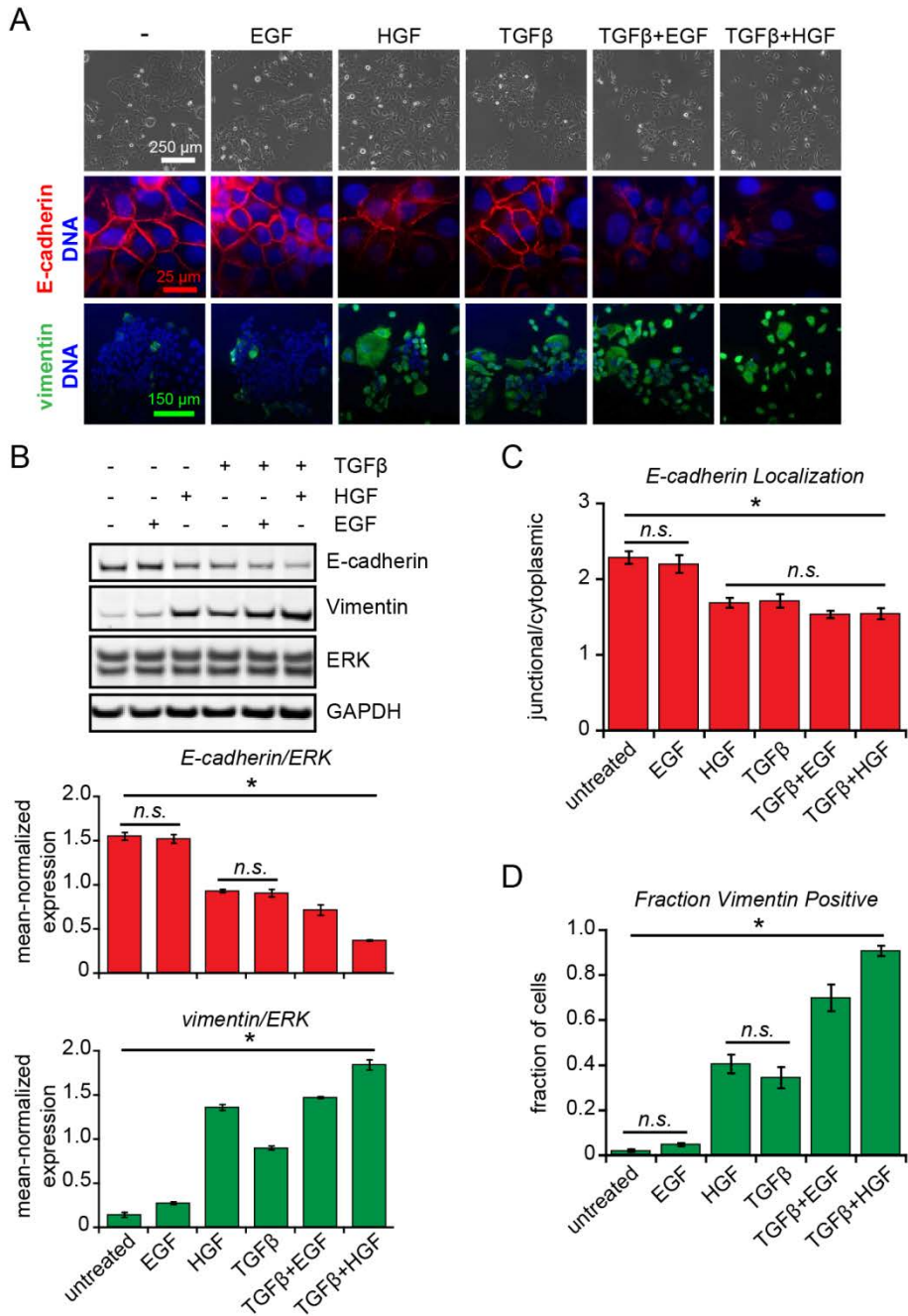


**Figure 4-1: EGF, HGF, and TGF $\beta$  induce differential changes in epithelial and mesenchymal marker expression and localization.**

HPAF-II cells were treated for five days with EGF (50 ng/mL), HGF (50 ng/mL), TGF $\beta$  (10 ng/mL), TGF $\beta$ +EGF, or TGF $\beta$ +HGF and subsequently imaged by phase contrast microscopy, prepared for immunofluorescence staining for E-cadherin and DNA or vimentin and DNA, or lysed for western blotting. **(A)** Representative phase contrast and immunofluorescence images are shown. **(B)** Lysates were analyzed by western blotting with antibodies against the indicated proteins. Densitometry values for each condition were normalized to the mean signal across conditions for

each of four independent experiments ( $n = 4$ ). **(C)** E-cadherin localization quantification comparing the relative intensity at cell-cell junctions versus peri-junctional regions was calculated as described in *Materials and Methods Section 4-3* for all junctions within an image. The mean ratio per image was averaged for four images from each of two independent experiments ( $n = 8$ ). **(D)** The percent of vimentin-positive cells was calculated as described in *Materials and Methods Section 4-3* for four images from each of two independent experiments ( $n = 8$ ). Data throughout are represented as mean  $\pm$  s.e.m; \*  $p < 0.01$  for all pairwise comparisons unless indicated not significant (*n.s.*).

#### *Measuring cell scatter in response to EMT-inducing growth factors*

Accompanying changes in protein expression and morphology, cells undergoing EMT become more motile and invasive [2, 168]. We assessed the ability of the growth factor conditions explored in Figure 4-1 to induce migration by using a cell scatter assay. As has been employed previously, monitoring the circularity index ( $CI = 4\pi(\text{area}/\text{perimeter}^2)$ ) of epithelial cell clusters in response to stimuli provides a quantitative measure of cellular scatter and migration and is related to the weakening of cell-cell junctions [139]. Quantifying circularity indices of clusters over 3 days of treatment revealed similar qualitative trends in the EMT-promoting capacity among the treatment conditions as seen for protein expression (Fig. 4-2). TGF $\beta$ +HGF again displayed the greatest effect, and HGF had the largest effect of the single growth factor treatments. Interestingly, TGF $\beta$ +EGF-mediated effects seemed dampened compared to the measurements based on protein expression in Figure 4-1, performing no better than HGF alone.

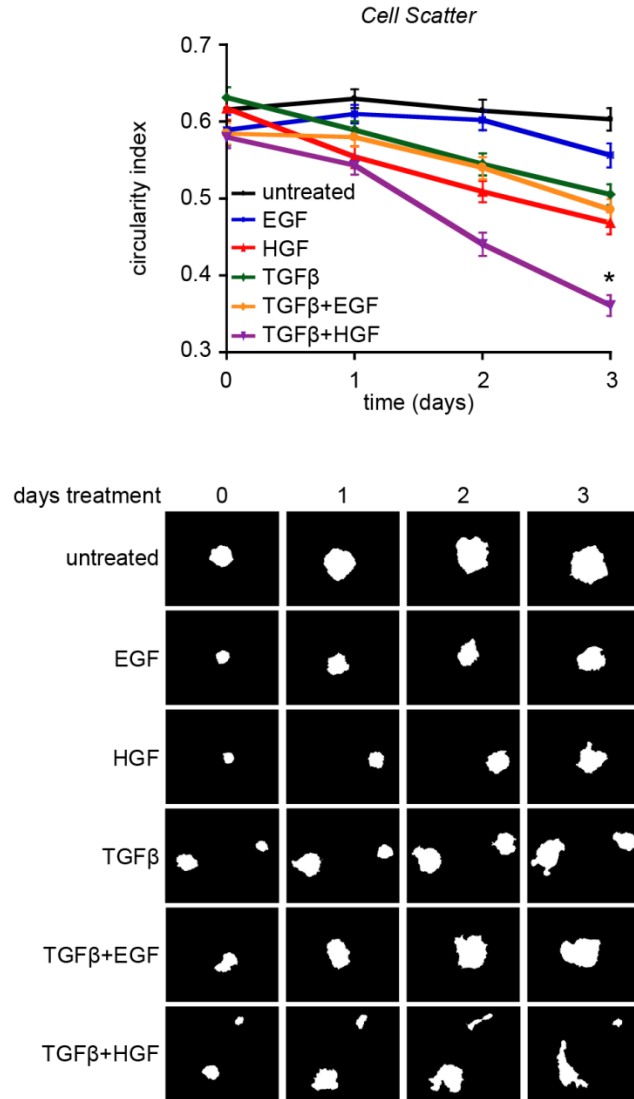


**Figure 4-2: EMT inducing growth factors promote cell scatter.**

HPAF-II cell clusters grown in 12-well plates from single cells were treated with EGF (50 ng/mL), HGF (50 ng/mL), TGFβ (10 ng/mL), TGFβ+EGF, or TGFβ+HGF and monitored for 3 days for cell scatter. Silhouettes from MATLAB analysis of representative cell cluster images are shown. Circularity indices versus time for clusters from twelve frames per condition in each of three independent experiments were quantified as described in *Materials and Methods Section 4-3* and are reported as averages ± s.e.m. ( $n > 45$ ); \*  $p < 0.05$  for all comparisons with TGFβ+HGF.

*Antibody microarray reveals EMT-relevant phosphorylated protein targets for further investigation*

Cellular integration of signaling through many networks in response to stimuli enables phenotype determination, including the ability for different growth factor treatments to elicit distinct extents of EMT induction. To identify the particular signaling nodes that differentiate among EMT states observed with different ligand treatments, we sought to quantitatively survey a large panel of signaling proteins to relate to the measured differences in EMT induction. Before focusing on quantitative evaluation of specific proteins, however, we interrogated a broad array of phosphorylation events in an unbiased screen using an antibody microarray with >1,300 distinct antibodies. We evaluated protein phosphorylation using antibody microarray in cells treated with TGF $\beta$ +EGF. After surveying a large number of time points by western blot (Fig. 4-3), a treatment time of 30 min was selected because it enabled measurement of both early and delayed phosphorylation events as detected by total phosphotyrosin (pY) western blotting.

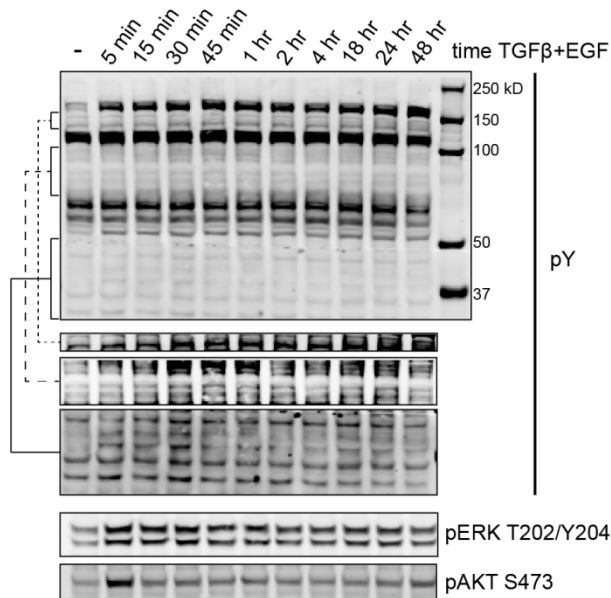


**Figure 4-3: Evaluating total phosphotyrosine content from TGF $\beta$ +EGF time course.**

HPAF-II cells in 6-well plates were maintained in complete medium and treated with TGF $\beta$  (10 ng/mL) and EGF (50 ng/mL) for the indicated times before lysis. Lysates were analyzed by western blotting with antibodies against the indicated proteins. Portions of the total phosphotyrosine (pY) scan are shown at higher contrast to visualize lower intensity bands. Images are representative of three independent experiments.

**Table 4-3 - Proteins with greatest induction of phosphorylation from microarray**

Phosphorylated Protein	Fold Change
NFkB-p65 Ser536	2.49
p27Kip1 Thr187	2.33
p53 Thr18	2.00
Cytokeratin 8 Ser431	1.86
CSFR Tyr561	1.83
ETK Tyr566	1.82
CASP2 Ser157	1.81
CD3Z Tyr142	1.79
HSP27 Ser15	1.78
CASP1 Ser376	1.78
NFkB-p100/p52 Ser869	1.77
ALK Tyr1507	1.76
NFkB-p100/p52 Ser865	1.76
Synapsin Ser62	1.76
CDK1/CDC2 Thr14	1.76
VAV1 Tyr174	1.76
CD5 Tyr453	1.75
Epo-R Tyr368	1.75
c-Jun Ser243	1.73
IKK-gamma Ser31	1.70
Tuberin/TSC2 Ser939	1.69
Calsenilin/KCNIP3 Ser63	1.69
Myc Ser62	1.67
Elk1 Thr417	1.67
Tuberin/TSC2 Thr1462	1.66

**Table 4-4 - Proteins with greatest decrease in phosphorylation from microarray**

Phosphorylated Protein	Fold Change
MAPKAPK2 Thr334	0.20
HDAC1 Ser421	0.24
4E-BP1 Ser65	0.37
MEK1 Thr291	0.47
Caspase-3 Ser150	0.53

Antibody microarray analysis, which tends to produce false negatives with low incidence of false positives, revealed a number of protein phosphorylation events that were increased (Table 4-3) or decreased (Table 4-4) in response to a 30 min treatment with TGF $\beta$ +EGF. Of note, four proteins of the top 25 hits for phosphorylation increase were in the NF $\kappa$ B pathway, including the first-ranked protein NF $\kappa$ B p65 phosphorylated at Ser<sup>536</sup>. Other notable proteins indicated were p27/Kip (a cell cycle regulator), ALK, p53, TSC2 (upstream of mTOR), 4E-BP1 (downstream of mTOR), MYC, and MAPKAPK2 (directly phosphorylated by p38). The connections to the AKT/mTOR, p38, and NF $\kappa$ B pathways, which have all been implicated in EMT induction, suggested inclusion of these pathways moving forward. Additionally, a necessary role for p27/Kip in EMT was recently described through promoting STAT3 activation in mammary epithelial cells [169], which argued for its inclusion as well.

*Partial least squares regression model predicts signaling events most relevant for EMT phenotype acquisition*

Using insight from the antibody microarray results and the literature, we measured phosphorylation of 45 proteins, listed in full in Tables 4-1 & 4-2, in response to all five growth factor treatments at five time points (15 min, 30 min, 1 hr, 4 hr, and 48 hr) by Luminex and western blotting. As described in *Materials and Methods Section 4-3*, 13 Luminex analytes were discarded from final PLSR model construction due to lack of linear signal. The phosphorylation profiles for the 32 remaining proteins included in our final data set are shown in Figure 4-4.

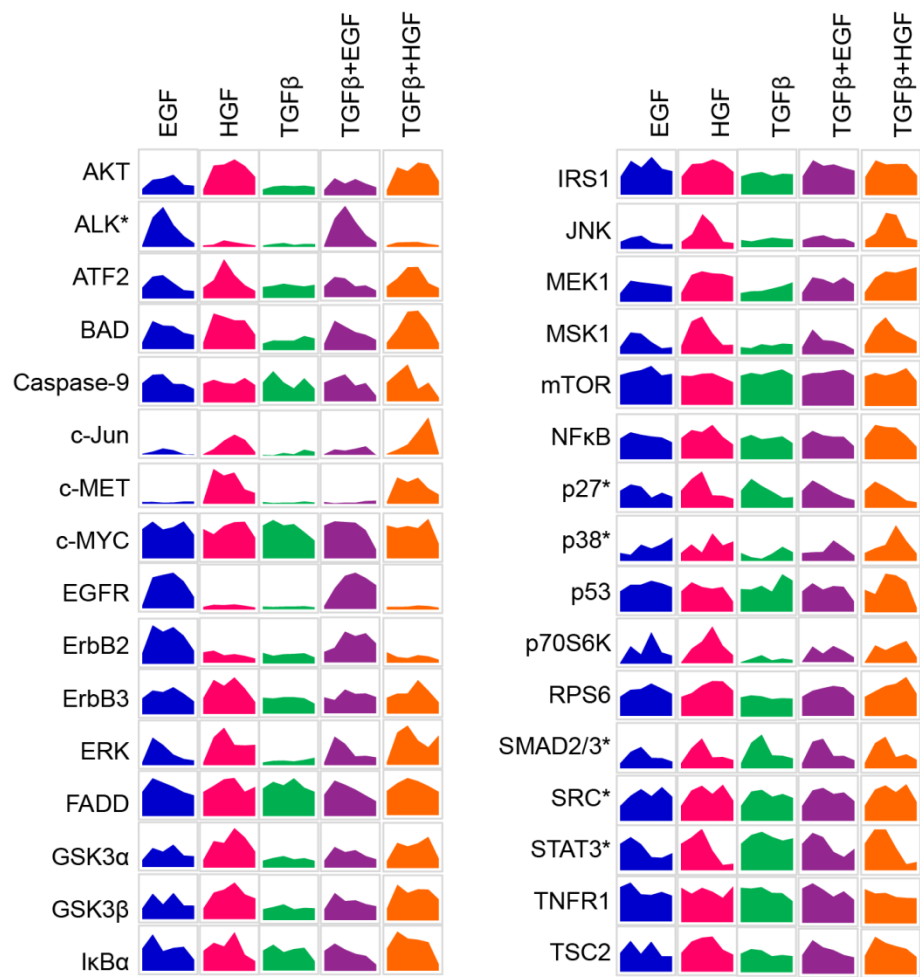


**Figure 4-4: Individual protein phosphorylation profiles reveal differences in growth factor-mediated signaling.**

HPAF-II cells plated in 6-wells were maintained in complete media, prior to addition of the indicated combinations of EGF (50 ng/mL), HGF (50 ng/mL), and TGF $\beta$  (10 ng/mL). Cells were lysed and lysates were analyzed by Luminex and western blotting according to *Materials and Methods Section 4-3*. Averaged triplicate Luminex and western blot-based measurements of protein phosphorylation are shown. \* indicates protein measured by western blot, all others by Luminex. Full list of phosphorylation sites measured is given in Tables 4-1 and 4-2.

A PLSR model was generated using the data in Figure 4-4 as the **X**-data with 160 X-variables and the phenotype measurements from Figures 4-1 and 4-2 for the **Y** data (Fig. 4-5). Inspection of the scores and weights plots revealed that the first principal component was positively correlated with epithelial characteristics with untreated cells and E-cadherin measures

having the highest scores and weights in PC1, respectively (Figure 4-5A,B). Conversely, the TGF $\beta$ +HGF treatment condition and vimentin measures had the most negative scores and weights values for PC1. Thus, PC1 provides a primary EMT axis, and X-variables weighted most negatively in PC1 are likely candidates for important roles in EMT induction. In the weights plot PC2 provided further separation between epithelial and mesenchymal phenotypes, again with positive values associated with epithelial characteristics, suggesting that there is additional information within PC2 regarding which variables contribute to EMT differences. The scores plot furthermore suggests that PC2 provides information distinguishing between single growth factor treatment conditions. Despite meaningful interpretation of the first few principal components, further analysis revealed that the overall model quality was not high (Fig. 4-5C). Though a two-component model captured the majority of Y information, the cross-validation of model prediction, given by  $Q^2$ , indicated a fairly low predictive ability of the model. These limitations may arise in PLSR models that are over-specified or when the PLSR model is built using X-data that is not Y-relevant.

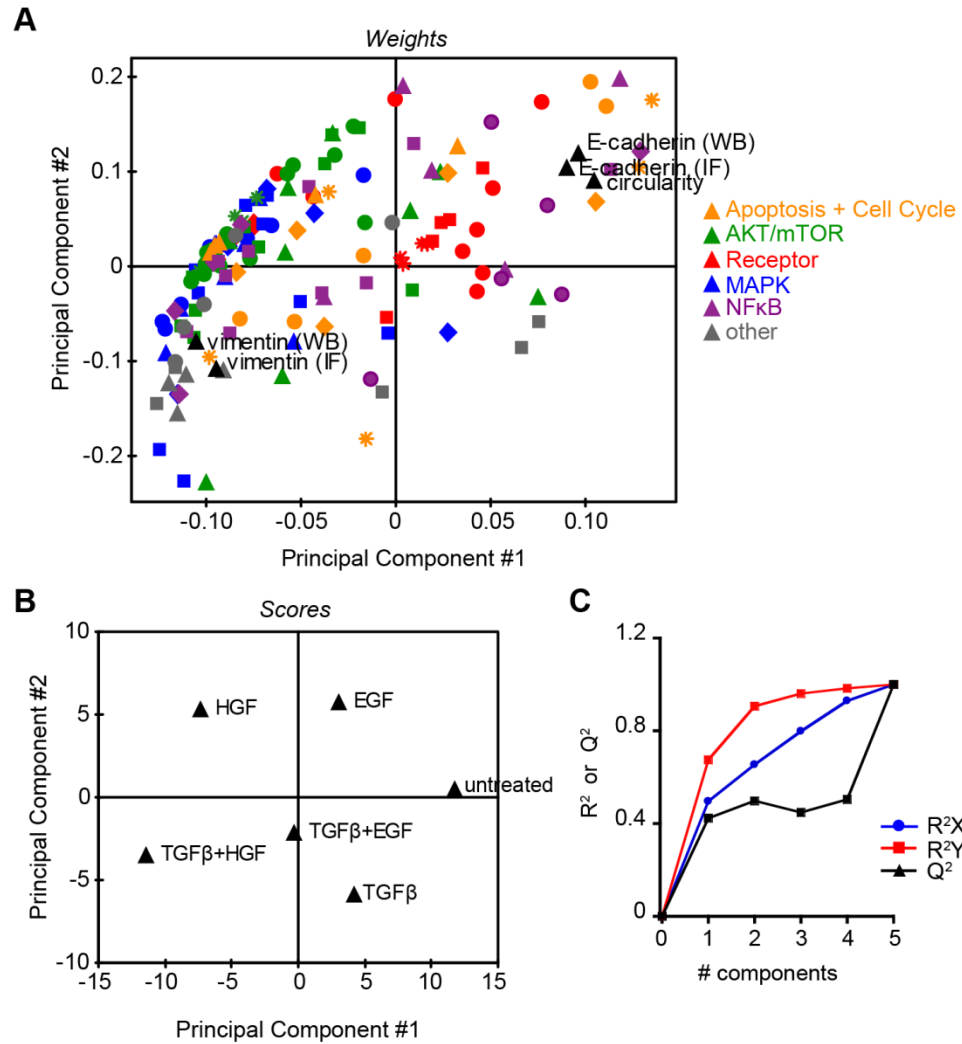


**Figure 4-5: A PLSR model reveals an EMT signaling axis.**

A PLSR model was built using phenotype and phosphorylated protein measurements from Figures 4-1, 4-2, and 4-4 as described in *Materials and Methods Section 4-3*. **(A)** Weights and **(B)** scores plots were generated for the first two principal components. In A dots are colored based on protein kit/function as shown in legend. **(C)** Cumulative measures of information captured,  $R^2X$  and  $R^2Y$ , and cross-validated prediction,  $Q^2$ , are shown for up to a 5-component model.

*Reducing the X dataset improves PLSR model prediction and reveals key EMT signaling nodes*

The results from Figure 4-5C suggested that there may have been  $Y$ -irrelevant information incorporated into the original  $X$  data set. Additionally, the considerable overlap of  $X$ -variables in the weights plot (Fig. 4-5A) indicated that many variables were providing redundant

information. To address these issues, we systematically evaluated the quality of information provided by each X-variable. First, we sought to eliminate redundant information provided by proteins within the same kit or pathway using a principal components analysis (PCA) for each time point (Fig. 4-S1). When two or more analytes from the same kit measured at the same time point were very proximal in a two-component PCA loadings plot, one representative analyte was chosen for model inclusion while the other(s) were removed. This analysis was performed for each time point. Next, the averaged data were inspected to reveal which time points showed no meaningful differences in protein level or activation. In this case, data processing prior to PLSR input would falsely separate these measurements from each other and thus provide misleading information for model inclusion. For example, in Figure 4-4 JNK phosphorylation returned to baseline values for all conditions by the 48 hr time point, indicating this should not be included as an x-variable for model construction.

This systematic approach led to a reduced **X** data set of 74 of the original 160 variables. A resulting PLSR model demonstrated quite similar separation of epithelial and mesenchymal Y-variables and conditions as the initial model (Fig. 4-5, 4-6A,B) with greatly improved model quality (Fig. 4-6C). In agreement with the known multivariate nature of EMT signaling, the distribution of variables in the weights plot indicates high correlation of EMT induction with all major signaling pathways measured for the overall model. Proteins within MAPK, AKT/mTOR, NFκB, STAT, and SMAD signaling pathways were all clustered near mesenchymal traits, and a number of variables within cell cycle and apoptosis pathways were distributed near epithelial traits. To rank the value of specific protein phosphorylation measurements for the overall two-component model, we analyzed the variable importance in the projection (VIP) scores for this reduced PLSR model (Fig. 4-7, Table 4-S1). A VIP score > 1 indicates a variable to be informative for the model, which was true of 38 variables in this model. This analysis again highlighted the multivariate nature of EMT signaling, with measurements of 26 separate proteins which spanned all pathways represented among the 38 variables with VIP score > 1.

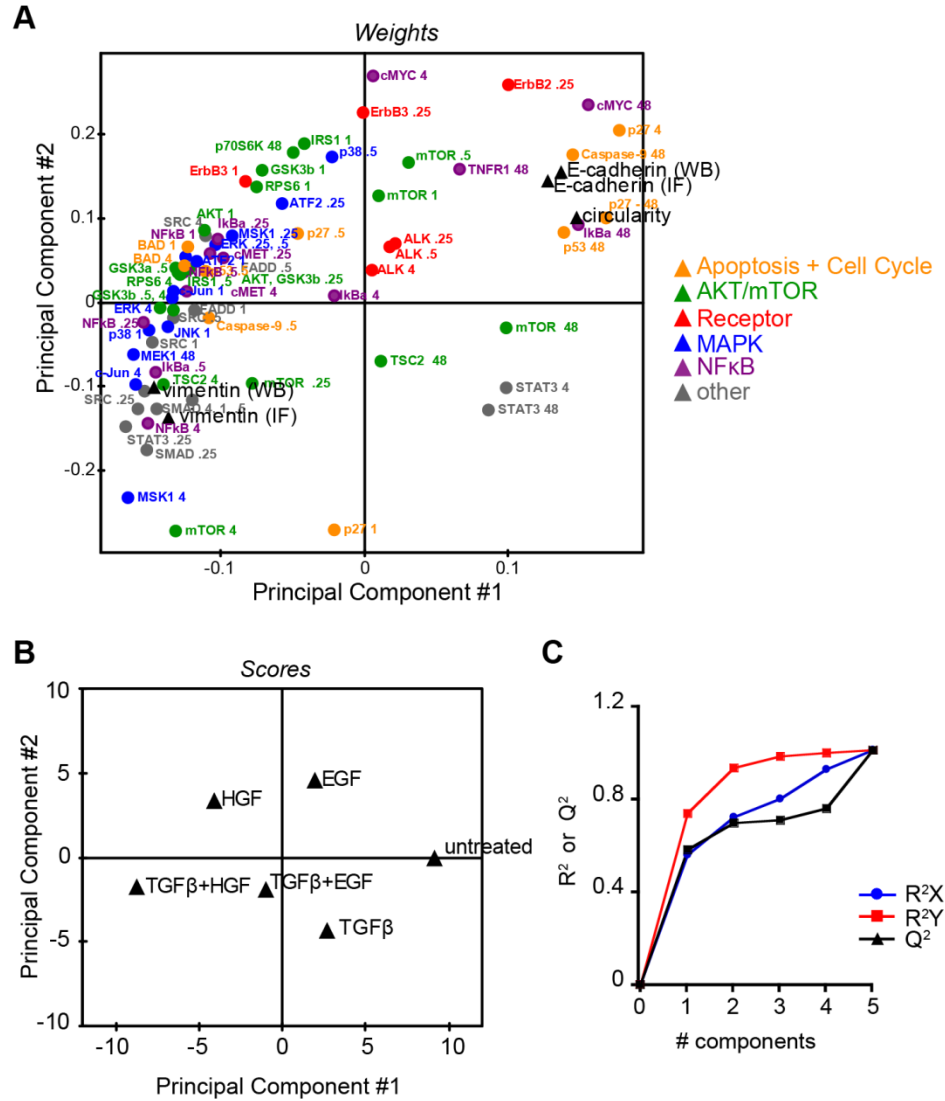


**Figure 4-6: Systematic reduction of X variables improves model quality.**

A PLSR model was built as in Figure 4-5 using a reduced  $X$  data set as described. (A) Weights and (B) scores plots were generated for the first two principal components. In A dots are colored based on protein kit/function as shown in legend. Text next to dots indicates protein and time point in hr. (C) Cumulative measures of information captured,  $R^2X$  and  $R^2Y$ , and cross-validated prediction,  $Q^2$ , are shown for up to a 5-component model.

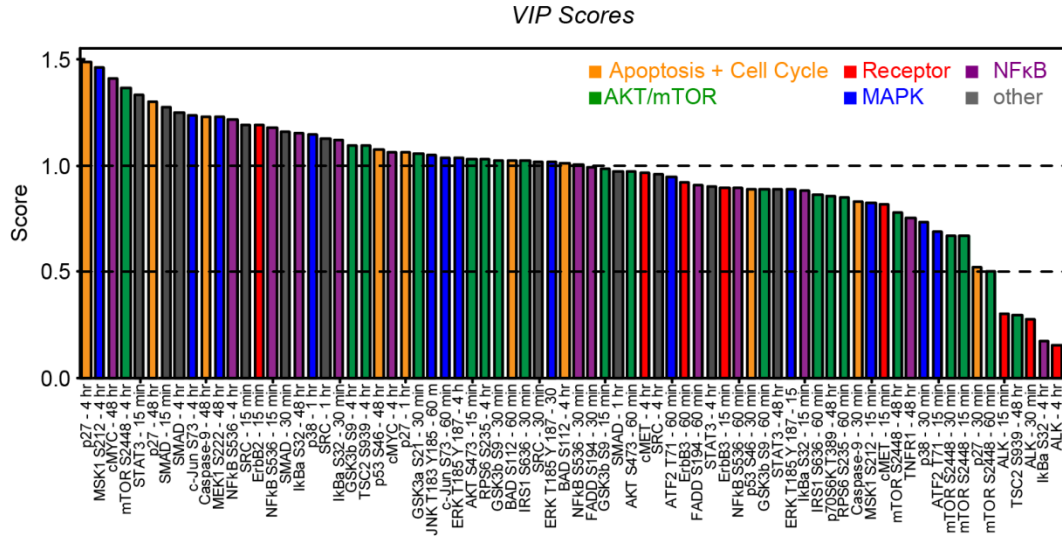


**Figure 4-7: VIP score analysis confirms multivariate EMT regulation.**

The VIP scores were calculated for the 74-variable PLSR model shown in Figure 4-6. Measurements are ranked by VIP score and colored according to pathway.

*A minimal PLSR model identifies key EMT signaling nodes for further validation*

Despite the obvious complexity of EMT signaling indicated by our analysis to this point, we wished to identify a subset of key variables predictive of EMT induction. A sequential VIP analysis was used to develop a minimal PLSR model using only 10 X-variables. First, the top-ranked measurement for each of the 26 proteins represented in the VIP scores in Table 4-S1 were used to generate a PLSR model. This model (not shown) had 10 variables with VIP score > 1, which were subsequently used to generate the minimal PLSR model (Fig. 4-8). The resulting model had altered distribution of variables and conditions in the two-component weights and scores plots compared to Figures 4-5 and 4-6 (Fig. 4-8A,B), despite some notable similarities. In this model, PC1 again provided the most meaningful separation between epithelial and mesenchymal states, whereas PC2 separated the different signaling pathways. Importantly, despite the vast reduction in input data for the model, the overall model quality was high (Fig. 4-8C). The minimal model included several proteins with negative weights, which suggests their

association with the mesenchymal state. The implicated signaling pathways would therefore represent promising targets for inhibiting or reversing mesenchymal phenotypes for future study.

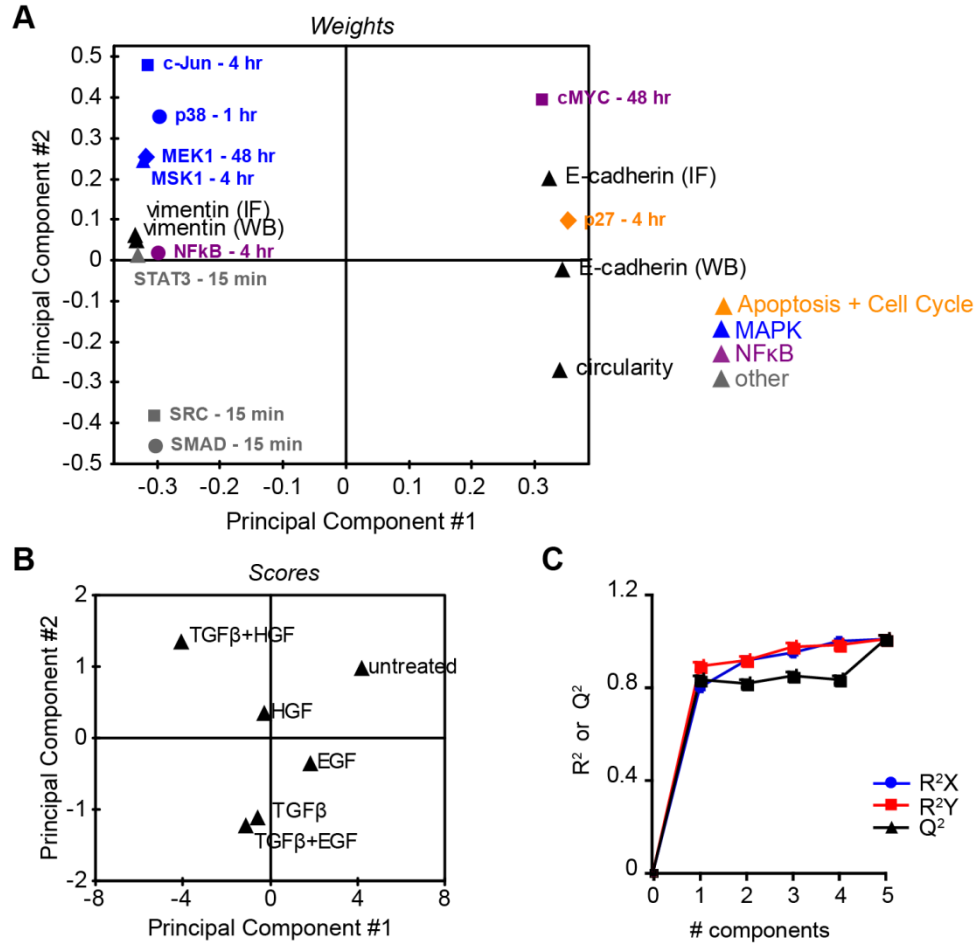


**Figure 4-8: A minimal PLSR model captures important EMT signaling.**

A PLSR model was built using a reduced **X** data set as described. **(A)** Weights and **(B)** scores plots were generated for the first two principal components. In **A** dots are colored based on protein kit/function as shown in legend. Text next to dots indicates protein and time point. **(C)** Cumulative measures of information captured,  $R^2X$  and  $R^2Y$ , and cross-validated prediction,  $Q^2$ , are shown for up to a 5-component model.

## 4-5 DISCUSSION

This study produced the first quantitative model directly connecting multivariate signaling events to the ability of different treatments to produce varying extents of EMT in pancreatic cancer cells. We quantified the ability of EGF, HGF, TGF $\beta$ , TGF $\beta$ +EGF, and TGF $\beta$ +HGF to induce differential changes in migration measured by cell scatter and expression and localization of E-cadherin and vimentin. TGF $\beta$ +HGF consistently displayed the greatest EMT-inducing capacity of all conditions across all phenotypes. We then undertook an unbiased screen of protein phosphorylation events under EMT-inducing conditions to identify key signaling events in EMT induction. Phosphorylation profiles for a panel of 32 proteins at 5 time points were quantitatively measured in response to all five growth factor treatment conditions. These protein phosphorylation measurements were combined with the quantified phenotype analysis in a PLSR model to identify signaling proteins whose activity covaried most with EMT status. Systematic reduction of phosphorylation measurements included in the model based on pruning of redundant or low confidence variables and VIP analysis led to identification of 10 key signaling measurements. These measurements produced a two-component PLSR model that captured >90% of the information in the EMT phenotype data.

The ten proteins from the minimal PLSR model provide promising potential targets for inhibiting or reversing mesenchymal phenotypes. In particular, the eight proteins with strongly negative weight into PC1 – c-Jun, p38, MEK, MSK1, NF $\kappa$ B, STAT3, SRC, and SMAD2/3 - are implicated as positive predictors of EMT induction. MEK, MSK1, c-Jun, and p38 are all MAPK signaling components, and their importance for EMT induction may not be surprising given previous reports particularly for MEK/ERK and p38 [47, 49, 57, 126]. c-Jun phosphorylation at Ser<sup>73</sup> after 4 hr of treatment was also among the most highly correlated with EMT induction in our model. The activity of JNK and c-Jun phosphorylation are less frequently implicated in EMT induction than ERK and p38, but a recent report identified c-Jun activation as crucial for mesenchymal differentiation from pluripotent stem cells [170]. These findings along with the present study, therefore, suggest JNK as a promising potential target for suppressing

mesenchymal cellular traits for future biochemical studies. An interesting aspect to this analysis could involve determining the reason for the delayed time scale of c-Jun activation and why this was unique to the combination of TGF $\beta$  and HGF (Fig. 4-4). SMAD2&3 are necessary effectors in TGF $\beta$ -mediated signaling, so the association of SMAD2/3 activity with TGF $\beta$ -mediated EMT induction is expected. Interestingly, though mTOR phosphorylation at 30 min had a high VIP score in the 74-variable model and many components of AKT/mTOR signaling were highly associated with EMT (Figs. 4-6 & 4-7), all of the measurements within the AKT/mTOR pathway were eventually dispensable for the minimal model generation. Further *in vitro* studies could reveal whether or not AKT/mTOR signaling is indeed dispensable for EMT induction as suggested by this analysis.

Among the proteins measured in this study, SRC/SFK phosphorylation at Tyr<sup>418</sup> was also among the most strongly correlated with EMT induction. Interestingly, SRC activity has been previously implicated as a driver of EMT induction with reported roles phosphorylating the type II TGF $\beta$  receptor [49] and EGFR [55] following TGF $\beta$  treatment. Additionally, following TGF $\beta$  treatment SFK can be activated by EGFR to suppress apoptotic signaling and promote full AKT activation [56]. These findings are in line with the implied role of SFK from our PLSR analysis and motivate further experimental analysis of the importance of SFK activity for EMT induction in response to different growth factor treatments. These investigations could employ siRNA or SFK inhibitors, which would each provide meaningful information. Small molecule inhibitors, such as PP2, have the ability to inhibit multiple SFK proteins simultaneously [171], which provides information of the general importance of SFK activity, but using PP2 would not enable evaluation of rank importance of specific SFK proteins. Alternatively, siRNA could be used to deplete specific SFK proteins such as c-SRC, FYN, LYN, and YES individually to determine which are particularly responsible for SFK-dependent EMT.

A notable finding from this study was the ability to improve model performance by reducing the input data incorporated in the model from 160 phosphoprotein measurements to 10 measurements. The ability to capture the majority of dependent variable variation using a

reduced PLSR model with ten or fewer independent variables has been reported previously [102, 166], and is in fact a strength of PLSR analysis. By identifying a small number of key parameters that predict cellular phenotypes, PLSR models such as the one reported here can be leveraged in the future for predicting responses to new treatments or in new contexts such as additional pancreatic cancer cell lines by making a minimal number of measurements. Further refinement and validation of the reduced PLSR model could provide a succinct list of key protein phosphorylation measurements that could be used to predict phenotypic responses in tumors or lead to the identification of nodes for inhibiting EMT induction.

#### **4-6 ACKNOWLEDGEMENTS**

The authors thank Dr. Carl June, for providing cells and thank staff at the Human Immunology Core at the University of Pennsylvania for help in designing and performing Luminex assay. Funding was provided by the University of Pennsylvania Pancreatic Cancer Translational Center of Excellence, a National Science Foundation (NSF) Graduate Research Fellowship to JMB (DGE-08220), and NSF CBET Award 1450751.

#### 4-7 SUPPLEMENTAL MATERIAL

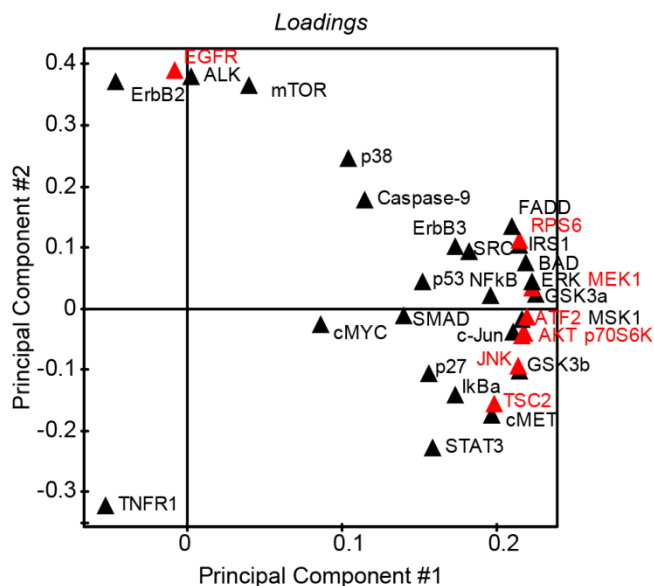


**Figure 4-S1: PCA analysis enables systematic exclusion of redundant X-variables.**

The loadings plot for a PCA model based only on measurements from the 30 min treatment conditions is shown. Analytes shown in red were excluded from subsequent PLSR analysis in Figure 4-6 due to their proximity to other analytes within the same kit/pathway. This systematic analysis was performed for each of the five time points (15 min, 30 min, 1 hr, 4 hr, and 48 hr) to identify variables for PLSR model exclusion.

**Table 4-S1: Protein measurements with VIP > 1.0 from 74-variable PLSR model**

Rank #	Protein/phosphorylation/time point
1	p27 T157 - 4 hr
2	MSK1 S212 - 4 hr
3	cMYC - 48 hr
4	mTOR S2448 - 4 hr
5	STAT3 Y705 - 15 min
6	p27 T 157 - 48 hr
7	SMAD2 S465/467 / SMAD3 S423/425 - 15 min
8	SMAD2 S465/467 / SMAD3 S423/425 - 4 hr
9	c-Jun S73 - 4 hr
10	Caspase-9 active - 48 hr
11	MEK1 S222 - 48 hr
12	NFkB S536 - 4 hr
13	SRC Y418 - 15 min
14	ErbB2 panY - 15 min
15	NFkB S536 - 15 min
16	SMAD2 S465/467 / SMAD3 S423/425 - 30 min
17	IkBα S32 - 48 hr
18	p38 - 1 hr
19	SRC Y418- 1 hr
20	IkBα S32 - 30 min
21	GSK3b S9 - 4 hr
22	TSC2 S939 - 4 hr
23	p53 S46 - 48 hr
24	cMYC - 4 hr
25	p27 T157 - 1 hr
26	GSK3a S21 - 30 min
27	JNK T183/Y185 - 60 min
28	c-Jun S73 - 60 min
29	ERK T185/Y187 - 4 hr
30	AKT S473 - 15 min
31	RPS6 S235 - 4 hr
32	GSK3b S9 - 30 min
33	BAD S112 - 60 min
34	IRS1 S636 - 30 min
35	SRC Y418 - 30 min
36	ERK T185 Y 187 - 30 min
37	BAD S112 - 4 hr
38	NFkB S536 - 30 min

Proteins are color-coded according to kit/function: cell cycle+apoptosis, AKT/mTOR, MAPK, NFkB, receptors, other

## CHAPTER 5: Conclusions and Future Work

### 5-1 SUMMARY

The work described in this thesis has enhanced the understanding of how EMT is regulated by specific cell signaling pathways and has identified potential routes for enhancing clinical outcomes in cancer. Of particular note was the development of a drug scheduling strategy aimed at enhancing EGFR inhibitor response after initial treatment with a MEK inhibitor in lung cancer cells (Chapter 2). In this study, MEK inhibition prevented EMT induction in response to TGF $\beta$  and EGF and promoted mesenchymal-epithelial transition (MET) in the absence of growth factors. The acquisition of epithelial traits from chronic MEK inhibition enhanced cell death in response to EGFR inhibition in cell lines characterized by both *de novo* or acquired resistance to EGFR inhibition. Though several recent studies have suggested the potential of MEK and EGFR coinhibition as a therapeutic strategy, this work suggests an alternative approach for combining these inhibitors sequentially to improve response. This work also demonstrated MEK-dependent acquisition of mesenchymal traits from ectopic expression of mutant KRAS, which is found in a significant portion of patients across cancer types.

The findings of Chapter 2 raised interest as to which ERK pathway components were responsible for transducing EMT-driving signals. In Chapter 3 we described a necessary role for the cytosolic phosphatase SHP2 in EMT and provided evidence that SHP2 activation states tune the extent of EMT observed in response to different ligands. Specifically, TGF $\beta$  treatment produced a partial EMT that corresponded to low SHP2 activity, which was nevertheless required for the observed EMT shifts. EGF co-administration with TGF $\beta$  led to induced SHP2 activity which greatly augmented the ability of TGF $\beta$  to promote mesenchymal dedifferentiation.

Experimental and computational approaches were then undertaken to survey additional signaling pathways that may also control EMT induction in Chapter 4. First, we observed that HGF and TGF $\beta$ +HGF treatments provide further diversity in the spectrum of EMT induction compared to treatments with EGF, TGF $\beta$ , or TGF $\beta$ +EGF. TGF $\beta$ +HGF produced the greatest

EMT of these conditions and HGF was the most efficient EMT inducer as a single agent. These findings were combined with quantitative protein phosphorylation measurements in response to each condition to generate a partial least squares regression computational model of which protein phosphorylation events are most predictive of the extent of EMT induction. These results provide a framework for developing novel strategies to inhibit mesenchymal phenotypes through combining targeted inhibitors. Implementing these strategies and the approach developed in Chapter 2 in preclinical and clinical models may demonstrate promising new therapeutic methods to improve cancer patient prognosis. The remainder of this chapter will elaborate on considerations for such preclinical and clinical models as well as other implications and future directions of this work.

## **5-2 EFFECTS OF CHRONIC MEK INHIBITION AND FURTHER INVESTIGATION**

The results of Chapter 2 suggested a novel strategy for enhancing therapeutic response to EGFR inhibitors in NSCLC. Specifically, the elevated gefitinib response observed after an MET from several days of MEK inhibition suggests that the sequential delivery of therapies wherein a MEK inhibitor is administered alone initially to promote an epithelial phenotype in cancer cells followed by addition of an EGFR inhibitor could enhance response to the EGFR inhibitor. Some studies have suggested the efficacy of EGFR and MEK inhibitor co-administration in gastric cancer [118], colorectal cancer [172], and pancreatic cancer cells [119], and current clinical trials are evaluating the combination of erlotinib with MEK inhibitors in NSCLC [84]. It seems, however, that response in these studies could potentially be increased by delaying initial administration of the EGFR inhibitor, since MEK inhibitor pretreatment enhanced or at least maintained EGFR inhibitor response in all cell lines tested in this work. Employing such a strategy could provide a clinical application for specific MEK inhibitors that could not be FDA-approved as single agents, such as CI-1040 [84], or an additional clinical indication for trametinib, the first FDA-approved MEK inhibitor, which is currently approved for metastatic melanoma patients with *BRAF* mutation [91, 92].

Before translating these strategies into the clinic, the efficacy of the proposed drug scheduling must be evaluated in more cell lines and in animal models. It is likely that similar effects of MEK inhibition could be observed in other cancer types in addition to NSCLC, since ERK activation drives EMT phenotypes in cells from oral cancers [173], melanoma [174], and pancreatic cancer [94]. These and other tumor types with mesenchymal-associated therapy resistance could be initially tested in *in vitro* experiments as in Chapter 2 before further analysis in animal models.

For *in vivo* work, the dose and schedule of inhibitors will likely require optimization since the time of maximal gefitinib response varied between cell lines and was not always associated with most epithelial marker expression. Qualitatively, response to MEK inhibition may also be improved overall *in vivo*, as suggested by recent results where EGFR-containing signaling complexes were much more abundant in some cells in subcutaneous xenografts compared to the same cells *in vitro* [175]. If these findings apply across cell lines, ERK activity may be generally enhanced *in vivo* which could broadly enhance phenotypic effects of MEK inhibition *in vivo*. These studies could initially rely upon subcutaneous xenograft experiments using a panel of cell lines or alternatively, patient-derived xenografts (PDXs), in which primary tumor cells from a patient are directly transplanted into the flank of a mouse. PDX samples recapitulate tumor heterogeneity seen in primary tissue and patient-to-patient variability [176, 177], and PDX studies have been used in lung [175], colorectal [172], breast [178], head and neck [179], renal cell [180], and ovarian [181] cancers to test therapeutic molecules and identify novel predictors of patient response. PDX cells are passaged between mice, which in future studies would enable matched comparison of different scheduling and combinations of MEK and EGFR inhibitors as an extension of the work in this thesis. Development of this therapeutic approach may prove an effective means of extracting value and clinical potential from therapeutic molecules that are clinically safe and biochemically effective but have not yet translated to clinical success.

### **5-3 SIGNALING TARGETS FOR EMT REVERSAL AND COMBINATION THERAPIES**

The pervasive nature of the malignant consequences from EMT induction in cancer has motivated studies to identify pharmacological targets to suppress mesenchymal traits [182]. Interestingly, this aim is in line with long-standing efforts toward 'differentiation therapy' for many malignancies [183, 184], which seeks to improve cancer therapeutic response in poorly differentiated tumors. To identify EMT targets, several studies have performed screens using libraries of available compounds or siRNAs to selectively target mesenchymal cells [129, 185], reduce migration [186], or promote E-cadherin expression [128, 187]. Though these techniques employ high-throughput screening to survey a very large number of targets for EMT suppression, they rarely incorporate integrated analysis of multiple EMT-relevant phenotypes, which may prove a limitation in finding broadly effective targets. More definitive identification of critical EMT regulators will require following up on these studies with more in-depth analysis of specific intermediates or with screens that incorporate several phenotypes.

The results in Chapter 2 and 3 provided a thorough analysis of ERK as an important signaling regulator that can be perturbed to control EMT phenotypes. However, several pieces of evidence indicated that other pathways play complimentary or overlapping roles to control EMT induction. For example, though MEK inhibition and SHP2 knockdown consistently and significantly inhibited mesenchymal dedifferentiation, these effects were sometimes incomplete and/or transient. In these cases, other pathways must, therefore, compensate for ERK when it is inhibited or play redundant roles in promoting EMT. In Chapter 4 we used a PLSR model to identify candidate EMT-relevant signaling intermediates by measuring phosphorylation of proteins from many signaling pathways against multiple phenotypic measures of EMT induction in response to growth factors. Future studies based on proteins indicated in the PLSR model will evaluate whether specifically targeting each protein or multiple proteins in combination can inhibit EMT induction, reverse mesenchymal traits, and potentially enhance therapeutic response.

One promising target for future investigation is the cytosolic kinase, SRC and other SRC-family kinases (SFKs). Previous work has demonstrated that TGF $\beta$ -mediated phenotypic shifts

depend upon SRC kinase activity [49, 56] through direct phosphorylation of TGF $\beta$  receptor II [49] and EGFR [55] after TGF $\beta$  treatment. In these studies, SRC kinase activity promoted signaling through p38 [49], ERK [55], and AKT [56] suggesting that SRC could potentially regulate signaling flux through multiple pathways controlling EMT induction. Additionally, EGFR-driven SFK activity promotes prolonged SHP2 activity [151], which may relate to the necessary role for SHP2 activity in EMT induction we described in Chapter 3. Importantly, many findings surrounding the role of SRC have relied on the pan-SFK inhibitor PP2 which has substantial affinity for other kinases including p38 [171], necessitating use of more specifically targeted tools for future investigation. The breadth of findings regarding the importance of SFK activity merits further analysis of the role of specific SFKs in EMT induction. Measuring response to TGF $\beta$  with or without EGF or HGF in cells with depletion of specific SFK proteins could reveal more conclusively the role for SFK proteins in EMT induction.

#### **5-4 SHP2 AS A THERAPEUTIC TARGET**

Given that SHP2 depletion prevented EMT induction in response to TGF $\beta$  with and without EGF in Chapter 3, targeting SHP2 activity may provide another potential strategy for promoting an epithelial phenotype in cancer cells. This fits within and contributes to the growing motivation to target SHP2 activity in cancer. SHP2-activating mutations occur in multiple cancers including juvenile myelomonocytic leukemia, acute myelogenous leukemia, and lung and colon carcinomas, as well as Noonan syndrome, a developmental disorder leading to increased risk of certain malignancies [81, 152]. SHP2 depletion, through suppressing ERK pathway activity, has been shown previously to confer gefitinib sensitivity in NSCLC cells [75], and SHP2 promotes tumorigenesis in xenograft studies of breast and brain cancer cells [82, 83]. The known roles of SHP2 and other PTPs in cancer and other diseases have motivated significant research efforts to develop specifically-targeted small molecule PTP inhibitors, which has been attainable for many kinases [188]. These efforts for PTPs have been quite challenging, however, due to the highly polar nature of and homology between PTP active sites, which introduce difficulties in

bioavailability and specificity, respectively [189, 190]. New strategies targeting allosteric binding sites unique to SHP2 [153, 154] and another phosphatase PTP1B [191] have shown promise toward improving specificity of PTP inhibitors. Since SHP2 drives malignancy in multiple cancers, further development of these newly-identified small molecule inhibitors would have great potential for preclinical and clinical investigations.

## **5-5 MEASURING SHP2 ASSOCIATIONS WITH HIGHER SENSITIVITY AND SPATIAL RESOLUTION**

Though we identified that EGF's ability to enhance TGF $\beta$ -mediated EMT depended upon SHP2 SH2 engagement by phosphotyrosines, additional questions remain regarding the specific molecular alterations underlying the ability of SHP2 to influence EMT. SHP2 was required for EMT induced by TGF $\beta$  alone, despite no detectable TGF $\beta$ -induced associations between SHP2 and phosphotyrosine-containing proteins. This may occur simply because basal SHP2 phosphatase activity in the absence of SH2 domain engagement is sufficient for TGF $\beta$ -mediated effects. Additionally, TGF $\beta$  mediates signaling through many pathways which could potentially involve SHP2 binding to proteins that are not detectable using phosphotyrosine western blotting. One recently-identified mechanism for SHP2 positively impacting TGF $\beta$ -mediated effects was through decreased SHP2 binding with Hook1, a negative regulator of SHP2 activity [192]. TGF $\beta$ -mediated unbinding of Hook1 from SHP2 provides a potential model for SHP2 activity being induced at a low level during TGF $\beta$  treatment without engagement by phosphotyrosine. SHP2 has additional signaling roles not assessed in this thesis. For example, SHP2 can regulate EMT-associated phenotypes through interactions with components of focal adhesions including focal adhesion kinase [148, 149] and the adherens junction protein  $\alpha$ -catenin [193], which could also be explored in the context of TGF $\beta$  treatment. Since these interactions were not detected through SHP2 immunoprecipitation western blotting higher sensitivity methods using proteomic mass spectrometry techniques for interaction mapping [194] could elucidate whether SHP2 binds to these proteins that may have lower abundance or to proteins that are not tyrosine

phosphorylated. Specific SHP2 interactions required for TGF $\beta$ -mediated effects could provide protein targets which have more potent small molecule inhibitors than SHP2 for inhibiting EMT induction. Such inhibitors could be combined with a MEK inhibitor, for example, to suppress multiple pathways influencing EMT induction.

In addition to enhancing our understanding of which proteins are engaged by SHP2 under different cellular conditions, the question of where this engagement occurs also merits a more thorough investigation. We identified SHP2-GAB1 interaction as critical for mediating EMT inducing signals in Chapter 3, motivating further characterization of factors influencing maintenance of this complex. In a recent study, we found that SFK activity maintains SHP2-GAB1 complexes distal from EGFR, which nucleates complex formation [151]. This complex persistence could allow SHP2 to dephosphorylate substrates distal from the receptor (e.g., the focal adhesion protein paxillin, [195]) by maintaining SHP2 activation as it diffuses away from the receptor. Computational modelling has enhanced the quantitative understanding of which kinetic parameters influence the ability of SHP2-GAB1 complexes to persist in the cell interior (unpublished results from Furcht et al.), though the spatially resolved persistence of complexes has not yet been measured in live cells. The abundance of SHP2 throughout the cell leads to high background in attempts to visualize co-localization of SHP2 and GAB1 in standard immunofluorescence staining and thus more sophisticated microscopy techniques are required to characterize SHP2-GAB1 spatial distribution.

Two methods for imaging protein co-localization in cells are fluorescence resonance energy transfer (FRET) microscopy and proximity ligation assay (PLA), which would each have advantages and disadvantages for the direct visualization of SHP2-GAB1 complexes. FRET utilizes the ability to detect energy transfer between two fluorophores when they are within 1-10 nm of each other (summarized in [196]). Using SHP2 and GAB1 genetically tagged with fluorescent proteins, FRET could thus enable high resolution temporal measurement of SHP2-GAB1 co-localization. Challenges in implementing FRET include proper selection and stoichiometric ratios of fluorophores and optimizing fluorophore placement on proteins such that

their inherent biochemical activities are retained while bringing the fluorophores close enough for FRET to occur [197]. Without resolved structures of full length SHP2 and GAB1 proteins bound together, optimal placement of fluorescent tags on the proteins is difficult to predict. FRET has historically relied on ectopic expression for genetic tagging of proteins, but recent advances in the CRISPR system for gene knock-in could allow for fluorescent tagging at the endogenous *SHP2* and *GAB1* loci for FRET experiments. Alternatively, PLA is an antibody-based method that uses *in situ* PCR to detect co-localization of two targets in fixed cells, which detects endogenous protein without concerns of fluorophore compatibility [198]. PLA has typically been used to detect the presence or extent of protein binding rather than intracellular distribution of complexes [175]. Therefore to study SHP2-GAB1 complex persistence using PLA, method verification with proper controls to distinguish between localization of SHP2-GAB1 complexes on endocytic vesicles versus in the cytosol would be necessary. Since PLA is performed on fixed samples, analysis is restricted to distinct time points rather than live-cell imaging in FRET, reducing the ease with which time-resolved detection of complex persistence could be achieved.

## **5-6 TGF $\beta$ SIGNALING**

As reviewed in Chapter 1, TGF $\beta$  binding to its receptors and subsequent TGF $\beta$  receptor-mediated signaling is complex and can be highly context dependent [4]. For example, in Chapter 3 TGF $\beta$  did not induce ERK phosphorylation (at the time points we investigated) in H322 and HPAF-II cells, despite direct links between TGF $\beta$  signaling and ERK activation in other cell settings [47]. Given the importance of ERK for EMT induction, it would be informative to investigate what cellular components determine the connectivity between TGF $\beta$  and ERK. For example, relative abundance of TGF $\beta$  type I and II receptors, SMAD2/3, or other signaling intermediates likely impact how TGF $\beta$ -mediated signals are transmitted through cellular networks. Since TGF $\beta$  type II receptor has low tyrosine kinase activity relative to serine/threonine kinase activity [48], higher abundance of TGF $\beta$  type II receptors could facilitate higher tyrosine phosphorylation of the receptor complexes, which favors recruitment of adapters in the MAPK

signaling cascades such as SHC [50, 51]. Therefore, it would be informative to determine relative abundance of TGF $\beta$  type I and II receptors and their phosphorylation at key residues following TGF $\beta$  treatment in H322 and HPAF-II cells compared to a cell line that displays TGF $\beta$ -induced ERK phosphorylation. Differences between these cell lines could suggest potential biochemical mechanisms determining pathway connectivity.

Chapter 3 revealed the importance of cell context on the density dependence of TGF $\beta$ -mediated EMT induction. Specifically, the pancreatic cancer cell line HPAF-II was highly sensitive to cell density for EMT induction, with no detectable EMT induced at high plating densities. The lung cancer cell line H322 showed no such dependence. Previous work in the human keratinocyte cell line HaCaT showed that TGF $\beta$ -induced formation of nuclear SMAD3-SMAD4 complexes detected by PLA was highly dependent on cell density, with significantly fewer complexes in cells plated at high density [145]. Recent investigation by Nallet-Staub and colleagues also captured the density dependence of SMAD nuclear localization in HaCaT cells as well as a melanoma cell line, but also showed that a mammary epithelial cell line did not display this density effect [146]. This cell context dependence provides further motivation to adapt these experimental techniques in H322 and HPAF-II as well as other cancer cell lines. PLA-based measurements of TGF $\beta$ -induced SMAD signaling could potentially reveal differences between H322 and HPAF-II, and the flexibility of PLA would enable detection of other EMT-relevant signaling complexes (e.g., TGF $\beta$  receptor type II-SRC and SHP2-GAB1 binding).

A downstream component in TGF $\beta$  signaling common to all SMAD signaling pathways is the co-regulator SMAD4, which facilitates translocation of SMAD2/3 complexes into the cell nucleus [4]. In addition to having a very high incidence of *KRAS* mutation (95%), pancreatic cancer is also characterized by mutation or deletion of *SMAD4* in roughly 50% of patient tumors [147]. Though SMAD4 is known to positively regulate TGF $\beta$ -mediated SMAD signaling, whether SMAD4 is required for TGF $\beta$ -mediated EMT remains unclear. Some investigations found that SMAD4 is involved in TGF $\beta$  tumor suppressive roles and not EMT response [199, 200], while other investigations determined that TGF $\beta$ -mediated EMT is distinctly dependent on SMAD4

activity [201]. HPAF-II, the pancreatic cancer cell line used in this thesis, harbors expected mutation of *KRAS* but is wild type for *SMAD4*. It would be informative to test whether *SMAD4* status affects the EMT induction patterns reported in this thesis. Correlative examination of *SMAD4* wild type versus mutant cell lines could reveal patterns in EMT dependence, but an isogenic cell line model to study *SMAD4* variants would provide a more robust framework for elucidating the EMT relevance of *SMAD4*. The CRISPR-Cas9 system is a recently adapted tool for modifying chromosomal DNA [202] that could be utilized to introduce mutations at the *SMAD4* locus or create a chromosomal deletion.

## **5-7 USING PLSR TO PREDICT CLINICALLY RELEVANT PHENOTYPES**

In Chapter 4, a PLSR model was developed to elucidate signaling processes underlying differential EMT induction in response to different growth factor conditions, which led to identification of targets to inhibit or suppress EMT for future investigation. The ability to adapt PLSR to any data set with corresponding independent and dependent variable data matrices for a given set of experimental conditions makes it a widely applicable computational tool. Moving forward, there will be many opportunities to develop additional PLSR models to study clinically relevant processes based on this thesis. For example, a PLSR model could be developed for prediction of response to the MEK inhibition strategy developed in Chapter 2. Though multiple cell lines with differing genotypes were sensitized to EGFR inhibition by MEK inhibitor pretreatment, other cell lines tested were not responsive to this strategy. A PLSR model built upon phosphorylation profiles in cells at rest and in response to MEK inhibition and corresponding cell death or proliferation measurements in response to EGFR inhibition could be used to predict response in additional panels of cell lines or future clinical samples. Such a model could also identify possible modes of adaptive resistance or escape from this strategy.

Another outstanding question in the EMT literature is determining what factors influence stable versus reversible mesenchymal dedifferentiation. *In vitro*, the extent and reversibility of TGF $\beta$ -mediated EMT is dependent on the concentration of TGF $\beta$  and length of treatment [203].

Metastatic colonization appears to rely on this reversibility of mesenchymal traits through MET induction [22, 23]. Since many carcinoma-derived cell lines (often with therapeutic resistance) display distinct permanent mesenchymal phenotypes [27, 141, 143], stable EMT induction also has clear relevance to understanding patient outcomes. Whether similar regulatory mechanisms are responsible for dynamic EMT induction and stable mesenchymal maintenance is unknown. PLSR analysis of EMT phenotypes using protein abundance and phosphorylation profiles in a large panel of cell lines across the spectrum of baseline epithelial and mesenchymal traits and cells undergoing growth factor-mediated EMT could reveal mechanisms underlying the distinction between permanent and transient EMT. Such a model could also incorporate measurements of response to EGFR inhibitors or chemotherapeutics to determine how the dynamics of EMT influence widely observed therapeutic resistance.

## BIBLIOGRAPHY

1. Yang, J. and R.A. Weinberg, *Epithelial-mesenchymal transition: at the crossroads of development and tumor metastasis*. Dev Cell, 2008. **14**(6): p. 818-29.
2. Kalluri, R. and R.A. Weinberg, *The basics of epithelial-mesenchymal transition*. J Clin Invest, 2009. **119**(6): p. 1420-8.
3. Thiery, J.P., *Epithelial-mesenchymal transitions in development and pathologies*. Curr Opin Cell Biol, 2003. **15**(6): p. 740-6.
4. Massague, J., *TGFbeta in Cancer*. Cell, 2008. **134**(2): p. 215-30.
5. Yilmaz, M. and G. Christofori, *EMT, the cytoskeleton, and cancer cell invasion*. Cancer Metastasis Rev, 2009. **28**(1-2): p. 15-33.
6. Schmidt, J.M., et al., *Stem-cell-like properties and epithelial plasticity arise as stable traits after transient Twist1 activation*. Cell Rep, 2015. **10**(2): p. 131-9.
7. Tam, W.L., et al., *Protein kinase C alpha is a central signaling node and therapeutic target for breast cancer stem cells*. Cancer Cell, 2013. **24**(3): p. 347-64.
8. Warzecha, C.C., et al., *An ESRP-regulated splicing programme is abrogated during the epithelial-mesenchymal transition*. EMBO J, 2010. **29**(19): p. 3286-300.
9. De Craene, B. and G. Berx, *Regulatory networks defining EMT during cancer initiation and progression*. Nat Rev Cancer, 2013. **13**(2): p. 97-110.
10. Wakefield, L.M. and A.B. Roberts, *TGF-beta signaling: positive and negative effects on tumorigenesis*. Curr Opin Genet Dev, 2002. **12**(1): p. 22-9.
11. Argast, G.M., et al., *Cooperative signaling between oncostatin M, hepatocyte growth factor and transforming growth factor-beta enhances epithelial to mesenchymal transition in lung and pancreatic tumor models*. Cells Tissues Organs, 2011. **193**(1-2): p. 114-32.
12. Saha, D., et al., *Synergistic induction of cyclooxygenase-2 by transforming growth factor-beta1 and epidermal growth factor inhibits apoptosis in epithelial cells*. Neoplasia, 1999. **1**(6): p. 508-17.
13. Docherty, N.G., et al., *TGF-beta1-induced EMT can occur independently of its proapoptotic effects and is aided by EGF receptor activation*. Am J Physiol Renal Physiol, 2006. **290**(5): p. F1202-12.
14. Grande, M., et al., *Transforming growth factor-beta and epidermal growth factor synergistically stimulate epithelial to mesenchymal transition (EMT) through a MEK-dependent mechanism in primary cultured pig thyrocytes*. J Cell Sci, 2002. **115**(Pt 22): p. 4227-36.
15. Bissell, M.J. and D. Radisky, *Putting tumours in context*. Nat Rev Cancer, 2001. **1**(1): p. 46-54.
16. O'Brien, L.E., M.M. Zegers, and K.E. Mostov, *Opinion: Building epithelial architecture: insights from three-dimensional culture models*. Nat Rev Mol Cell Biol, 2002. **3**(7): p. 531-7.
17. Reginato, M.J., et al., *Bim regulation of lumen formation in cultured mammary epithelial acini is targeted by oncogenes*. Mol Cell Biol, 2005. **25**(11): p. 4591-601.
18. Mehlen, P. and A. Puisieux, *Metastasis: a question of life or death*. Nat Rev Cancer, 2006. **6**(6): p. 449-58.

19. Weigelt, B., J.L. Peterse, and L.J. van 't Veer, *Breast cancer metastasis: markers and models*. Nat Rev Cancer, 2005. **5**(8): p. 591-602.
20. Tarin, D., E.W. Thompson, and D.F. Newgreen, *The fallacy of epithelial mesenchymal transition in neoplasia*. Cancer Res, 2005. **65**(14): p. 5996-6000; discussion 6000-1.
21. Rhim, A.D., et al., *EMT and dissemination precede pancreatic tumor formation*. Cell, 2012. **148**(1-2): p. 349-61.
22. Celia-Terrassa, T., et al., *Epithelial-mesenchymal transition can suppress major attributes of human epithelial tumor-initiating cells*. J Clin Invest, 2012. **122**(5): p. 1849-68.
23. Tsai, J.H., et al., *Spatiotemporal regulation of epithelial-mesenchymal transition is essential for squamous cell carcinoma metastasis*. Cancer Cell, 2012. **22**(6): p. 725-36.
24. Singh, A. and J. Settleman, *EMT, cancer stem cells and drug resistance: an emerging axis of evil in the war on cancer*. Oncogene, 2010. **29**(34): p. 4741-51.
25. Garofalo, M., et al., *EGFR and MET receptor tyrosine kinase-altered microRNA expression induces tumorigenesis and gefitinib resistance in lung cancers*. Nat Med, 2011. **18**(1): p. 74-82.
26. Thomson, S., et al., *Kinase switching in mesenchymal-like non-small cell lung cancer lines contributes to EGFR inhibitor resistance through pathway redundancy*. Clin Exp Metastasis, 2008. **25**(8): p. 843-54.
27. Yauch, R.L., et al., *Epithelial versus mesenchymal phenotype determines in vitro sensitivity and predicts clinical activity of erlotinib in lung cancer patients*. Clin Cancer Res, 2005. **11**(24 Pt 1): p. 8686-98.
28. Wilson, C., et al., *AXL inhibition sensitizes mesenchymal cancer cells to antimetabolic drugs*. Cancer Res, 2014. **74**(20): p. 5878-90.
29. Shrader, M., et al., *Molecular correlates of gefitinib responsiveness in human bladder cancer cells*. Mol Cancer Ther, 2007. **6**(1): p. 277-85.
30. Frederick, B.A., et al., *Epithelial to mesenchymal transition predicts gefitinib resistance in cell lines of head and neck squamous cell carcinoma and non-small cell lung carcinoma*. Mol Cancer Ther, 2007. **6**(6): p. 1683-91.
31. Maseki, S., et al., *Acquisition of EMT phenotype in the gefitinib-resistant cells of a head and neck squamous cell carcinoma cell line through Akt/GSK-3beta/snail signalling pathway*. Br J Cancer, 2012. **106**(6): p. 1196-204.
32. Yin, T., et al., *Expression of snail in pancreatic cancer promotes metastasis and chemoresistance*. J Surg Res, 2007. **141**(2): p. 196-203.
33. Li, X., et al., *Intrinsic resistance of tumorigenic breast cancer cells to chemotherapy*. J Natl Cancer Inst, 2008. **100**(9): p. 672-9.
34. Suda, K., et al., *Epithelial to mesenchymal transition in an epidermal growth factor receptor-mutant lung cancer cell line with acquired resistance to erlotinib*. J Thorac Oncol, 2011. **6**(7): p. 1152-61.
35. Yao, Z., et al., *TGF-beta IL-6 axis mediates selective and adaptive mechanisms of resistance to molecular targeted therapy in lung cancer*. Proc Natl Acad Sci U S A, 2010. **107**(35): p. 15535-40.
36. Kemper, K., et al., *Phenotype switching: tumor cell plasticity as a resistance mechanism and target for therapy*. Cancer Res, 2014. **74**(21): p. 5937-41.

37. Bonnet, D. and J.E. Dick, *Human acute myeloid leukemia is organized as a hierarchy that originates from a primitive hematopoietic cell*. Nat Med, 1997. **3**(7): p. 730-7.
38. Al-Hajj, M., et al., *Prospective identification of tumorigenic breast cancer cells*. Proc Natl Acad Sci U S A, 2003. **100**(7): p. 3983-8.
39. O'Brien, C.A., et al., *A human colon cancer cell capable of initiating tumour growth in immunodeficient mice*. Nature, 2007. **445**(7123): p. 106-10.
40. Mani, S.A., et al., *The epithelial-mesenchymal transition generates cells with properties of stem cells*. Cell, 2008. **133**(4): p. 704-15.
41. Antoniou, A., et al., *Cancer stem cells, a fuzzy evolving concept: a cell population or a cell property?* Cell Cycle, 2013. **12**(24): p. 3743-8.
42. Floor, S., et al., *Cancer cells in epithelial-to-mesenchymal transition and tumor-propagating-cancer stem cells: distinct, overlapping or same populations*. Oncogene, 2011. **30**(46): p. 4609-21.
43. Lemmon, M.A. and J. Schlessinger, *Cell signaling by receptor tyrosine kinases*. Cell, 2010. **141**(7): p. 1117-34.
44. Schlessinger, J. and M.A. Lemmon, *SH2 and PTB domains in tyrosine kinase signaling*. Sci STKE, 2003. **2003**(191): p. RE12.
45. Zavadil, J., et al., *Genetic programs of epithelial cell plasticity directed by transforming growth factor-beta*. Proc Natl Acad Sci U S A, 2001. **98**(12): p. 6686-91.
46. Gonzalez, D.M. and D. Medici, *Signaling mechanisms of the epithelial-mesenchymal transition*. Sci Signal, 2014. **7**(344): p. re8.
47. Zhang, Y.E., *Non-Smad pathways in TGF-beta signaling*. Cell Res, 2009. **19**(1): p. 128-39.
48. Lawler, S., et al., *The type II transforming growth factor-beta receptor autophosphorylates not only on serine and threonine but also on tyrosine residues*. J Biol Chem, 1997. **272**(23): p. 14850-9.
49. Galliher, A.J. and W.P. Schiemann, *Src phosphorylates Tyr284 in TGF-beta type II receptor and regulates TGF-beta stimulation of p38 MAPK during breast cancer cell proliferation and invasion*. Cancer Res, 2007. **67**(8): p. 3752-8.
50. Galliher-Beckley, A.J. and W.P. Schiemann, *Grb2 binding to Tyr284 in TbetaR-II is essential for mammary tumor growth and metastasis stimulated by TGF-beta*. Carcinogenesis, 2008. **29**(2): p. 244-51.
51. Lee, M.K., et al., *TGF-beta activates Erk MAP kinase signalling through direct phosphorylation of ShcA*. EMBO J, 2007. **26**(17): p. 3957-67.
52. Xie, L., et al., *Activation of the Erk pathway is required for TGF-beta1-induced EMT in vitro*. Neoplasia, 2004. **6**(5): p. 603-10.
53. Lo, H.W., et al., *Epidermal growth factor receptor cooperates with signal transducer and activator of transcription 3 to induce epithelial-mesenchymal transition in cancer cells via up-regulation of TWIST gene expression*. Cancer Res, 2007. **67**(19): p. 9066-76.
54. Savagner, P., K.M. Yamada, and J.P. Thiery, *The zinc-finger protein slug causes desmosome dissociation, an initial and necessary step for growth factor-induced epithelial-mesenchymal transition*. J Cell Biol, 1997. **137**(6): p. 1403-19.

55. Joo, C.K., et al., *Ligand release-independent transactivation of epidermal growth factor receptor by transforming growth factor-beta involves multiple signaling pathways*. *Oncogene*, 2008. **27**(5): p. 614-28.
56. Murillo, M.M., et al., *Involvement of EGF receptor and c-Src in the survival signals induced by TGF-beta1 in hepatocytes*. *Oncogene*, 2005. **24**(28): p. 4580-7.
57. Uttamsingh, S., et al., *Synergistic effect between EGF and TGF-beta1 in inducing oncogenic properties of intestinal epithelial cells*. *Oncogene*, 2008. **27**(18): p. 2626-34.
58. Salt, M.B., S. Bandyopadhyay, and F. McCormick, *Epithelial-to-mesenchymal transition rewires the molecular path to PI3K-dependent proliferation*. *Cancer Discov*, 2014. **4**(2): p. 186-99.
59. Jahn, S.C., et al., *An in vivo model of epithelial to mesenchymal transition reveals a mitogenic switch*. *Cancer Lett*, 2012. **326**(2): p. 183-90.
60. Shilo, B.Z., *Regulating the dynamics of EGF receptor signaling in space and time*. *Development*, 2005. **132**(18): p. 4017-27.
61. Wieduwilt, M.J. and M.M. Moasser, *The epidermal growth factor receptor family: biology driving targeted therapeutics*. *Cell Mol Life Sci*, 2008. **65**(10): p. 1566-84.
62. Mukohara, T., et al., *Expression of epidermal growth factor receptor (EGFR) and downstream-activated peptides in surgically excised non-small-cell lung cancer (NSCLC)*. *Lung Cancer*, 2003. **41**(2): p. 123-30.
63. Aldape, K.D., et al., *Immunohistochemical detection of EGFRvIII in high malignancy grade astrocytomas and evaluation of prognostic significance*. *J Neuropathol Exp Neurol*, 2004. **63**(7): p. 700-7.
64. Frederick, L., et al., *Diversity and frequency of epidermal growth factor receptor mutations in human glioblastomas*. *Cancer Res*, 2000. **60**(5): p. 1383-7.
65. Chong, C.R. and P.A. Janne, *The quest to overcome resistance to EGFR-targeted therapies in cancer*. *Nat Med*, 2013. **19**(11): p. 1389-400.
66. Lynch, T.J., et al., *Activating mutations in the epidermal growth factor receptor underlying responsiveness of non-small-cell lung cancer to gefitinib*. *N Engl J Med*, 2004. **350**(21): p. 2129-39.
67. Sordella, R., et al., *Gefitinib-sensitizing EGFR mutations in lung cancer activate anti-apoptotic pathways*. *Science*, 2004. **305**(5687): p. 1163-7.
68. Helfrich, B.A., et al., *Antitumor activity of the epidermal growth factor receptor (EGFR) tyrosine kinase inhibitor gefitinib (ZD1839, Iressa) in non-small cell lung cancer cell lines correlates with gene copy number and EGFR mutations but not EGFR protein levels*. *Clin Cancer Res*, 2006. **12**(23): p. 7117-25.
69. Kobayashi, S., et al., *EGFR mutation and resistance of non-small-cell lung cancer to gefitinib*. *N Engl J Med*, 2005. **352**(8): p. 786-92.
70. Pao, W., et al., *Acquired resistance of lung adenocarcinomas to gefitinib or erlotinib is associated with a second mutation in the EGFR kinase domain*. *PLoS Med*, 2005. **2**(3): p. e73.
71. Engelman, J.A., et al., *MET amplification leads to gefitinib resistance in lung cancer by activating ERBB3 signaling*. *Science*, 2007. **316**(5827): p. 1039-43.
72. Ercan, D., et al., *Reactivation of ERK Signaling Causes Resistance to EGFR Kinase Inhibitors*. *Cancer Discov*, 2012. **2**(10): p. 934-947.

73. Takeyama, Y., et al., *Knockdown of ZEB1, a master epithelial-to-mesenchymal transition (EMT) gene, suppresses anchorage-independent cell growth of lung cancer cells*. *Cancer Lett*, 2010. **296**(2): p. 216-24.
74. Lazzara, M.J., et al., *Impaired SHP2-mediated extracellular signal-regulated kinase activation contributes to gefitinib sensitivity of lung cancer cells with epidermal growth factor receptor-activating mutations*. *Cancer Res*, 2010. **70**(9): p. 3843-50.
75. Furcht, C.M., et al., *Diminished functional role and altered localization of SHP2 in non-small cell lung cancer cells with EGFR-activating mutations*. *Oncogene*, 2013. **32**(18): p. 2346-55, 2355 e1-10.
76. Gu, H. and B.G. Neel, *The "Gab" in signal transduction*. *Trends Cell Biol*, 2003. **13**(3): p. 122-30.
77. Barford, D. and B.G. Neel, *Revealing mechanisms for SH2 domain mediated regulation of the protein tyrosine phosphatase SHP-2*. *Structure*, 1998. **6**(3): p. 249-54.
78. Neel, B.G., H. Gu, and L. Pao, *The 'Shp'ing news: SH2 domain-containing tyrosine phosphatases in cell signaling*. *Trends Biochem Sci*, 2003. **28**(6): p. 284-93.
79. Pluskey, S., et al., *Potent stimulation of SH-PTP2 phosphatase activity by simultaneous occupancy of both SH2 domains*. *J Biol Chem*, 1995. **270**(7): p. 2897-900.
80. Chan, G., D. Kalaitzidis, and B.G. Neel, *The tyrosine phosphatase Shp2 (PTPN11) in cancer*. *Cancer Metastasis Rev*, 2008. **27**(2): p. 179-92.
81. Mohi, M.G. and B.G. Neel, *The role of Shp2 (PTPN11) in cancer*. *Curr Opin Genet Dev*, 2007. **17**(1): p. 23-30.
82. Aceto, N., et al., *Tyrosine phosphatase SHP2 promotes breast cancer progression and maintains tumor-initiating cells via activation of key transcription factors and a positive feedback signaling loop*. *Nat Med*, 2012. **18**(4): p. 529-37.
83. Furcht, C.M., et al., *Multivariate signaling regulation by SHP2 differentially controls proliferation and therapeutic response in glioma cells*. *J Cell Sci*, 2014. **127**(Pt 16): p. 3555-67.
84. Neuzillet, C., et al., *MEK in cancer and cancer therapy*. *Pharmacol Ther*, 2014. **141**(2): p. 160-71.
85. Roberts, P.J. and C.J. Der, *Targeting the Raf-MEK-ERK mitogen-activated protein kinase cascade for the treatment of cancer*. *Oncogene*, 2007. **26**(22): p. 3291-310.
86. Cox, A.D., et al., *Drugging the undruggable RAS: Mission possible?* *Nat Rev Drug Discov*, 2014. **13**(11): p. 828-51.
87. Der, C.J., T.G. Krontiris, and G.M. Cooper, *Transforming genes of human bladder and lung carcinoma cell lines are homologous to the ras genes of Harvey and Kirsten sarcoma viruses*. *Proc Natl Acad Sci U S A*, 1982. **79**(11): p. 3637-40.
88. Parada, L.F., et al., *Human EJ bladder carcinoma oncogene is homologue of Harvey sarcoma virus ras gene*. *Nature*, 1982. **297**(5866): p. 474-8.
89. Cox, A.D. and C.J. Der, *The raf inhibitor paradox: unexpected consequences of targeted drugs*. *Cancer Cell*, 2010. **17**(3): p. 221-3.
90. Heidorn, S.J., et al., *Kinase-dead BRAF and oncogenic RAS cooperate to drive tumor progression through CRAF*. *Cell*, 2010. **140**(2): p. 209-21.
91. Flaherty, K.T., et al., *Improved survival with MEK inhibition in BRAF-mutated melanoma*. *N Engl J Med*, 2012. **367**(2): p. 107-14.

92. Robert, C., et al., *Improved overall survival in melanoma with combined dabrafenib and trametinib*. N Engl J Med, 2015. **372**(1): p. 30-9.
93. Shin, S., et al., *ERK2 but not ERK1 induces epithelial-to-mesenchymal transformation via DEF motif-dependent signaling events*. Mol Cell, 2010. **38**(1): p. 114-27.
94. Botta, G.P., et al., *Constitutive K-RasG12D activation of ERK2 specifically regulates 3D invasion of human pancreatic cancer cells via MMP-1*. Mol Cancer Res, 2011. **10**(2): p. 183-96.
95. Liu, X., et al., *PTPN14 interacts with and negatively regulates the oncogenic function of YAP*. Oncogene, 2012.
96. Wong, V.C., et al., *Tumor suppressor dual-specificity phosphatase 6 (DUSP6) impairs cell invasion and epithelial-mesenchymal transition (EMT)-associated phenotype*. Int J Cancer, 2011. **130**(1): p. 83-95.
97. Zhou, X.D. and Y.M. Agazie, *Inhibition of SHP2 leads to mesenchymal to epithelial transition in breast cancer cells*. Cell Death Differ, 2008. **15**(6): p. 988-96.
98. Wendt, M.K., J.A. Smith, and W.P. Schiemann, *Transforming growth factor-beta-induced epithelial-mesenchymal transition facilitates epidermal growth factor-dependent breast cancer progression*. Oncogene, 2010. **29**(49): p. 6485-98.
99. Blumenschein, G.R., Jr., et al., *Phase II study of cetuximab in combination with chemoradiation in patients with stage IIIA/B non-small-cell lung cancer: RTOG 0324*. J Clin Oncol, 2011. **29**(17): p. 2312-8.
100. Spigel, D.R., et al., *Randomized, double-blind, placebo-controlled, phase II trial of sorafenib and erlotinib or erlotinib alone in previously treated advanced non-small-cell lung cancer*. J Clin Oncol, 2011. **29**(18): p. 2582-9.
101. Xu, L., et al., *Combined EGFR/MET or EGFR/HSP90 Inhibition Is Effective in the Treatment of Lung Cancers Codriven by Mutant EGFR Containing T790M and MET*. Cancer Res, 2012. **72**(13): p. 3302-3311.
102. Lee, M.J., et al., *Sequential application of anticancer drugs enhances cell death by rewiring apoptotic signaling networks*. Cell, 2012. **149**(4): p. 780-94.
103. Zavadil, J. and E.P. Bottinger, *TGF-beta and epithelial-to-mesenchymal transitions*. Oncogene, 2005. **24**(37): p. 5764-74.
104. Witta, S.E., et al., *Restoring E-cadherin expression increases sensitivity to epidermal growth factor receptor inhibitors in lung cancer cell lines*. Cancer Res, 2006. **66**(2): p. 944-50.
105. Zhang, Z., et al., *Activation of the AXL kinase causes resistance to EGFR-targeted therapy in lung cancer*. Nat Genet, 2012. **44**(8): p. 852-60.
106. Furcht, C.M., et al., *Diminished functional role and altered localization of SHP2 in non-small cell lung cancer cells with EGFR-activating mutations*. Oncogene, 2012.
107. Lund, K.A., et al., *Quantitative analysis of the endocytic system involved in hormone-induced receptor internalization*. J Biol Chem, 1990. **265**(26): p. 15713-23.
108. Wiley, H.S. and D.D. Cunningham, *The endocytotic rate constant. A cellular parameter for quantitating receptor-mediated endocytosis*. J Biol Chem, 1982. **257**(8): p. 4222-9.
109. Singh, A., et al., *A gene expression signature associated with "K-Ras addiction" reveals regulators of EMT and tumor cell survival*. Cancer Cell, 2009. **15**(6): p. 489-500.

110. Basu, D., et al., *Evidence for mesenchymal-like sub-populations within squamous cell carcinomas possessing chemoresistance and phenotypic plasticity*. *Oncogene*, 2010. **29**(29): p. 4170-82.
111. Basu, D., et al., *Detecting and targeting mesenchymal-like subpopulations within squamous cell carcinomas*. *Cell Cycle*, 2011. **10**(12): p. 2008-16.
112. Zhou, W., et al., *Novel mutant-selective EGFR kinase inhibitors against EGFR T790M*. *Nature*, 2009. **462**(7276): p. 1070-4.
113. Janda, E., et al., *Ras and TGF[ $\beta$ ] cooperatively regulate epithelial cell plasticity and metastasis: dissection of Ras signaling pathways*. *J Cell Biol*, 2002. **156**(2): p. 299-313.
114. Lehmann, K., et al., *Raf induces TGF $\beta$  production while blocking its apoptotic but not invasive responses: a mechanism leading to increased malignancy in epithelial cells*. *Genes Dev*, 2000. **14**(20): p. 2610-22.
115. Peinado, H., M. Quintanilla, and A. Cano, *Transforming growth factor beta-1 induces snail transcription factor in epithelial cell lines: mechanisms for epithelial mesenchymal transitions*. *J Biol Chem*, 2003. **278**(23): p. 21113-23.
116. von Thun, A., et al., *ERK2 drives tumour cell migration in three-dimensional microenvironments by suppressing expression of Rab17 and liprin-beta2*. *J Cell Sci*, 2012. **125**(Pt 6): p. 1465-77.
117. Han, M., et al., *Antagonism of miR-21 Reverses Epithelial-Mesenchymal Transition and Cancer Stem Cell Phenotype through AKT/ERK1/2 Inactivation by Targeting PTEN*. *PLoS One*, 2012. **7**(6): p. e39520.
118. Yoon, Y.K., et al., *Combination of EGFR and MEK1/2 inhibitor shows synergistic effects by suppressing EGFR/HER3-dependent AKT activation in human gastric cancer cells*. *Mol Cancer Ther*, 2009. **8**(9): p. 2526-36.
119. Diep, C.H., et al., *Synergistic effect between erlotinib and MEK inhibitors in KRAS wild-type human pancreatic cancer cells*. *Clin Cancer Res*, 2011. **17**(9): p. 2744-56.
120. Wang, D., et al., *Clinical experience of MEK inhibitors in cancer therapy*. *Biochim Biophys Acta*, 2007. **1773**(8): p. 1248-55.
121. Xing, H., et al., *Activation of fibronectin/PI-3K/Akt2 leads to chemoresistance to docetaxel by regulating survivin protein expression in ovarian and breast cancer cells*. *Cancer Lett*, 2008. **261**(1): p. 108-19.
122. Pratilas, C.A., et al., *Genetic predictors of MEK dependence in non-small cell lung cancer*. *Cancer Res*, 2008. **68**(22): p. 9375-83.
123. Chaffer, C.L. and R.A. Weinberg, *A perspective on cancer cell metastasis*. *Science*, 2011. **331**(6024): p. 1559-64.
124. Tan, T.Z., et al., *Epithelial-mesenchymal transition spectrum quantification and its efficacy in deciphering survival and drug responses of cancer patients*. *EMBO Mol Med*, 2014. **6**(10): p. 1279-93.
125. Arumugam, T., et al., *Epithelial to mesenchymal transition contributes to drug resistance in pancreatic cancer*. *Cancer Res*, 2009. **69**(14): p. 5820-8.
126. Buonato, J.M. and M.J. Lazzara, *ERK1/2 blockade prevents epithelial-mesenchymal transition in lung cancer cells and promotes their sensitivity to EGFR inhibition*. *Cancer Res*, 2014. **74**(1): p. 309-19.
127. Davis, F.M., et al., *Targeting EMT in cancer: opportunities for pharmacological intervention*. *Trends Pharmacol Sci*, 2014. **35**(9): p. 479-488.

128. Dragoi, A.M., et al., *Novel strategies to enforce an epithelial phenotype in mesenchymal cells*. *Cancer Res*, 2014. **74**(14): p. 3659-72.
129. Wilson, C., et al., *Overcoming EMT-associated resistance to anti-cancer drugs via Src/FAK pathway inhibition*. *Oncotarget*, 2014. **5**(17): p. 7328-41.
130. Hof, P., et al., *Crystal structure of the tyrosine phosphatase SHP-2*. *Cell*, 1998. **92**(4): p. 441-50.
131. Eck, M.J., et al., *Spatial constraints on the recognition of phosphoproteins by the tandem SH2 domains of the phosphatase SH-PTP2*. *Nature*, 1996. **379**(6562): p. 277-80.
132. Lechleider, R.J., et al., *Activation of the SH2-containing phosphotyrosine phosphatase SH-PTP2 by its binding site, phosphotyrosine 1009, on the human platelet-derived growth factor receptor*. *J Biol Chem*, 1993. **268**(29): p. 21478-81.
133. Sugimoto, S., et al., *Activation of the SH2-containing protein tyrosine phosphatase, SH-PTP2, by phosphotyrosine-containing peptides derived from insulin receptor substrate-1*. *J Biol Chem*, 1994. **269**(18): p. 13614-22.
134. Kapoor, G.S., et al., *Distinct domains in the SHP-2 phosphatase differentially regulate epidermal growth factor receptor/NF-kappaB activation through Gab1 in glioblastoma cells*. *Mol Cell Biol*, 2004. **24**(2): p. 823-36.
135. O'Reilly, A.M. and B.G. Neel, *Structural determinants of SHP-2 function and specificity in Xenopus mesoderm induction*. *Mol Cell Biol*, 1998. **18**(1): p. 161-77.
136. Stewart, R.A., et al., *Phosphatase-dependent and -independent functions of Shp2 in neural crest cells underlie LEOPARD syndrome pathogenesis*. *Dev Cell*, 2010. **18**(5): p. 750-62.
137. Li, S., et al., *SHP2 Positively Regulates TGFbeta1-induced Epithelial-mesenchymal Transition Modulated by Its Novel Interacting Protein Hook1*. *J Biol Chem*, 2014.
138. Loerke, D., et al., *Quantitative imaging of epithelial cell scattering identifies specific inhibitors of cell motility and cell-cell dissociation*. *Sci Signal*, 2012. **5**(231): p. rs5.
139. Caslavsky, J., Z. Klimova, and T. Vomastek, *ERK and RSK regulate distinct steps of a cellular program that induces transition from multicellular epithelium to single cell phenotype*. *Cell Signal*, 2013. **25**(12): p. 2743-51.
140. Ventura, A., et al., *Cre-lox-regulated conditional RNA interference from transgenes*. *Proc Natl Acad Sci U S A*, 2004. **101**(28): p. 10380-5.
141. Thomson, S., et al., *Epithelial to mesenchymal transition is a determinant of sensitivity of non-small-cell lung carcinoma cell lines and xenografts to epidermal growth factor receptor inhibition*. *Cancer Res*, 2005. **65**(20): p. 9455-62.
142. Rajasekaran, S.A., et al., *HPAF-II, a cell culture model to study pancreatic epithelial cell structure and function*. *Pancreas*, 2004. **29**(3): p. e77-83.
143. Deer, E.L., et al., *Phenotype and genotype of pancreatic cancer cell lines*. *Pancreas*, 2010. **39**(4): p. 425-35.
144. Gotzmann, J., et al., *A crucial function of PDGF in TGF-beta-mediated cancer progression of hepatocytes*. *Oncogene*, 2006. **25**(22): p. 3170-85.
145. Zieba, A., et al., *Intercellular variation in signaling through the TGF-beta pathway and its relation to cell density and cell cycle phase*. *Mol Cell Proteomics*, 2012. **11**(7): p. M111013482.

146. Nallet-Staub, F., et al., *Cell Density Sensing Alters TGF-beta Signaling in a Cell-Type-Specific Manner, Independent from Hippo Pathway Activation*. Dev Cell, 2015. **32**(5): p. 640-51.
147. Schutte, M., et al., *DPC4 gene in various tumor types*. Cancer Res, 1996. **56**(11): p. 2527-30.
148. Hartman, Z.R., M.D. Schaller, and Y.M. Agazie, *The tyrosine phosphatase SHP2 regulates focal adhesion kinase to promote EGF-induced lamellipodia persistence and cell migration*. Mol Cancer Res, 2013. **11**(6): p. 651-64.
149. Lee, H.H., et al., *Shp2 plays a crucial role in cell structural orientation and force polarity in response to matrix rigidity*. Proc Natl Acad Sci U S A, 2013. **110**(8): p. 2840-5.
150. Wendt, M.K. and W.P. Schiemann, *Therapeutic targeting of the focal adhesion complex prevents oncogenic TGF-beta signaling and metastasis*. Breast Cancer Res, 2009. **11**(5): p. R68.
151. Furcht, C.M., J.M. Buonato, and M.J. Lazzara, *EGFR-activated Src Family Kinases Maintain GAB1-SHP2 Complexes Distal from EGFR*. Science Signaling, 2015. **Accepted**.
152. Bentires-Alj, M., et al., *Activating mutations of the noonan syndrome-associated SHP2/PTPN11 gene in human solid tumors and adult acute myelogenous leukemia*. Cancer Res, 2004. **64**(24): p. 8816-20.
153. Yu, B., et al., *Targeting protein tyrosine phosphatase SHP2 for the treatment of PTPN11-associated malignancies*. Mol Cancer Ther, 2013. **12**(9): p. 1738-48.
154. Chio, C.M., C.S. Lim, and A.C. Bishop, *Targeting a cryptic allosteric site for selective inhibition of the oncogenic protein tyrosine phosphatase shp2*. Biochemistry, 2015. **54**(2): p. 497-504.
155. Vincent, A., et al., *Pancreatic cancer*. Lancet, 2011. **378**(9791): p. 607-20.
156. Costello, E., W. Greenhalf, and J.P. Neoptolemos, *New biomarkers and targets in pancreatic cancer and their application to treatment*. Nat Rev Gastroenterol Hepatol, 2012. **9**(8): p. 435-44.
157. Bakin, A.V., et al., *p38 mitogen-activated protein kinase is required for TGFbeta-mediated fibroblastic transdifferentiation and cell migration*. J Cell Sci, 2002. **115**(Pt 15): p. 3193-206.
158. Maier, H.J., et al., *NF-kappaB promotes epithelial-mesenchymal transition, migration and invasion of pancreatic carcinoma cells*. Cancer Lett, 2010. **295**(2): p. 214-28.
159. Nagai, T., et al., *Sorafenib inhibits the hepatocyte growth factor-mediated epithelial mesenchymal transition in hepatocellular carcinoma*. Mol Cancer Ther, 2011. **10**(1): p. 169-77.
160. Albeck, J.G., G.B. Mills, and J.S. Brugge, *Frequency-modulated pulses of ERK activity transmit quantitative proliferation signals*. Mol Cell, 2013. **49**(2): p. 249-61.
161. Birchmeier, C., et al., *Met, metastasis, motility and more*. Nat Rev Mol Cell Biol, 2003. **4**(12): p. 915-25.
162. Purvis, J.E. and G. Lahav, *Encoding and decoding cellular information through signaling dynamics*. Cell, 2013. **152**(5): p. 945-56.
163. Geladi, P. and B.R. Kowalski, *Partial Least-Squares Regression - a Tutorial*. Analytica Chimica Acta, 1986. **185**: p. 1-17.

164. Wold, S., M. Sjostrom, and L. Eriksson, *PLS-regression: a basic tool of chemometrics*. Chemometrics and Intelligent Laboratory Systems, 2001. **58**(2): p. 109-130.
165. Janes, K.A. and M.B. Yaffe, *Data-driven modelling of signal-transduction networks*. Nat Rev Mol Cell Biol, 2006. **7**(11): p. 820-8.
166. Kumar, N., et al., *Modeling HER2 effects on cell behavior from mass spectrometry phosphotyrosine data*. PLoS Comput Biol, 2007. **3**(1): p. e4.
167. Kim, H.D., et al., *Signaling network state predicts twist-mediated effects on breast cell migration across diverse growth factor contexts*. Mol Cell Proteomics, 2011. **10**(11): p. M111 008433.
168. Wong, I.Y., et al., *Collective and individual migration following the epithelial-mesenchymal transition*. Nat Mater, 2014. **13**(11): p. 1063-71.
169. Zhao, D., et al., *Cytoplasmic p27 promotes epithelial-mesenchymal transition and tumor metastasis via STAT3-mediated Twist1 upregulation*. Oncogene, 2015.
170. Liu, J., et al., *The oncogene c-Jun impedes somatic cell reprogramming*. Nat Cell Biol, 2015. **17**(7): p. 856-67.
171. Bain, J., et al., *The selectivity of protein kinase inhibitors: a further update*. Biochem J, 2007. **408**(3): p. 297-315.
172. Misale, S., et al., *Blockade of EGFR and MEK intercepts heterogeneous mechanisms of acquired resistance to anti-EGFR therapies in colorectal cancer*. Sci Transl Med, 2014. **6**(224): p. 224ra26.
173. Judd, N.P., et al., *ERK1/2 regulation of CD44 modulates oral cancer aggressiveness*. Cancer Res, 2012. **72**(1): p. 365-74.
174. Weiss, M.B., et al., *TWIST1 is an ERK1/2 effector that promotes invasion and regulates MMP-1 expression in human melanoma cells*. Cancer Res, 2012. **72**(24): p. 6382-92.
175. Smith, M.A., et al., *Annotation of human cancers with EGFR signaling-associated protein complexes using proximity ligation assays*. Sci Signal, 2015. **8**(359): p. ra4.
176. Peng, S., et al., *Tumor grafts derived from patients with head and neck squamous carcinoma authentically maintain the molecular and histologic characteristics of human cancers*. J Transl Med, 2013. **11**: p. 198.
177. Siolas, D. and G.J. Hannon, *Patient-derived tumor xenografts: transforming clinical samples into mouse models*. Cancer Res, 2013. **73**(17): p. 5315-9.
178. Wang, K., et al., *PEST Domain Mutations in Notch Receptors Comprise an Oncogenic Driver Segment in Triple-Negative Breast Cancer Sensitive to a gamma-Secretase Inhibitor*. Clin Cancer Res, 2015. **21**(6): p. 1487-96.
179. Klinghammer, K., et al., *A comprehensively characterized large panel of head and neck cancer patient-derived xenografts identifies the mTOR inhibitor everolimus as potential new treatment option*. Int J Cancer, 2014.
180. Schuller, A., et al., *The MET inhibitor AZD6094 (Savolitinib, HMPL-504) induces regression in papillary renal cell carcinoma patient derived xenograft models*. Clin Cancer Res, 2015.
181. Dobbin, Z.C., et al., *Using heterogeneity of the patient-derived xenograft model to identify the chemoresistant population in ovarian cancer*. Oncotarget, 2014. **5**(18): p. 8750-64.
182. Davis, F.M., et al., *Targeting EMT in cancer: opportunities for pharmacological intervention*. Trends Pharmacol Sci, 2014. **35**(9): p. 479-88.

183. Leszczyniecka, M., et al., *Differentiation therapy of human cancer: basic science and clinical applications*. Pharmacol Ther, 2001. **90**(2-3): p. 105-56.
184. Sachs, L., *Control of normal cell differentiation and the phenotypic reversion of malignancy in myeloid leukaemia*. Nature, 1978. **274**(5671): p. 535-9.
185. Gupta, P.B., et al., *Identification of selective inhibitors of cancer stem cells by high-throughput screening*. Cell, 2009. **138**(4): p. 645-59.
186. Chua, K.N., et al., *A cell-based small molecule screening method for identifying inhibitors of epithelial-mesenchymal transition in carcinoma*. PLoS One, 2012. **7**(3): p. e33183.
187. Hirano, T., et al., *Identification of novel small compounds that restore E-cadherin expression and inhibit tumor cell motility and invasiveness*. Biochem Pharmacol, 2013. **86**(10): p. 1419-29.
188. Fabbro, D., et al., *Targeting cancer with small-molecular-weight kinase inhibitors*. Methods Mol Biol, 2012. **795**: p. 1-34.
189. Barr, A.J., *Protein tyrosine phosphatases as drug targets: strategies and challenges of inhibitor development*. Future Med Chem, 2010. **2**(10): p. 1563-76.
190. He, R., et al., *Small molecule tools for functional interrogation of protein tyrosine phosphatases*. FEBS J, 2013. **280**(2): p. 731-50.
191. Krishnan, N., et al., *Targeting the disordered C terminus of PTP1B with an allosteric inhibitor*. Nat Chem Biol, 2014. **10**(7): p. 558-66.
192. Li, S., et al., *SHP2 positively regulates TGFbeta1-induced epithelial-mesenchymal transition modulated by its novel interacting protein Hook1*. J Biol Chem, 2014. **289**(49): p. 34152-60.
193. Burks, J. and Y.M. Agazie, *Modulation of alpha-catenin Tyr phosphorylation by SHP2 positively effects cell transformation induced by the constitutively active FGFR3*. Oncogene, 2006. **25**(54): p. 7166-79.
194. Vasilescu, J. and D. Figeys, *Mapping protein-protein interactions by mass spectrometry*. Curr Opin Biotechnol, 2006. **17**(4): p. 394-9.
195. Ren, Y., et al., *Roles of Gab1 and SHP2 in paxillin tyrosine dephosphorylation and Src activation in response to epidermal growth factor*. J Biol Chem, 2004. **279**(9): p. 8497-505.
196. Jares-Erijman, E.A. and T.M. Jovin, *FRET imaging*. Nat Biotechnol, 2003. **21**(11): p. 1387-95.
197. Piston, D.W. and G.J. Kremers, *Fluorescent protein FRET: the good, the bad and the ugly*. Trends Biochem Sci, 2007. **32**(9): p. 407-14.
198. Soderberg, O., et al., *Characterizing proteins and their interactions in cells and tissues using the in situ proximity ligation assay*. Methods, 2008. **45**(3): p. 227-32.
199. Levy, L. and C.S. Hill, *Smad4 dependency defines two classes of transforming growth factor {beta} (TGF-{beta}) target genes and distinguishes TGF-{beta}-induced epithelial-mesenchymal transition from its antiproliferative and migratory responses*. Mol Cell Biol, 2005. **25**(18): p. 8108-25.
200. Zhao, S., et al., *Inhibition of STAT3 Tyr705 phosphorylation by Smad4 suppresses transforming growth factor beta-mediated invasion and metastasis in pancreatic cancer cells*. Cancer Res, 2008. **68**(11): p. 4221-8.

201. Bardeesy, N., et al., *Smad4 is dispensable for normal pancreas development yet critical in progression and tumor biology of pancreas cancer*. *Genes Dev*, 2006. **20**(22): p. 3130-46.
202. Doudna, J.A. and E. Charpentier, *Genome editing. The new frontier of genome engineering with CRISPR-Cas9*. *Science*, 2014. **346**(6213): p. 1258096.
203. Zhang, J., et al., *TGF-beta-induced epithelial-to-mesenchymal transition proceeds through stepwise activation of multiple feedback loops*. *Sci Signal*, 2014. **7**(345): p. ra91.